



Dipl.-Ing. Lukas Schwalt, BSc

Lightning Phenomena in the Alpine Region of Austria

DOCTORAL THESIS

to achieve the university degree of
Doktor der technischen Wissenschaften
submitted to

Graz University of Technology

Supervisor

Ao.Univ.-Prof. Dipl.-Ing. Dr.techn. Stephan Pack

Institute of High Voltage Engineering and System Performance

Univ.-Prof. Dr.-Ing. Uwe Schichler

AFFIDAVIT

I declare that I have authored this thesis independently, that I have not used other than the declared sources/resources, and that I have explicitly indicated all material which has been quoted either literally or by content from the sources used. The text document uploaded to TUGRAZonline is identical to the present doctoral thesis.

Date

Signature

Graz University of Technology
Institute of High Voltage Engineering and System Performance
Inffeldgasse 18
8010 Graz
Austria

Head of Institute

Univ.-Prof. Dr.-Ing. Uwe Schichler

Supervisor

Ao.Univ.-Prof. Dipl.-Ing. Dr.techn. Stephan Pack

Reviewer

Prof. Farhad Rachidi

A Dissertation by

Dipl.-Ing. Lukas Schwalt, BSc

September 2019

Danksagung – Acknowledgement

Diese Arbeit stellt den letzten Punkt meiner Studienlaufbahn an der Technischen Universität Graz dar. Diesen Rahmen möchte ich nutzen, um all jenen Dank auszusprechen, die mich fachlich, praktisch und mental unterstützt haben.

Ein großer Dank geht an meinen Doktorats-Betreuer Ao.Univ.-Prof. Dipl.-Ing. Dr.techn. Stephan Pack, welcher jederzeit ein offenes Ohr für meine Anliegen hatte und mir mit Expertise stets hilfsbereit, kompetent und mit Engagement zur Seite stand. Auch bei Institutsleiter Univ.-Prof. Dr.-Ing. Uwe Schichler möchte ich mich für die Unterstützung und das mir entgegengebrachte Vertrauen bedanken.

Besonderer Dank gebührt dem Team des Österreichischen Blitzortungssystems ALDIS, allen voran Dr. Wolfgang Schulz, der mich über die ganze Projektlaufzeit professionell unterstützt hat, mit mir wissenschaftliche Diskussionen führte und Ideen stets positiv aufnahm. Weiter gilt mein Dank Dr. Gerhard Diendorfer und DI Hannes Pichler, welche beide fachlich wie organisatorisch in jedem Moment bemüht um den positiven Verlauf des Projekts waren.

Georg Pistotnik hat mir über zwei Messperioden täglich projektspezifisch Auskunft über Wetterlage und Gewitterwahrscheinlichkeit gegeben. Danke für deine selbstverständliche und unkomplizierte Art zu helfen.

All meinen Freunden und Arbeitskollegen, welche sich während der Zeit an der TU Graz meine Gedanken und Ideen angehört und das Arbeitsleben erheitert haben, möchte ich danken. Hier geht mein Dank vor allem an Alex, Anton, Bernhard, Christoph, Dennis, Florian, Gernot, Jürgen, Oliver, Mark und Marlene. Dem restlichen Team am Institut, wie auch Christian Vergeiner sei hier mein Dank ausgesprochen.

Ein einfacher Dank reicht nicht, um meiner Familie das zu sagen was mir ihre Unterstützung bedeutet. Ohne sie hätte ich dieses Ziel wahrscheinlich nicht erreicht. Der notwendige Ehrgeiz für diese Arbeit wurde durch sie stetig bestärkt. Ihr Rückhalt, Mitfiebern und Verständnis haben mich über die ganze Zeit meines Studiums begleitet.

Meine Partnerin Viktoria wusste von Anfang an, dass ich mein Dissertationsvorhaben mit Erfolg meistern werde. Dieses uneingeschränkte Vertrauen in mich und mein Tun ist etwas, das ich jedem nur wünschen kann. Danke.

Last but not least I would like to thank Prof. Farhad Rachidi as one of the Experts willing to be part of the examination board and escorting me across the finish line.

Abstract

Cloud-to-ground (CG) lightning phenomena in the Alpine region of Austria and associated analyzes of recorded data represent the research focus of the present thesis. First, on-site measurements of CG flashes were performed to generate a ground truth data set. A high speed Video camera (recording speed of 2000 frames per second) and an electric Field Recording System (VFRS) was used for this purpose. The VFRS measurements have been conducted at 21 different measurement locations. 531 CG flashes including 1639 CG strokes have been recorded on 51 days during warm season thunderstorms in the years 2015, 2017 and 2018. The recorded ground truth VFRS data were correlated with Lightning Location System (LLS) data of the Austrian Lightning Detection and Information System (ALDIS) to complement the data set. This data set was used to analyze characteristic parameters of the recorded flashes and to calculate annual and total performance parameters of the LLS. The results of the analyses are then compared with former findings from the literature.

Flashes in the Alpine region of Austria show a particularly high amount of negative single stroke flashes compared to other regions in the world. Mean multiplicity values determined with the VFRS data are comparable to the previous results for measurements in the Austrian Alps but the values are situated at the lower end compared to previous studies for other countries. Analyses for negative first return stroke peak current estimations by the LLS show a significant difference compared to the used values in standards, derived from direct current measurements. The hypothesis that larger return stroke peak currents of subsequent strokes than the first stroke of LLS grouped flashes are resulting from first strokes to a new ground strike point cannot be confirmed. The analysis of LLS performance parameters for negative flashes revealed a median location accuracy value of 100 m and LLS flash detection efficiency (DE) values constantly higher than 96 % have been detected for all three investigated years. DE percentages for strokes show a higher variance over the three years. Analyses of the positive flash data revealed a rather low single stroke flash percentage compared to previous analyses for Austria but the percentage is situated within the range of previously published values for other countries whereas LLS median return stroke peak current show a comparatively high value. Mean multiplicity as well as DE values for positive flashes show similar results than for previous studies. A rare stepwise analysis of VFRS data of direct lightning strikes to wind turbines and a railway transmission line correlated with system operator data completes this work.

Kurzfassung

Die Erforschung von Wolke-Erde-Blitzen im österreichischen Alpenraum und die damit verbundene Auswertung aufgezeichneter Daten, stellt den Schwerpunkt der vorliegenden Arbeit dar. Zunächst wurden reale Abläufe von Wolke-Erde-Blitzen vor Ort aufgezeichnet, um einen sogenannten „ground truth“ Datensatz (reale Bodeneinschläge) von Blitzentladungen zu generieren. Zu diesem Zweck wurden eine Hochgeschwindigkeits-Videokamera (Aufnahmen mit 2000 Bildern pro Sekunde) und ein elektrisches Feldmesssystem (VFRS) verwendet. Die VFRS-Messungen wurden an 21 verschiedenen Messstandorten durchgeführt und dabei wurden 531 Wolke-Erde-Flashes (Gesamtblitzentladungen), mit 1639 Wolke-Erde-Strokes (Teilblitze), an 51 Tagen zwischen Mai und August in den Jahren 2015, 2017 und 2018 aufgezeichnet. Diese „ground truth“-VFRS-Daten wurden mit Daten des Österreichischen Blitzortungssystems (LLS) „Austrian Lightning Detection and Information System (ALDIS)“ korreliert, um den Datensatz zu ergänzen. Der Datensatz wurde verwendet, um charakteristische Parameter der aufgezeichneten Blitze zu analysieren und Leistungsparameter des LLS für die jeweiligen Jahre zu berechnen. Zusätzlich wurden diese Analysen mit Ergebnissen vorangegangener Studien verglichen.

Die Anzahl negativer „Single Stroke Flashes“ im österreichischen Alpenraum ist im Vergleich zu anderen Regionen der Welt besonders hoch. Die mittlere „Multiplicity“ für negative Blitze ist mit vorangegangenen Messergebnissen in den österreichischen Alpen vergleichbar, liegt jedoch im internationalen Vergleich im unteren Ergebnisfeld. Analysen der negativen Blitzstromamplituden (LLS Daten) zeigen wesentlich niedrigere Werte als in den Normen verwendete Werte direkter Blitzstrommessungen. Die Hypothese, dass größere Blitzstromamplitudenwerte in einem Flash von Teil-Strokes zu einem neuen Bodenfußpunkt herrühren, welche dem Erst-Stroke eines Flashes folgen, kann nicht bestätigt werden. Die Werte der „LLS-Location-Accuracy“ liegen für negative Blitze im Mittel bei 100 m und die der „LLS-Flash-Detection-Efficiency (DE)“ liegen konstant über 96 %, für alle drei untersuchten Jahre. Die Prozentsätze der Stroke-DE zeigen über die drei Jahre eine höhere Varianz. Auswertungen für Flashes mit positiver Polarität ergaben im Vergleich zu früheren Auswertungen für Österreich einen eher geringen „Single Stroke Flash-Anteil“. Der Wert liegt jedoch im Bereich der zuvor veröffentlichten Ergebnisse für andere Länder, während der Median der Blitzstromamplituden einen vergleichsweise hohen Wert aufweist. Die mittlere „Multiplicity“ sowie die DE-Werte für positive Blitze zeigen ähnliche Ergebnisse wie frühere Studien. Eine schrittweise Analyse zweier Spezialfälle von direkten Blitzeinschlägen in Windkraftanlagen und eine Eisenbahn-Fahrdrahtleitung, aufgezeichnet mit dem VFRS und korreliert mit Daten der Systembetreiber, vervollständigt diese Arbeit.

Contents

1	Introduction.....	1
1.1	Motivation	1
1.2	Aim of the Work	3
1.3	Method	5
1.4	Field of Research.....	6
2	Cloud-to-Ground Lightning.....	7
2.1	Lightning Discharge	7
2.2	Lightning in the Alpine Region of Austria	11
3	Measurement Systems, Setup and Tools	15
3.1	Video and Field Recording System.....	15
3.2	Lightning Location System.....	18
3.3	On-Site Setup of the VFRS.....	22
4	Data.....	25
4.1	General Information	25
4.2	Data of Cloud-to-Ground Flashes	26
4.3	Lightning Location System (LLS) Data.....	27
4.4	Additional Meteorological Data	28
4.5	Additional Information of Wind Farm and Railway Operator.....	28
5	Methodology	29
5.1	Research Parameters.....	29
5.2	VFRS and LLS Data Analysis	29
5.2.1	Correlation.....	29
5.2.2	Single Stroke Flashes and Multiplicity	30
5.2.3	Return Stroke Peak Current Analyses.....	32
5.2.4	Location Accuracy (LA)	34

5.2.5	Detection Efficiency (DE).....	36
6	Results	37
6.1	Negative Single Stroke Flashes.....	37
6.1.1	Data of Single Stroke Flashes	37
6.1.2	Single Stroke Flashes Detected by VFRS and LLS	38
6.1.3	Analysis of Negative Single Stroke Flashes by Thunderstorm Type for Data from 2009 to 2018	39
6.1.4	Comparison with Values Available in the Literature	42
6.2	Mean Multiplicity and Multiplicity Distribution of Negative Flashes	45
6.2.1	Analysis of the Multiplicity of VFRS and LLS Data.....	45
6.2.2	Multiplicity Distribution of VFRS and LLS Data	46
6.2.3	Comparison with Values Available in the Literature	46
6.3	Negative Return Stroke Peak Currents of LLS Detections	48
6.3.1	Return Stroke Peak Currents for Flashes, all Strokes, FI and SU Strokes ...	48
6.3.2	Return Stroke Peak Current distribution for all Strokes, FI and SU Strokes and Flashes	50
6.3.3	Return Stroke Peak Current Analysis for Ground Strike Points.....	52
6.3.4	Comparison with Values Available in the Literature	55
6.4	Location Accuracy of the LLS for Negative Flashes	57
6.4.1	Location Accuracy Distribution	57
6.4.2	Location Accuracy for Particular Channel Geometries.....	58
6.4.3	Comparison with Recent Values Available in the Literature	62
6.5	Detection Efficiency of the LLS for Negative Flashes	64
6.5.1	Analysis of the Detection Efficiency	64
6.5.2	Reason for Flash and Stroke Detection Efficiency Variations	65
6.5.3	Comparison with Recent Values Available in the Literature	65
6.6	Analyses of Positive Flashes	67
6.6.1	Single Stroke Flashes	67
6.6.2	Multiplicity.....	69

6.6.3	Positive Return Stroke Peak Currents of LLS Detections	70
6.6.4	Detection Efficiency	71
6.7	Direct Impact of Lightning Discharges on Power Generation and Transmission Systems	73
6.7.1	Lightning Strikes to two Wind Turbines.....	73
6.7.2	Lightning Strike to a Railway Overhead Line	76
7	Discussion	81
7.1	Negative Single Stroke Flashes	81
7.2	Mean Multiplicity and Multiplicity Distribution of Negative Flashes	84
7.3	Negative Return Stroke Peak Currents of LLS Detections	86
7.4	Location Accuracy of the LLS for Negative Flashes	89
7.5	Detection Efficiency of the LLS for Negative Flashes	91
7.6	Analyses of Positive Flashes	93
7.7	Direct Impact of Lightning Discharges on Power Generation and Transmission Systems	94
8	Conclusion	97
9	Summary	103
10	Abbreviations.....	107
11	References	109
12	List of Figures.....	117
13	List of Tables	121
14	Publications by the Author	125
14.1	Publications with Scientific Relation to the Present Thesis.....	125
14.2	Other Publications by the Author	126
15	Appendix	127

1 Introduction

1.1 Motivation

The motivation for the present investigation is to gather lightning ground truth data for the Austrian Alpine region over three years out of measurements from on-site Video and Field Recording System (VFRS) data. This region shows high lightning activity, especially in the southeastern part of the country (see section 2.2). The VFRS measurements shall be conducted in different measurement locations to observe individual thunderstorms and their lightning characteristics over a large area. The used VFRS consists of two main components: a high speed video camera and an electric field measurement system.

Measurements with the VFRS have been carried out for the first time in 2015 at the Institute of High Voltage Engineering and System Performance. To enhance the research in this field, the project “Lightning Observation in the Alps (LiOn)” was established in 2017 at Graz University of Technology.

The analyzed VFRS measurements for the present thesis have been recorded during 2015, 2017 and 2018. To gather the ground truth data of cloud-to-ground (CG) discharges, measurements have been carried out during warm season thunderstorms. Even though the CG processes represent just around 25 % of the total lightning activity (Rakov, 2014 [1]) the analysis in the present thesis has its main focus on this section. The research in this field shall provide a contribution to a better understanding of the physical processes of CG discharges in continental and mountainous regions of Austria during the main storm period from May to August. The investigated CG discharges, e.g., can have a direct impact on existing power generation and transmission systems as well as living beings. Parameters for technical applications and characteristic values for future work in lightning protection can be derived from the recorded data sets in the best case. The data of the used high speed video camera gives proof of the occurrence of flashes and strokes and provides additional information about ground strike points (GSP), multiplicity, leader propagation properties and continuing current durations for example. Dependencies of lightning parameters from different thunderstorm types will be analyzed especially for negative single stroke flashes.

The recorded ground truth VFRS data is correlated with data of the Austrian Lightning Detection and Information System (ALDIS) to complement the data set of each lightning flash. On the one hand data recording with a portable video and field recording system has the advantage of recording lightning discharges over a large area but on the other hand such

VFRS measurements cannot provide ground truth information about the return stroke peak current for example. Such a correlated data set of VFRS and Lightning Location System (LLS) data offers the possibility of analyzing quality parameters of the LLS in addition. Therefore the analysis of the LLS location accuracy and detection efficiency parameters for each year and in total have been chosen as secondary goal for the present work. All analyses will additionally be compared with former findings for the Austrian region and recent international investigations in the field of lightning ground truth data analyses as well as with analyses regarding quality parameters of large-scale LLS.

Figure 1 shows the region under investigation with its measurement locations on an elevation map of Austria. Variations in altitude above sea level depending on the area of investigation can be extracted from Figure 1 too. The area of investigation includes flat terrain in the southeast and northeast, pre-alpine terrain in the center of the country and the central alpine area with mountains up to a height of 3800 m. In addition, sensor locations of ALDIS and sensor positions of the surrounding countries, which are combined in the EUCLID¹ system, are illustrated.

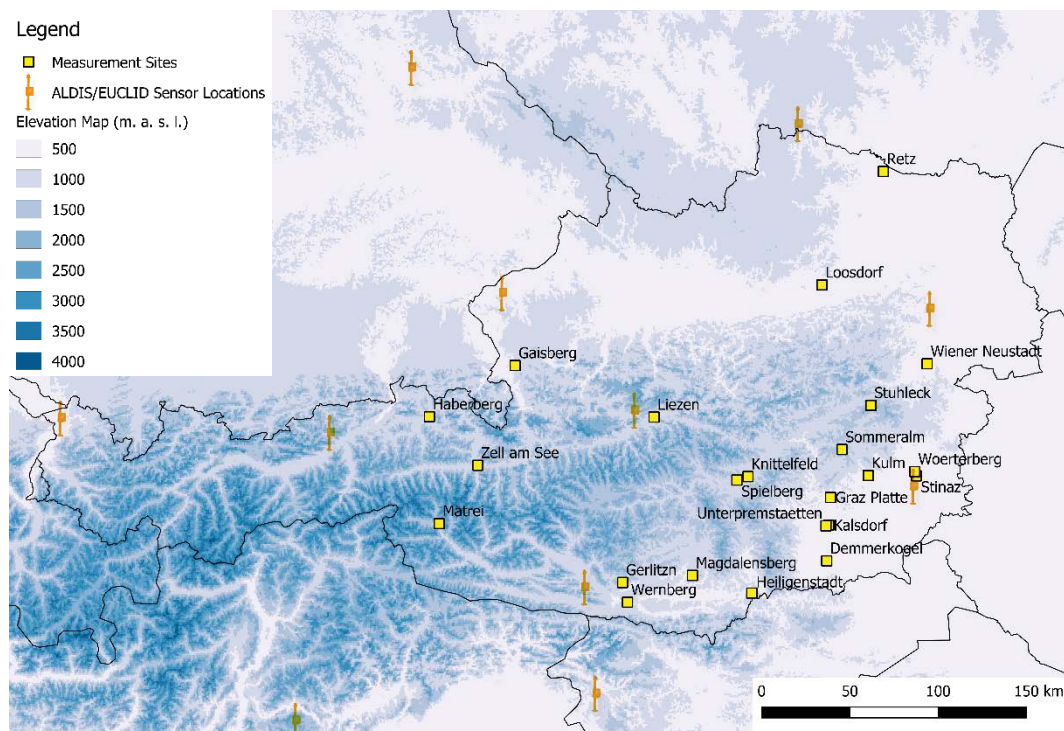


Figure 1: VFRS measurement locations of the research project and sensor locations of ALDIS/EUCLID on an elevation map

¹ European Cooperation of Lightning Detection (EUCLID)

1.2 Aim of the Work

As declared in the previous section, ground truth data from on-site VFRS measurements, conducted during 2015, 2017 and 2018, and the correlated data set of VFRS and LLS will be analyzed for the present thesis. First, investigated lightning parameters and second, investigated parameter for the LLS shall be described in detail in the present section.

The correlated data set of VFRS recordings and LLS data of CG lightning is categorized in lightning flashes with a negative, positive and bipolar polarity. For this analysis, only data of negative and positive lightning flashes will be analyzed regarding their main lightning parameters and their associated LLS quality parameters.

At first lightning parameters, the percentage of single stroke flashes and the multiplicity shall be analyzed. Single stroke flashes are CG flashes that consist of one stroke only (see section 2.1). Due to the analysis of ground truth lightning observation data from the alpine region (on-site VFRS measurements), every stroke can be assigned unambiguously to a flash. The percentage of single stroke flashes influences the multiplicity statistics, which describes the number of strokes per flash. The multiplicity is one of the main characteristics of lightning flashes and is, for example, relevant for the protection principles of transmission lines (Anderson and Eriksson, 1980 [2]). Mean multiplicity values for each year and in total shall be analyzed for VFRS and LLS data. Since our data set consists of a combination of LLS data and information derived from the VFRS data, a comparison of parameters, such as multiplicity and the percentage of single stroke flashes, for data of both systems, will be carried out additionally. The relation between thunderstorm types and its lightning characteristics will be analyzed as well. A classification of the thunderstorms shall be done in two alternative ways for each measurement day: a manual classification according to radar characteristics and a classification based on the strength of vertical wind shear. Results regarding the single stroke flash percentage and the mean multiplicity values shall be compared with former results for the Austrian region and international publications, conducted in various regions all over the world during the last decades.

Return stroke peak currents of the LLS data shall be analyzed for the investigated periods too. For this analysis LLS detected return stroke peak currents and their distributions for flashes, first (FI) strokes, subsequent (SU) strokes and all strokes will be carried out. All stroke categories shall be analyzed regarding their median, mean and 95 % return stroke peak current values. The return stroke peak currents for FI strokes versus SU strokes in multiple-stroke flashes will be investigated too. Because high speed video data allows to identify clearly which stroke belongs to which GSP, return stroke peak currents of FI and SU strokes within

the same GSP (multiple-strokes only) shall be analyzed in a second step. The probability of higher SU peak currents within a flash and for strokes terminating in the same GSP versus the FI stroke peak currents will be analyzed in particular. Dividing flashes, classically grouped by time and spatial parameters by the LLS, into strokes per GSP leads to a multiplicity per GSP. Both multiplicity distributions (per flash and per GSP) shall be analyzed versus return stroke peak currents.

To analyze performance criteria of the LLS, the location accuracy (LA) and the detection efficiency (DE) shall be analyzed for the entire CG flash data set. First, the LA will be analyzed for each year and in total. If a flash consists of at least two strokes following the same channel to ground, the LA of the LLS can be evaluated. For such strokes, it can be assumed that they have the same GSP and the LLS should estimate the same position for every stroke in the same channel. The VFRS video data shall again be used to categorize strokes striking the same GSP. Second, the DE of the LLS will be analyzed. For analyses of the DE of the LLS, the flash and the stroke DE will be analyzed separately. The DE is defined as percentage of detected strokes by the LLS to really occurred strokes (detected in the video record). All calculations will be carried out for flashes and strokes for the three individual years and for the merged data set. Since continuous technical improvements of the LLS over the last decades strongly influence the resulting LA and DE, only values in more recent publications shall be compared with the calculated LA and DE values of the present analysis.

Finally, to gain some knowledge about processes and impacts of lightning strikes to power generation and transmission systems, two particular and specific cases of lightning strikes to a wind turbine and lightning to a railway track will be analyzed. Out of these analyses, information derived from the merged data set of correlated VFRS and LLS data with additional data of system operators for each case can be examined. The analysis of each case shall show the entire process and information gathering out of the recorded data sets, the LLS parameter verification and its evaluation. Furthermore, the needed details for a correlation of VFRS and LLS data with data from system operators and the so gathered information shall be discussed.

1.3 Method

The method of investigation for the present thesis comprises two parts: the on-site measurements of ground truth CG lightning for the Austrian Alpine region, recorded with the VFERS at the different measurement locations and the correlation of the recorded VFERS data with LLS data. This correlated VFERS and LLS data set is analyzed regarding characteristic parameters of CG lightning in the investigated area and regarding performance parameters of the LLS.

The transportable VFERS allows observing thunderstorms at different locations. With this system on-site observations at selected places, where thunderstorms are predicted for a certain time, shall be carried out. As described in the preceding sections, electric field and video data of naturally occurring CG flashes were recorded in the observed area in 2015, 2017 and 2018. The VFERS system consists of two main components: a high speed camera, to capture the leader propagation and GSP of each stroke and an electric field measurement system, to record the transient electric field. The synchronization of both components to GPS time provided the proper conjunction and comparability of the data of each lightning discharge.

Collecting data with a portable VFERS has the advantage of recording lightning discharges over a large area and insights about lightning characteristics can so be gathered over the country. Such VFERS measurements cannot provide ground truth information about the return stroke peak current. Therefore, data of the LLS shall be used to complement the ground truth data for this investigation.

The measurements shall be conducted at different measurement locations to observe individual thunderstorms and their lightning characteristics over a large area. The investigations are backed by an active exchange about weather forecasts, and especially thunderstorm predictions, with the national meteorological and geophysical service "Zentralanstalt für Meteorologie und Geodynamik (ZAMG)". Highly accurate weather forecasts made planned observations at measurement sites distributed all over Austria possible.

For the correlation and analysis, the recorded VFERS measurement data will be first correlated with the ALDIS LLS data by using a time criterion for a specific analysis of each flash. The video and electric field data will then be analyzed and documented. For the electric field measurement system, a software tool called DataViewer and provided by ALDIS, is used. This software tool allows the correlation of LLS data with the analyzed electric field record by loading the data of events detected by the LLS for the given time period. Using the time information of the LLS, each video frame containing information about the CG process in the

video record, is analyzed. Video analyses are carried out with the Vision Research Phantom Camera Control (PCC) software.

The conducted correlation of VFRS video and electric field data with LLS data of all records is analyzed regarding characteristic parameters of CG flashes as well as LLS performance parameters. Additionally, the calculated values of the present analysis of the VFRS measurements and the correlated LLS data will be compared with values from former national and international studies. More information about the VFRS measurements and the individual analyses of CG lightning parameters for VFRS and LLS data can be found in chapter 3 and 5, respectively.

1.4 Field of Research

The following assumptions shall characterize the main field of research of the present thesis in detail:

- (1) Analysis of lightning phenomena in the Alpine region of Austria based on video and electric field recordings of cloud-to-ground lightning discharges
- (2) Correlation of VFRS and LLS data and analysis of characteristic parameters for cloud-to-ground flashes. Comparison with values from the literature and similar older investigations
- (3) Analysis of single stroke flashes and their occurrence regarding different thunderstorm types
- (4) Observation of processes and impacts of lightning discharges on power generation and transmission systems

2 Cloud-to-Ground Lightning

2.1 Lightning Discharge

The following section shall give an overview on the used terminology describing lightning discharges. The principles of lightning processes in general and for CG lightning in specific are described in addition. The process of these lightning strikes as well as their formation and characteristics will be explained as well.

A number of terms are used to describe naturally occurring lightning discharge processes. An overall discharge process itself is usually termed as a flash, regardless of whether it strikes ground or not. If a flash finds its path to ground or a ground based structure it can consist of a number of components, so-called strokes (Rakov and Uman, 2003 [3]). It can occur that the CG flash may end after the first stroke (i.e. single stroke flash) but most of the flashes in tempered regions consist of 3 to 5 strokes, which lower negative charge to ground. Global lightning activity shows a percentage of 75 % of discharges in clouds or between clouds. The remaining percentage involves ground or ground based structures (Rakov, 2014 [1]). The used terminology for the four different types of discharges are:

- intercloud discharges
- intracloud discharges
- cloud to air discharges and
- cloud-to-ground (CG) discharges.

All four types of lightning discharges are visualized in Figure 2. CG discharges are of main interest for the present thesis because of their impact on the ground. Intercloud and intracloud discharges are not analyzed in the present thesis (IC is used as abbreviation for both type of discharges). The CG flashes can again be discriminated in downward and upward lightning strikes. Downward lightning strikes start propagating from the cloud in direction to ground. Upward lightning strikes start their evolution from ground based objects, especially from high buildings or exposed mountain tops (Rakov and Uman, 2003 [3]). Both downward and upward lightning strikes can have an initial leader depositing either negative or positive charge along the leader channel. A downward-propagating leader with negative charge initiates around 90 % of global CG lightning flashes (Dwyer and Uman, 2014 [4]).

To generate the environment for lightning discharges, several pre-processes are needed. Lightning is linked to thunderclouds in general (Rakov, 2014 [1]). These thunderclouds have

to contain sufficiently large charge deposits, which create field strengths that exceeds the dielectric strength level of air for lightning to occur (Dwyer and Uman, 2014 [4]). For the generation of such a thundercloud, containing sufficient charge deposits, first warm air masses of sufficient humidity have to be available. Second, an updraft is necessary to transport the warm air masses at higher altitudes. The transport of humid air mass into high altitude levels initiates a cooling process of the matter. In this case, the humid air mass starts first to condensate and forms small fair-weather clouds (cumulus) with its start at the condensation level (cloud base). If the temperature decrease is high enough, this newly formed cloud and the contained water droplets will rise with the updraft. The cloud structure can change in this phase from cumulus to cumulonimbus (decrease of the temperature with increasing height has to be larger than moist-adiabatic lapse rate). The water droplets will change its stage of aggregation into graupel, small ice crystals or become super-cooled water (freezes immediately after contact with other droplets) arriving at the 0 °C isotherm. By getting to this state, the charge separation starts. If the separated charge deposits are large enough, IC or CG discharges can occur (Rakov and Uman, 2003 [3]).

Figure 2 shows possible charge structures of thunderclouds. The dipole-like structure with the main positive charge region in the upper portion and the more or less equal negative one found below the positive charge area should be seen as an idealized charge distribution (Dwyer and Uman, 2014 [4]).

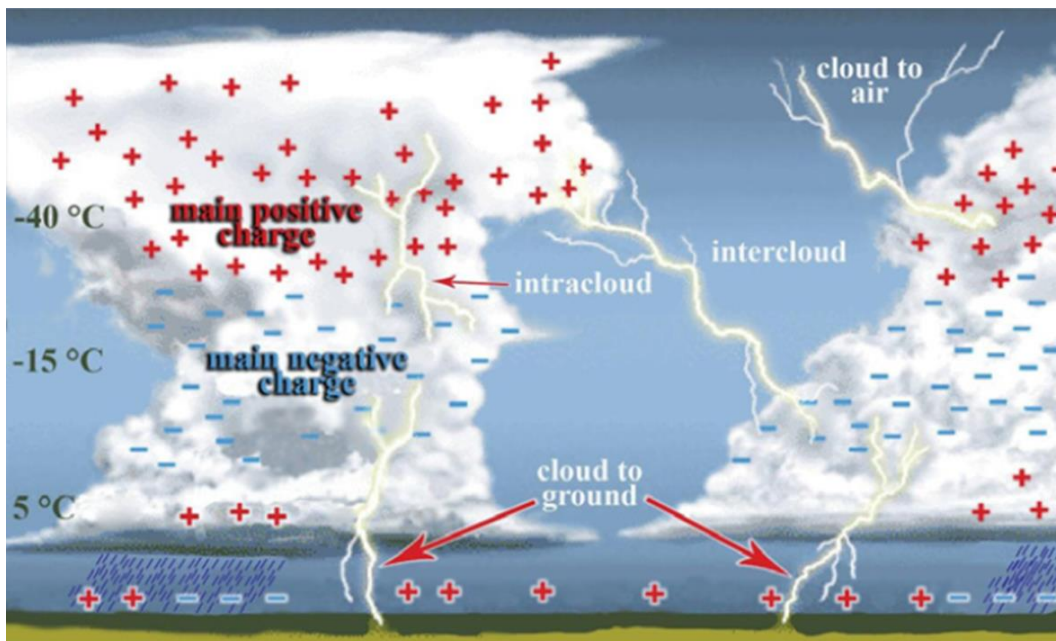


Figure 2: Charge structure of two thunderclouds and lightning types (Dwyer and Uman, 2014 [4])

The shown small positive charge at the bottom of the thundercloud in Figure 2 can lead to a tripole-charge structure, if its charge is increased (Cooray, 2014 [5]). However, the charge structure of a real thundercloud can be much more complex than shown in Figure 2 and vary from storm to storm. In addition, a change of the positions of the main positive and negative charged areas is possible (Dwyer and Uman, 2014 [4]).

From these charged areas an initial or preliminary breakdown can initiate a lightning process. Further, the processes of a negative CG flash shall be described in more detail. After the preliminary breakdown, one or several faint leader branches start to grow stepwise towards ground. This stepping phenomenon is called stepped leader. Cooray, 2014 [5] described the optically determined properties of this steps in direction towards ground with a length of 10 to 100 m. Saba et al., 2006 [6] showed an average stepped leader speed of 3×10^5 m/s for recent measurements using high speed video cameras. If a negative charged leader comes close to ground a positively charged upward connecting leader starts, particularly from high, exposed, sharp-edged and good electrically conducting objects, to grow from the ground until both, the positive upward and the negative downward leader, connect. After this contact, the return stroke occurs with a velocity of the return stroke front of about a third of the speed of light, moving from ground to the cloud and discharging the deposited electric charge along the leader channel. If a flash ends after this completed discharge process it would be called a single stroke flash (see description above). If not, one or more subsequent strokes can occur in the ionized lightning channel of the first stroke, within an average time interval of 40 to 50 ms between each stroke (Dwyer and Uman, 2014 [4]). During the time interval between the first stroke and the subsequent stroke so-called K- and J-processes can occur. Both processes can be viewed as transients in the cloud (Rakov and Uman, 2003 [3]). To initiate a subsequent return stroke, a so-called dart leader propagates from cloud to ground and deposits again charge along the remaining channel of the first return stroke. After that the second return stroke occurs similar to the return stroke process of the first stroke. If a subsequent stroke uses the existing channel, ionized by the first return stroke, a so-called dart leader initiates the subsequent return stroke sequence. If the ionized channel is interrupted or disturbed (e.g. due to heavy wind), it can occur that one of the subsequent strokes has to restart the stepping-process and create a new channel. Such a phenomenon is called dart-stepped-leader. The new path to ground formed by the dart-stepped leader of a subsequent stroke leads to the fact that about one-third to one-half of the CG lightning contact the ground in more than one point, so called ground strike points (GSPs) (Dwyer and Uman, 2014 [4]). Figure 3 shows the above-described processes and a time wise resolution of milliseconds for this negative CG flash comprising two strokes. The processes of main interest for the present thesis are highlighted.

The electromagnetic frequency spectra of the described processes ranges from a few hertz for long continuing currents (long lasting return stroke current in the channel with slow charge transfer) to 10^{20} Hz for radiated x-rays. The knowledge about the frequency range of CG and IC strokes is important for studying their properties (Rakov, 2008 [7]). The frequency range of radiated fields affects the design of an LLS sensor too. The return stroke process of CG strokes shows the most powerful electromagnetic radiation in the very low frequency (VLF) and low frequency (LF) section. The vertically-polarized transient electromagnetic field pulses of CG flashes, which propagate along the surface or bouncing between earth surface and ionosphere can be used to quantify and analyze their properties (Diendorfer et al., 2010 [8]). For that reason the sensors used for medium range, ground based LLS (distances between sensors of 150 to 400 km) are designed to detect electromagnetic signals in this frequency spectra (Nag et al., 2015 [9]). Additional information about the LLS and its sensor technology can be found in section 3.2.

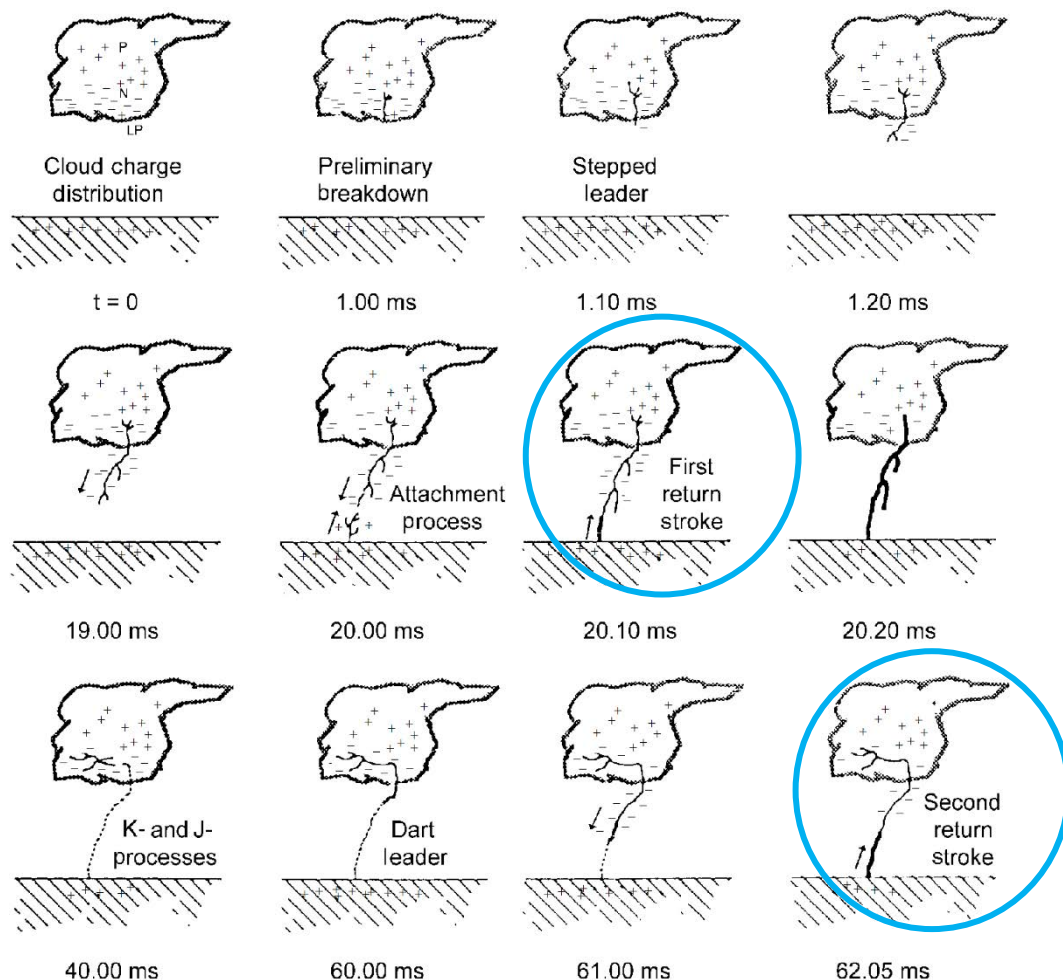


Figure 3: Process of CG flash comprising two strokes; processes of main interest for the present thesis are highlighted; adapted from (Rakov and Uman, 2003 [3])

2.2 Lightning in the Alpine Region of Austria

In this section lightning activity in the Alpine region of Austria shall be described. Monthly and regional variations can both be observed from LLS data for the investigated country. Annual variations of lightning characteristics detected by the LLS underline the need of observations over periods of several years. For that reason, on-site observations with the VFERS have been carried out in 2015, 2017 and 2018, to get a spread data set with sufficient data for an analysis of characteristic lightning parameters (see section 5.1). Anderson et al., 1979 [10] actually recommended that the average annual flash density should be calculated from a measurement period of a minimum of eleven continuous years, because of the annual occurrence variations. Variations for the LLS performance parameters (e.g. location accuracy, detection efficiency) can be identified as well, if ground-truth observations are carried out over longer periods.

Lightning activity in Austria shows a high density, especially in the southeastern part of the country. Figure 4 shows the ground flash density for ALDIS/EUCLID LLS data from 2010 to 2018 separated per political district (deep grey coloured area shows district with the highest flash density).

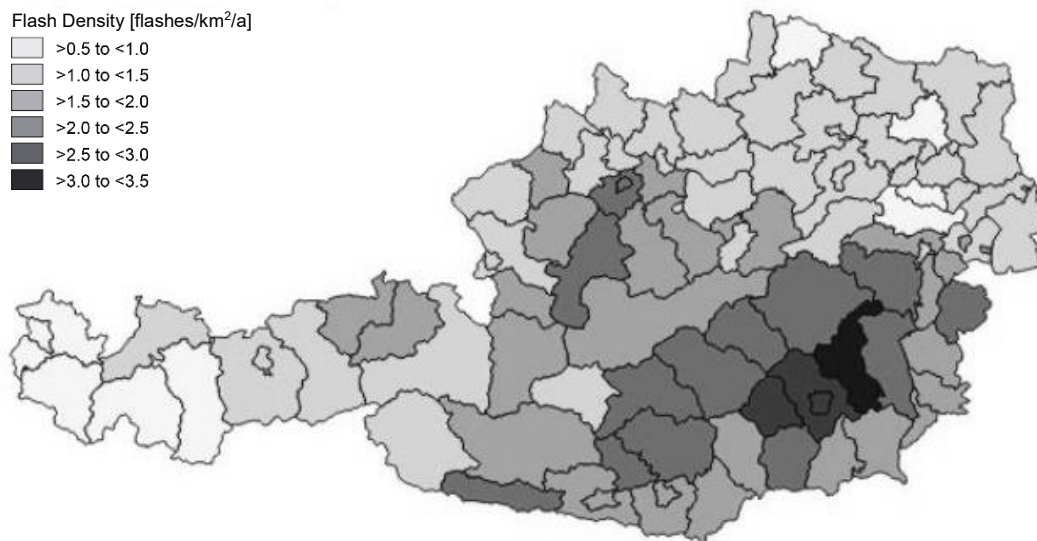


Figure 4: Flash density map for political districts of Austria calculated from ALDIS/EUCLID data of 2010 to 2018 for flashes per square km per year; deep grey coloured areas show the districts with highest flash density²

² Adapted from <https://www.aldis.at/blitzstatistik/blitzdichte/bezirke-karte> (downloaded on August 20th 2019)

Poelman et al., 2016 [11] showed a graphical distributions of annual and monthly lightning flash densities for Europe detected by the EUCLID system for data from 2006 to 2014. They found the highest flash densities at the cross-border section between Austria, Slovenia and Italy (7 flashes/km²/a; location south-east). Results shown in Figure 4 for ALDIS/EUCLID LLS data go along with the findings by Poelman et al., 2016 [11] and show again a higher flash density in the southeastern region of the country. The district with the highest flash density in Figure 4 is Weiz, with a ground flash density of 3.02 flashes per square km and year. The lowest flash density was detected in the most western region of Feldkirch (0.73 flashes/km²/a).

The analysis of EUCLID LLS data by Poelman et al., 2016 [11] of the mean monthly distribution of all detected flashes shows the highest number of flashes within the months of May to September (EUCLID LLS data of 2006 to 2014). They stated that nearly 85 % of all detected flashes occurred during this period (Poelman et al., 2016 [11]). Schulz et al., 2005 [12] showed the same analysis for the mean monthly distribution and its standard deviation of all detected flashes for ALDIS LLS data from 1992 to 2001 for Austria (see Figure 5). The findings by Schulz et al., 2005 [12] can be seen as confirmation for the highest lightning activity between May and September for the country too, with a strong decrease of the number of flashes in September. The observation period for the measurements of ground truth data with VFRS carried out in this thesis was therefore set from May to August for all three years of observation.

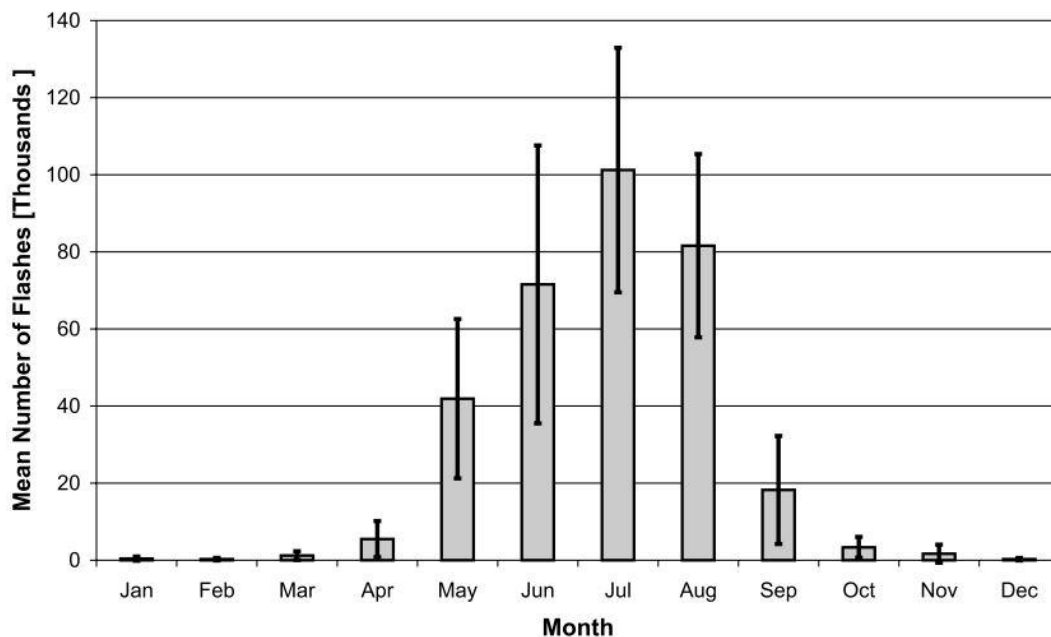


Figure 5: Mean monthly number of flashes with bars representing a ±1 standard deviation based on ALDIS data from 1992 to 2001 for Austria shown by Schulz et al., 2005 [12]

Unlike for monthly and annual variations, there is no specific indication regarding regional variations of lightning parameters in the literature. Rakov et al. (CIGRE TB 549, 2013 [13]) stated that a possible dependence of lightning parameters on geographical location has been pointed out for several years (e.g. Anderson and Eriksson, 1980 [2]), but no conclusive evidence has been reported until now. Their investigation had its focus on negative CG flashes and compared lightning parameters on geographical dependency but no general evidence has been found, even if there may be some variations regarding current intensity for first and subsequent return stroke peak currents. However, they explicitly noted that the observed differences in the current measurements could be linked neither directly to geographical location nor to seasonal variations. Two main reasons have been addressed why no explicit statement about the geographical dependency can be made. First, obtaining statistically significant data samples has its difficulties. Second, different instrumentation and data analysis methodologies are used at various locations for their observations. With the information available, the hypothesis regarding the dependence of negative CG flashes on geographical location cannot be confirmed and was refused at that time (CIGRE TB 549, 2013 [13]). These findings underline the need for high quality, ground truth data sets recorded over a long time by VFRS for example.

3 Measurement Systems, Setup and Tools

3.1 Video and Field Recording System

The Video and Field Recording System (VFRS) was used to record ground truth data of lightning discharges in Austria. With such a system a targeted deployment for on-site observations at selected places, where thunderstorms are particularly likely on a given day, is possible. The transportable system allows observation of thunderstorms at variable locations, contrary to measurements at instrumented towers or rocket-triggered lightning. For naturally occurring CG flashes, electric field and video data have been recorded in the given area (see Figure 1). The system consists of two main components: a high speed video camera and an electric field measurement system. Technical specifications and selected settings of the VFRS are listed in appendix 15A. The synchronization of both components to GPS time provides the proper conjunction and comparability of the data of each lightning discharge.

To record real occurring lightning discharges in the region of interest, the VFRS was set up ahead of the initiation of the predicted thunderstorm activity. Even if the camera and field recording system were operated in parallel, both systems were build up independently; just the manual trigger box contained the connectors for both systems.

The used camera was a Vision Research Phantom v9.1 (see Figure 6). This type of camera has a monochrome sensor with an image bit depth of 14 bit and can record up to 153.846 frames per second (fps). A Nikon wide-angle lens (type AF-S NIKKOR 24 mm, 1:1.4G ED) was mounted during the observations. A red filter was mounted on the lens during daytime observations to achieve a higher contrast for the video records. The camera model had an available internal memory of 6 GB and a maximum resolution of 1632 x 1200 pixels. As a setup for the records of lightning discharges, the following parameters have been chosen:

- Resolution 1344 x 400 pixels
- Framerate 2000 fps
- Image depth 14 bit
- Record length 1.6 s

These general settings seemed most appropriate for our purposes (see Vergeiner et al., 2016 [14]). A framerate of 2000 fps results in a maximum exposure time of 500 μ s. This frame rate allows to clearly follow the discharge process from cloud towards ground. As the frame rate influences the maximum resolution and the length of each video a compromise of all three

settings had to be found. An important issue for such observations is the fact that a natural process should be banned on camera. A wide picture was chosen for that reason, even if the observed height had then to be reduced. Due to the necessity of a minimum distance of several kilometers from the lightning events during the measurements (security issues etc.) it showed that the 400 pixels in vertical direction is enough to get an image from the cloud base to the ground. The setting of framerate and resolution led to a maximum video length of 3.2 s. The camera memory was split to save two video records of 1.6 s each. That means that two videos can be saved on the internal memory of the camera before they have to be transferred to the control-device (Laptop) via local Ethernet. The camera software allows setting a pre-trigger. The pre-trigger was set to one third to one half of the time duration of the total video length. To use this function, the camera has to continuously save images to the buffer (ring buffer operated with “first in, first out” principle) and store the frames from the point of the pre-setup time on (pre-trigger) in case of a trigger impulse. Each VFRS record was manually triggered, after a flash occurred within the camera’s field of view. To get an appropriate time synchronization to GPS time, an external GPS module was connected to the camera system via coaxial cable (IRIG-B standard).

To record the transient electric field of lightning discharges, a flat plate antenna was used. The overall electric field measurement system is composed of the flat plate antenna (see Figure 6 and Figure 7), an integrator circuit and an amplifier, a fiber optic link, a digitizer and a PXI system as processing unit. This PXI system includes a Windows based computer system and two additional hardware modules, a GPS time receiver (National Instruments NI PXI-6683H GPS) and a digitizer module (ADLINK PXI-9816H/512 AD digitizer card, 4 channels).



Figure 6: High speed video camera (left) and flat plate antenna (right)

The antenna consists of a rectangular aluminum housing, which was placed on ground for the necessary connection to ground potential. The actual sensor is an insulated aluminum

plate in the center of the antenna system. Mair, 2000 [15] calculated a needed plate size of 25 cm diameter to record distant electric fields of lightning discharges. The plate is surrounded by a small air gap between sensor plate and the aluminum housing, to avoid an enhancement of the electric field, and has a distance to ground of 5 cm. By building the sensor plate much smaller than the wavelength of the emitted electric field of lightning discharges, the antenna will operate as a capacitive voltage source. The variation of the background electric field in time results in a variation of induced charges on the antenna, generating a measurable current in the circuit (Cooray, 2014 [5]). The integrator circuit then processes this current so that a variable voltage signal (± 15 V) can be transmitted via fiber optic link to the digitizer of the PXI system.

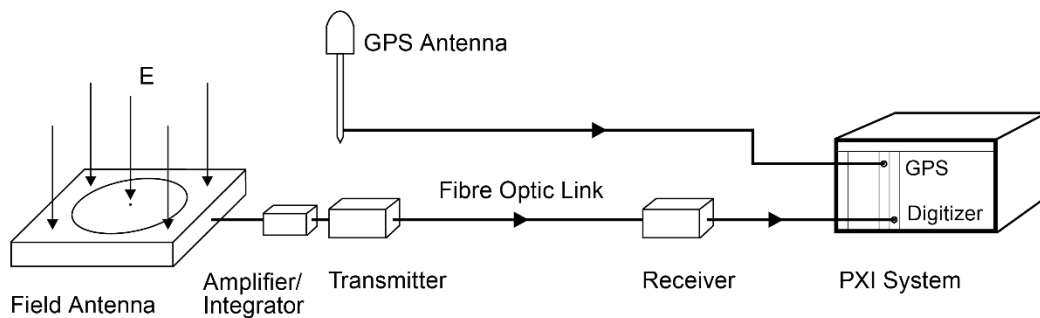


Figure 7: Components of the electric field measurement system

The overall system was first developed, calibrated³ and tested by ALDIS. During this project the system had a bandwidth of 3000 Hz to ~ 1.0 MHz (see appendix 15A). The bandwidth of the integrator and amplifier limits the overall bandwidth of the system. The analog/digital sampling rate of the used digitizer is 10 MS/s for all four channels. The vertical resolution of the digitizer is 16 bits. For the electric field measurement, just one of the channels is used. In the case of a trigger impulse, five seconds (the actual second, two seconds before and two after the trigger impulse) are recorded, in order to not miss any stroke. The recording software was developed by H. Pichler (ALDIS) and is LabVIEW based. This software also synchronizes the measurements to GPS time.

After recording the lightning discharges, all VFRS measurement data are first correlated with the ALDIS LLS data by using time criteria (both systems are synchronized to GPS time). These leads to an accurate temporal correlation within micro seconds. The video and electric

³ The calibration of the electric field system was conducted at the beginning of the measurements by ALDIS. No changes on the system side were made over the entire measurement period.

field data are then analyzed and documented. For the electric field measurement system, the software tool “Data Viewer”, developed by C. Diendorfer and adapted by H. Pichler (ALDIS) was in use. This program allows to correlate LLS data directly with the analyzed electric field record by loading the data of LLS detected events for the given time period (5 s of recording time) and the geographical area (100 km radius around the measurement location).

With the precise time information of the LLS, the video frame in the video record can then be analyzed. The electric field measurement record was used to examine the polarity of each stroke. Absolute electric field values of the electric field measurement system have not been used for the analyses in the present thesis. Video analyses have been carried out with the Vision Research Phantom Camera Control software. Appendix 0 shows the analysis of the electric field and video record by using the software analysis tools for a lightning strike to a railway overhead line, recorded in 2018 (VFRS electric field signal in green, vertical blue line shows LLS time stamp for the analyzed stroke). This specific case will be analyzed in subsection 6.7.2 in more detail. All analyses of recorded flashes have been carried out on spreadsheets for each year.

The correlation of VFRS video and electric field data with LLS data of all records allows to determine the percentage of single stroke flashes, flash multiplicity and return stroke peak currents distribution of CG flashes, LLS location accuracy and LLS detection efficiency. The results of these analyses will be shown in chapter 6.

3.2 Lightning Location System

The sensors of the Austrian Lightning Detection and Information System ALDIS were first installed in fall 1991. The system consisted and still consists of eight sensors based on Vaisala Inc. technology and started its full operation in 1992. The nationwide installation of this Lightning Location System (LLS) gave the possibility to monitor the lightning activity in Austria for the first time (Diendorfer, 2016 [16]). From the early years on, validation and performance of the system had been in focus too (direct current measurements at the Gaisberg Tower; see for example Diendorfer et al., 2010 [17], Diendorfer et al., 2011 [18] as well as VFRS observations). In 2001 ALDIS became one of the processing centers of the European Cooperation for Lightning Detection (EUCLID) and is therefore processing the data of currently 166 sensors distributed all over Europe (Poelman et al., 2016 [11], Schulz et al., 2016 [19]).

From the early stages of single-station lightning location systems (e.g. Pierce, 1956 [20]) to correlated electric and magnetic fields from return strokes (e.g. Uman et al., 1975 [21]) to nowadays used lightning location sensor systems, a significant technology improvement was made. ALDIS started in 1994 to use the IMPACT sensor type (Vaisala Inc.) that combined the magnetic direction finding (MDF) technology and benefits of the time of arrival (TOA) technology. The ALDIS and EUCLID sensor system can be classified as mid-range system with a maximum distance of 400 km between two sensors (Nag et al., 2015 [9]). The used sensors have been designed to detect lightning electromagnetic radiation in the VLF and LF range (see section 2.1).

Strike points of the strokes can be calculated by using the information of the arrival time or the direction to the stroke in general. For the MDF the electromagnetic field information, radiated by the upward propagating return stroke and measured by the sensors crossed loop antennas, is used (Cummins and Murphy, 2009 [22]). The strike point location calculation is based on time stamps derived from the measured electromagnetic fields. Those time stamps are related to field onsets, which are related to processes in the lightning channel from the GSP up to an altitude of a few hundred meters. The TOA method is based on the principle of arrival times of the travelling wave. The radiated field caused by a lightning strike propagates in every direction with the speed of light. Due to the use of precise GPS time synchronization, accurate time stamps for all sensors are given. Moreover at least three sensors have to report a stroke to calculate a strike point (Diendorfer, 2007 [23], Cummins and Murphy, 2009 [22]). It should be kept in mind that under particular geographic conditions, calculations of detections with the TOA method by using three sensors only can lead to ambiguous locations. The use of the combined data set of MDF and TOA would offer the opportunity to calculate stroke locations with the data of only two sensors only because of redundant information about latitude, longitude and discharge time. (Diendorfer, 2007 [23]).

After replacing the IMPACT sensors in 2005 and 2006, ALDIS upgraded all of their eight sensors to the LS7000 and finally to the LS7002 in 2015 (all from Vaisala Inc.). IMPACT sensors and also LS700x sensors provide both, TOA and MDF, and combine the two calculation methods.

Several updates of the software, at the sensor side as well as for the main processing unit have been carried out too. The update to a new location algorithm in 2008, the sensor based onset time calculation in 2011, and the propagation correction as well as proper consideration of the index of refraction in 2012 are the major changes until the upgrade to the LS7002 in 2015. A propagation correction was introduced to take the landscape structure in Austria into account. A significant part of the Austrian region is located in the pre-alpine and alpine area

(see Figure 1). The need of the ground based waves of lightning discharges to travel along ground surface leads to longer way paths up and down the mountainsides. The heights of these structures cause a time delay. Thus, a time correction model was implemented where the areas and mountains surrounding each sensor were taken into account. Schulz, 2015 [24] shows the improvement of this update by comparing LA at the Gaisberg Tower location (direct strikes) before and after the implementation of the time correction model.

For the LS7002 sensor system an improvement of IC/CG lightning detection was determined (see Buck et al., 2014 [25]). They pointed out additional improvements among the sensors and the central processing unit with effects on DE and LA. Regarding DE higher sensitivity of the sensor to low amplitudes, additional provided waveform parameter for each stroke and digital filtering, to reach a better signal-to-noise ratio, should help to increase this factor. It is stated, that an accuracy of 80 to 90 % of correct classification of IC and CG can be achieved using additional waveform parameters for the classification (see Buck et al., 2014 [25]). LA should be improved by the use of waveform onset corrections (i.e. the determination of the arrival time of the electromagnetic waveform) which reduces the timing error and therefore increases the accuracy of the geolocation (Honma et al., 2013 [26]). Additional improvements regarding propagation across uneven terrain, varying ground conductivity, and improved handling of electromagnetic wave propagation in the central processing unit should lead to a further improvement of the LA (Buck et al., 2014 [25]).

The ongoing comparison of strokes detected by the ALDIS LLS with ground truth data, as recorded by VFRS or at the instrumented Gaisberg Tower, helps to determine the performance of the system regarding LA, DE and stroke peak current detection in general and especially after the above-described adaptations in the system.

The return stroke peak currents of the LLS data are calculated from electromagnetic fields by using a field-to-current conversion factor (Uman et al., 1975 [27]). The used conversion factor is based on the relation of the return stroke peak current I_p to the far-field peak E_p and the return stroke speed. Equation (1) shows this relation. This equation is valid for a constant return stroke velocity, a perfectly conducting ground and if the return-stroke front has not reached the top of the channel (see Diendorfer et al., 2007 [23]):

$$I_p = \frac{2\pi * \epsilon_0 * c^2 * D}{v} * E_p \quad (1)$$

The abbreviation v indicates the return stroke velocity in m/s, c is the speed of light ($2.99*10^8$ m/s) and D the distance from the sensor to the lightning channel. For this linear relationship between the measured far-field peak E_p and the return stroke peak current I_p , a velocity of

$v = 1 \cdot 10^8$ m/s and a distance of $D = 100$ km can be chosen. These assumptions lead to the following equation (2):

$$I_p [kA] = 5 * E_p [V/m] \quad (2)$$

The manufacturer Vaisala Inc. scale their output signals in LLP units. They are directly proportional to the electric field peak E_p in V/m. The following relation can be used for conversion:

$$E_p = 52 \frac{V}{m} \triangleq 1158 \text{ LLP units} \quad (3)$$

The combination of equation (2) and (3) leads to the direct conversion equation (4) of the peak current in kA to the range normalized signal strength (RNSS, normalized to 100 km using an e-folding length to take into account attenuation (CIGRE TB 376, 2009 [28]) in LLP units:

$$I_p [kA] \cong 0.185 * RNSS [\text{LLP units}] \quad (4)$$

The variability of key parameters, as the return stroke velocity, makes a highly accurate field to current conversion for individual strokes difficult. However, it has been shown that a statistical estimation is possible (see Rachidi et al., 2004 [29]). In general, it should be kept in mind that the used current conversion factor is only validated for negative subsequent strokes, with a return stroke peak current lower than -60 kA (Diendorfer et al., 2007 [28]). Return stroke peak currents of negative SU strokes, estimated by LLS have been compared with direct current measurements at the Gaisberg Tower (see Schulz et al., 2016 [19]) for EUCLID LLS data and (Mallick et al., 2014 [30]) for triggered lightning detected by the US NLDN. A median peak current error of -5 % was detected for NLDN data correlated with rocket triggered lightning data and +4 % for EUCLID LLS data compared to direct current measurements at the Gaisberg Tower. A validation of peak current estimates for negative first return strokes and positive return strokes is still needed (CIGRE TB 376, 2009 [28]).

The used grouping algorithm of CG strokes into flashes is described in Diendorfer et al., 2007 [23]. The two main criteria for a grouping are time and spatial criteria. First, a stroke is grouped to a flash if it occurs within a second after the first stroke and within an interstroke interval of less than 500 ms. As a second criteria the stroke location has to be within a radius of 10 km around the first stroke (see Diendorfer et al., 2007 [23], Cummins et al., 1998 [31]). The NLDN LLS allows a maximum of 15 strokes being grouped to one flash. If more strokes occur which fulfill the above-described grouping criteria, the strokes will be split up into two flashes (Buck et al., 2014 [25]). For ALDIS/EUCLID no maxima of strokes per flash is or was set.

Using the standard deviation of angle and time measurements as well as the number and relative position of sensors, which are used for the calculation of a stroke location, the location algorithm of the LLS calculates the length of the semi-major axis, eccentricity and orientation of the 50 % confidence ellipse for each stroke. This 50 % confidence ellipse surrounds the calculated strike point, and shows the area where the probability is 50 % that the stroke occurred within this ellipse (Diendorfer et al., 2014 [32]).

Due the above described continuous adaptations and improvements of the system the median LA decreased to values around 100 m (Diendorfer, 2016 [16]). Selected analyses of performance parameters as LA, DE, multiplicity and accuracy of the peak current of the system are shown in Schwalt et al., 2018 [33], Poelman et al., 2016 [11], Diendorfer et al., 1998 [34], Schulz and Diendorfer, 2006 [35], Schulz et al., 2016 [19].

3.3 On-Site Setup of the VFRS

For on-site measurements, three parameters are of special interest in general and specifically for mountainous regions:

- high visibility (up to 50 km),
- low electric field interferences, and
- road access.

Good visibility is necessary for visual observations such as high speed video records. For the selected measurement locations, a free view to all directions is the best case scenario. That was mostly the case on flat terrain. To find such conditions on mountainous terrain is a hard task, because public road access to mountaintops is rare. Electric interferences are again a larger problem for measurement locations on flat terrain and the pre-alpine area because of transmission and distribution lines. Before selecting new measurement locations, analyses of the surrounding of the locations via satellite images have been carried out (see Vergeiner et al., 2016 [14]).

To successfully record VFRS data on the preselected measurement locations weather forecasts have to be as accurate as possible. An active communication about the actual weather forecast and especially the thunderstorm prediction with the national meteorological and geophysical service “Zentralanstalt für Meteorologie und Geodynamik (ZAMG)” was carried out for that reason and was very important for these investigations. A planned observation with measurement sites distributed all over Austria needs an accurate scheduling

of the day of measurement and an update of changes of forecast and information about actual meteorological data over the day.

In order to operate the system at variable measurement locations a mobile power generator was used as an external power supply. The main components of the recording systems (camera and its GPS system, PXI system) have been operated via uninterruptible power supply to protect the system from long-lasting interrupts during operation. This was primarily necessary to keep the GPS time synchronization continuous and to finish the record of the actual measurements during an interruption of the power supply.

Figure 8 shows a compact view of the measurement equipment. During real measurements, the full length of 20 m of the fibre optic link was used to avoid any interferences of the power generator and the equipment as good as possible. For that reason, also the power generator was positioned more than 15 m away from the measurement vehicle during real operation.

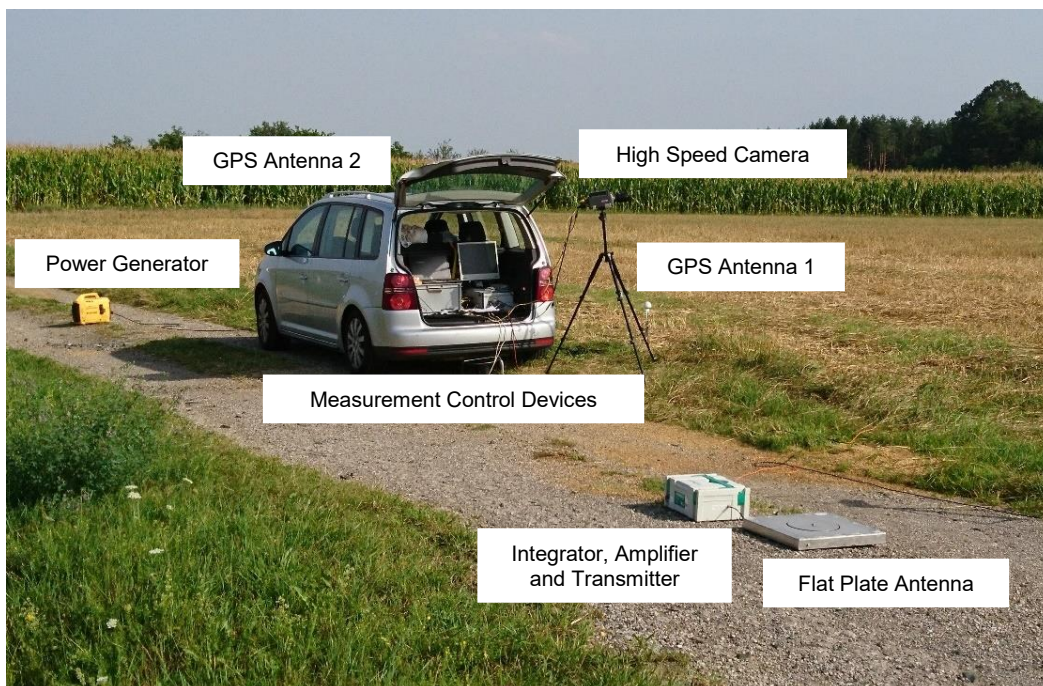


Figure 8: General measurement setup and components (GPS antenna 1 for E-field system, GPS antenna 2 for camera system)

4 Data

4.1 General Information

The measurements for this research project were performed during warm season thunderstorms in 2015, 2017 and 2018. As shown in section 2.2 this season starts in May and lasts until August. This period represents the main thunderstorm season for the investigated area (see again section 2.2 and Poelman et al., 2014 [36], Schulz et al. [12]). During the years of 2015, 2017 and 2018 measurements have been conducted in total at 21 selected measurement spots. Figure 9 shows the VFRS measurement sites and the recorded data for negative, positive and bipolar CG flashes for 2015, 2017 and 2018. Overall, 531 CG flashes including 1639 CG strokes were recorded during 51 different thunderstorm days during the three years and have been analyzed. The recorded data can be divided in CG flashes with negative (87.2 %), positive (11.1 %) and bipolar (1.7 %) polarity. The main analyses in this thesis will be focused on negative CG flashes and strokes (see section 6.1 to 6.5). Additionally, also some analyses of positive flashes and strokes are given (see section 6.6). For analyses regarding negative single stroke flashes by thunderstorm type additional data of VFRS measurements campaigns in 2009, 2010 and 2012 have been included (see subsection 6.1.3).

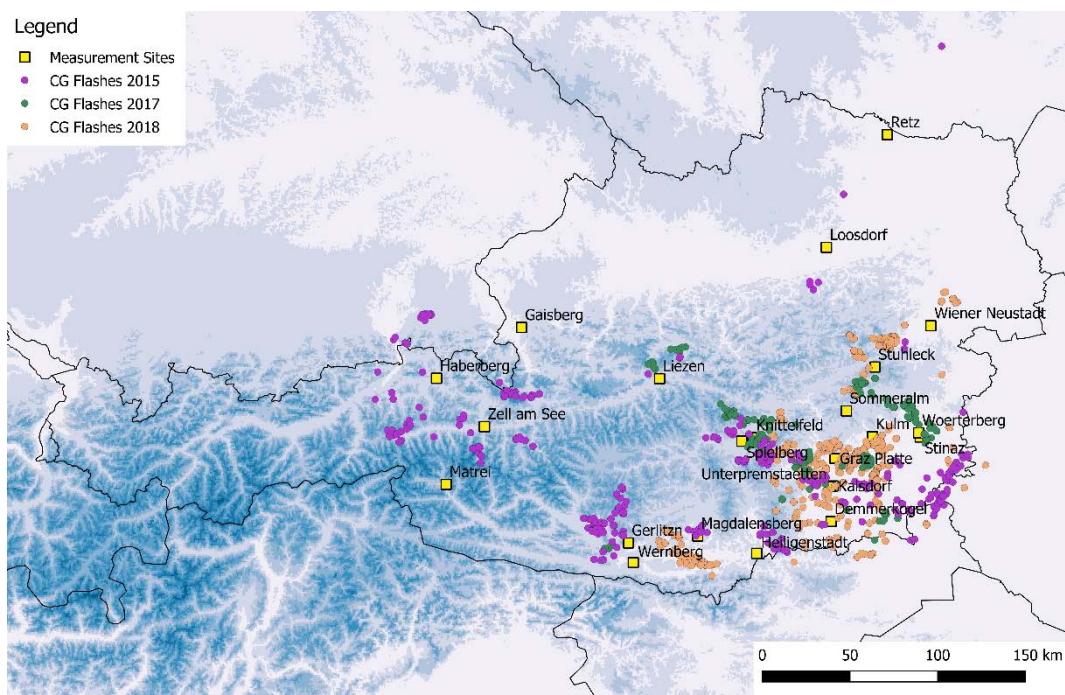


Figure 9: VFRS measurement sites and recorded data for negative, positive and bipolar CG flashes for 2015, 2017 and 2018; elevation map in the background

Every VFRS data set was analyzed manually to determine the sequence of each stroke from cloud to ground (e.g. same or different GSP, channel characteristics) and to analyze the characteristic parameters for each stroke. The individual ground truth data set are only taken into account for this analysis, if the stroke channel and its GSP was visible in the video and the electric field measurement was without any significant interference of other, simultaneously ongoing lightning events (IC same as CG events).

The next section shows the recorded data for negative, positive and bipolar flashes and strokes, LLS and additional meteorological data as well as information of railway system and wind farm operator in detail.

4.2 Data of Cloud-to-Ground Flashes

This section shows all recorded VFRS data for all polarities, which were correlated with LLS records. In total 463 negative CG flashes and 1527 negative CG strokes were recorded in Austria during 51 days. Table 1 shows the analyzed thunderstorms, the number of negative CG flashes and strokes for all three years and in total.

Table 1: Analyzed thunderstorms, total flashes and strokes for each year and in total for negative CG flashes in the VFRS data

Year	Thunderstorms	Total Flashes	Total Strokes
2015	24	153	514
2017	13	94	317
2018	14	216	696
Total	51	463	1527

59 flashes with 71 CG strokes of positive polarity were recorded during 20 days spread over the three years. Table 2 shows the analyzed thunderstorms, the number of positive CG flashes and strokes for all three years and in total.

Table 2: Analyzed thunderstorms, total flashes and strokes for each year and in total for positive CG flashes in the VFRS data

Year	Thunderstorms	Total Flashes	Total Strokes
2015	9	28	34
2017	4	4	4
2018	7	27	33
Total	20	59	71

Regarding bipolar CG flashes (a flash including at least one stroke with a different polarity as the other ones) 9 flashes including 41 CG strokes were recorded on 9 days spread over the three years. Table 3 shows the thunderstorms, the number of bipolar CG flashes and strokes for all three years and in total. In 2017, no bipolar CG flashes have been recorded. The data set for bipolar flashes includes type 3 flashes only (return strokes with opposite polarity; see Rakov, 2005 [37]). The data set of bipolar CG flashes was not analyzed for the present thesis.

Table 3: Thunderstorms, total flashes and strokes for each year and in total for bipolar CG flashes in the VFRS data

Year	Thunderstorms	Total Flashes	Total Strokes
2015	6	6	24
2017	-	-	-
2018	3	3	17
Total	9	9	41

4.3 Lightning Location System (LLS) Data

The data shown in section 4.2 have been correlated with ALDIS LLS data, first to get additional information for our analysis (e.g. stroke locations, stroke peak current) and second to analyze the LLS performance regarding DE and LA. For all the following investigations, LLS data sets have only been taken into account, if each and every assignment of the LLS (e.g. polarity, categorization as CG stroke) was confirmed with the VFRS data as correct. Only for DE analyses, data of misclassified strokes have been used additionally. Information about the

lightning location (latitude, longitude), stroke peak currents, IC/CG classifications and the 50 % confidence ellipse of the LLS data has been used for analyses of all recorded cases.

In section 3.2 the used flash grouping algorithm (CIGRE TB 376, 2009 [28]) and the calculation methods of LLS peak currents (via field-to-current conversion factor, see Uman et al., 1975 [27]) are described. It shall be pointed out again that the variability of the return stroke speed makes a highly accurate field to current conversion for individual strokes difficult. However, it has been shown that a statistical estimation is possible (see Rachidi et al., 2004 [29]).

4.4 Additional Meteorological Data

To analyze the given VFRS data regarding different thunderstorm types, radar data of the Austrian radar network, operated by the Aeronautical Meteorological Service (Austrocontrol GmbH) was used. To get an overall radar picture of Austria, data of five different radar stations are merged into a composite data set, which provides a three-dimensional picture of precipitation intensity at a spatial resolution of one kilometer and a temporal resolution of five minutes. As a second additional data source, the wind vector at an altitude of 6 km is taken into account. Data of the latest and closest available radiosonde; either Vienna, Udine or Munich at 12 UTC have been used to characterize the wind vector at 6 km height. The surface wind vector is extracted from the nearest meteorological station of the Austrian national meteorological system operator ZAMG, whose data are available at ten-minute intervals. In order to minimize random noise, an average value of the wind measurements over the last hour before the onset of the investigated thunderstorm was calculated.

4.5 Additional Information of Wind Farm and Railway Operator

During the measurement season of 2018 two very specific cases of direct lightning strikes on power generation and transmission systems have been recorded and shall be analyzed in section 6.6. The first case shows a lightning strike to two wind turbines, situated on a pre-alpine mountain ridge. For this case, data of the VFRS, the LLS and the network fault protocol of the wind farm operator were correlated and analyzed. The second case shows a strike to a railway overhead transmission line. Again, VFRS and LLS data were analyzed. The digital fault recorder data and the network fault protocol of this event were provided by the Austrian railway operator “Österreichische Bundesbahnen” in addition and have been correlated and analyzed.

5 Methodology

5.1 Research Parameters

In the following sections, characteristic parameters of data of the negative CG lightning discharges recorded over the three measurement periods will be analyzed. A comparison of particular values obtained in this study and previously published ones will also be carried out. An analysis of the single stroke flash distribution regarding thunderstorm type was carried out for the data set of negative CG flashes. The same data set was analyzed regarding their mean multiplicity for each year and in total and their flash multiplicity distribution. LLS detected return stroke peak currents and their distributions for flashes, first strokes, subsequent strokes and all strokes shall be carried out for the data set of negative CG flashes. To analyze the quality criteria for the LLS the location accuracy (LA) and the detection efficiency (DE) has been calculated again for the negative CG flash data set.

The present data set of positive flashes has been analyzed regarding single stroke flash percentage, flash multiplicity, LLS return stroke peak current and DE. The data set of bipolar CG flash data shall not be analyzed within this thesis.

Interstroke intervals as well as continuing currents are two additional parameters, which were not analyzed in this thesis for any type of discharge.

5.2 VFRS and LLS Data Analysis

5.2.1 Correlation

To correlate the VFRS data with the corresponding LLS data, the GPS time stamp in universal time (UTC) provided by the measurement systems have been used. The nanosecond time resolution of this time stamp allows a correct time correlation for all strokes within microseconds.

Each VFRS measurement data set is first correlated with the ALDIS LLS data by using the GPS time stamp. For this step, the DataViewer software (see section 3.1) was used. A typical data output of such a correlation is shown in appendix 0 (see Figure 36 to Figure 38; electric field signal of the VFRS in green, vertical blue line shows LLS time stamp for the analyzed

stroke). The video and electric field data for each individual stroke are then analyzed and documented. During this step, also the LLS data entries for the specific time and location are analyzed and verified. The whole data were separated in detected and completely correctly detected strokes. A stroke is categorized as completely correctly detected, if every assignment of the LLS detection (e.g. polarity, categorization as CG stroke) is confirmed as correct by the VFRS data. Only completely correct detected strokes have been used for analyses of single stroke flash percentages, multiplicity, return stroke peak current analyses and the LA calculations. Just for the DE analyses detected strokes have been analyzed too. Additionally, each individual ground truth measurement data set was only taken into account for this analysis, if the GSP was visible in the video. Otherwise, the data set was ignored. The LLS return stroke peak current was only taken into account if the stroke was correctly detected too. Electric field measurements have been analyzed for every stroke and peak values of the detected field have been extracted. For this investigation, the electric field data were just taken into account to check for the correct assignment of the polarity of the LLS return stroke peak current calculation. No peak current calculations have been carried out by using the electric field data. To check CG and IC assignments the video data and the electric field data are used. The video data have been used for the assignment of the GSP of the individual strokes (same GSP or new GSP as previous stroke), for the categorization of leader channel in straight or inclined, and for the identification of special phenomena like forked stroke channels, etc.

5.2.2 Single Stroke Flashes and Multiplicity

For the present thesis, the occurrence of single stroke flashes in the Alpine region is analyzed in more detail. The detections of single stroke flashes by the VFRS and the LLS are compared for each year and over the whole measurement period. The differences of the percentage of single stroke flashes over the different measurement days or measurement locations and years are analyzed as well. In addition the values of the percentage of single stroke flashes obtained from the VFRS measurements are compared with values from former national and international studies of this topic.

In order to investigate whether the structure of different thunderstorm types systematically influences their lightning characteristics, a classification into single cells, multicells, supercells, and lines was carried out. This classification is done in two alternative ways: based on radar characteristics (weather radar data) and based on the underlying vertical wind shear (data of radiosondes; see section 4.4). For this investigation Mag. Georg Pistotnik, meteorologist at the

Austrian Meteorological Service ZAMG analyzed and categorized the thunderstorms in the two ways by using radar data and data of radiosondes.

Characteristic features of single cells, multicells, supercells or lines in radar data are used to undertake a manual classification of the thunderstorms whose ground truth lightning data have been recorded. For example, the asymmetric position of the updraft and downdraft within multicells and supercells results in a v-shaped appearance and in deviant motions, in contrast to round single cells, which just move with the mean wind. While this classification is based on expert's knowledge, it cannot be discounted that a small rest of subjectivity is left.

The results are therefore corroborated by using vertical wind shear information as an alternative classification, which is related to the atmospheric background conditions on a given day instead of each individual thunderstorm's behavior, but can be better objectified. Single cells usually dominate with "deep-layer shear" (DLS) below 10 m/s, multicells between 10 and 20 m/s and supercells above 20 m/s (Markowski and Richardson, 2010 [38]).

The so called DLS is the most widely used measure for vertical wind shear between the surface and 6 km height. DLS is the best discriminator between the occurrences of different thunderstorm types (Craven and Brooks, 2004 [39]). Under weak vertical wind shear, a thundercloud is almost vertical. It is built by a brief updraft of warm and moist air, which is then overwhelmed by a rain-cooled downdraft as soon as precipitation forms. As vertical wind shear increases, it starts to tilt the updraft; as a result, the precipitation falls in a separated area and does not choke off the updraft anymore. Note that the characteristic fuzzy ice shield ("anvil") which forms the cloud top is more or less symmetric in case of a single cell, whereas it becomes more and more asymmetric as the vertical wind shear and the thunderstorm organization increase.

Thunderstorms tend to live longer and become more intense when they organize into multicells (regenerated by repeated pulses of new updrafts at one particular side), and finally, under strong vertical wind shear, into supercells (sustained by a continuous inflow and updraft at this particular side). In addition to these types of discrete thunderstorms, convection may also organize into a line, which is favored when unstable air is lifted over an elongated area (e.g. along a cold front) and vertical wind shear is strong.

The term flash/GSP multiplicity describes the number of strokes per flash or per GSP. Strokes do not have to follow the same channel to ground to be counted for the flash multiplicity. LLS derived multiplicities for flashes are based on LLS sensor detections and depend on the quality of the LLS LA and the quality of the LLS IC/CG categorisation. To determine the multiplicity distribution and to calculate the mean multiplicity, for each year and

in total, the VFRS and LLS data of the same events shall be compared. The calculated VFRS multiplicity values are compared additionally with values from former national and international studies of this topic.

The results regarding negative single stroke flashes obtained from VFRS and LLS data, the single stroke flashes by thunderstorm type and the comparison with literature values are shown in section 6.1. The results of mean multiplicity values, its distribution and the comparison with values available in the literature are shown in section 6.2.

5.2.3 Return Stroke Peak Current Analyses

For analyses regarding the return stroke peak current correlated ALDIS LLS data of each analyzed return stroke have been used. Peak currents were not determined from VFRS electric field peaks. The estimation of LLS return stroke peak currents from electromagnetic fields is described in detail in section 3.2.

For this investigation, only flashes with absolute stroke peak currents greater than 2 kA, shown as lower limit of stroke peak currents in Berger's distribution (Berger et al., 1975 [40]) and confirmed in a theoretical way by Cooray and Rakov, 2012 [41] are used.

As return stroke peak current of a flash detected by the LLS, the return stroke peak current of the first detected stroke in this flash is assigned as flash peak current. The return stroke peak currents for all other strokes than first strokes in a multiple-stroke flash are just being categorized as SU strokes, irrespective of whether some of these strokes terminated eventually in a new GSP (see section 3.2). By using the ground truth video data in correlation with the LLS data, the grouped flashes can now be split up into strokes to individual GSPs. In this case, more FI peak currents will be taken into account for the calculation of lightning current distribution, because every first stroke to a new GSP is assigned as a FI stroke.

For analyzes regarding the median, mean and 95 % return stroke peak currents of flashes (all FI1 strokes), all strokes, FI and SU strokes have been analyzed separately. In addition, for every category (flashes, all strokes, FI and SU strokes) their peak current distribution is shown.

Further, analyses of return stroke peak currents per GSPs have been carried out. Every data set was analyzed manually to determine each individual FI or SU stroke per GSP by using the VFRS video data. Such ground truth data allows a clear assignment for strokes to the same or individual GSPs, as an alternative to the given LLS flash grouping assignment. These ground truth assignments of strokes to GSP can then be used to analyze various parameters.

Figure 10 and Figure 11 show an example of the above-described GSP assignment. This flash was recorded in the center of the Alps on July 7th 2018 at 11:49:15 UTC and includes four strokes with individual GSPs. The second stroke (FI2) strikes the ground in a distance of 1.41 km to the first stroke (FI1). The following third stroke (FI3) has a calculated distance to the FI1 of 2.68 km and a distance of 1.37 km to FI1 for the fourth (FI4) stroke was determined. All distances are calculated by using LLS location data. The strokes appeared all within the same second and show interstroke intervals from 61.6 to 91.3 ms. For this case the LLS estimated return stroke peak current of -29.1 kA for the FI4 stroke was higher than the -17.7 kA for the FI1 stroke.

The estimated LLS values for the return stroke peak currents shall be compared additionally with values from former national and international analyses for flashes and for return stroke peak current analyses per GSP.

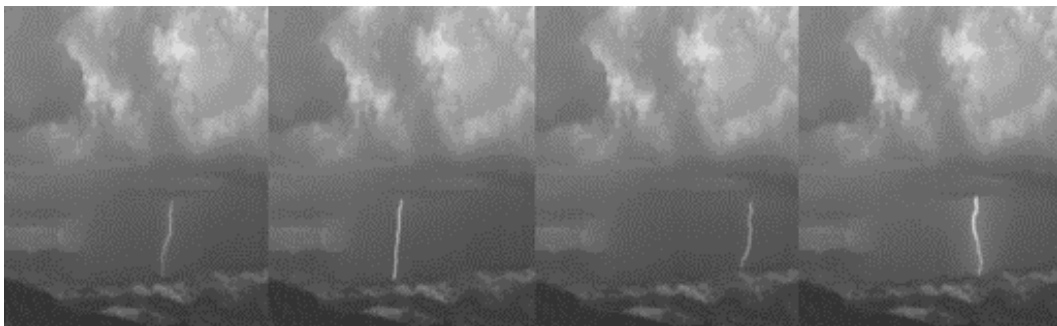


Figure 10: First (FI1), second (FI2), third (FI3) and fourth (FI4) stroke terminating in a different GSP (from left to right)

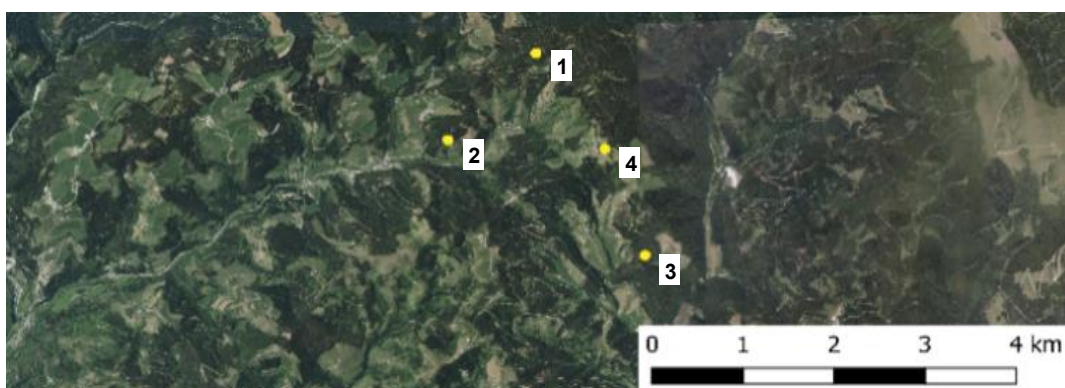


Figure 11: LLS detection of the four strokes in the flash. Position 1 to 4 for each GSP (FI1 to FI4); ESRI satellite map in the background

The results of the analyzed negative return stroke peak currents of LLS detections for flashes, all strokes, FI and SU strokes, the return stroke peak current analysis for GSPs and the comparison with values available in the literature are shown in section 6.3.

5.2.4 Location Accuracy (LA)

To analyze the LA of the LLS only strokes following the same channel from the cloud to the ground were used. For such strokes, it can be assumed that they have the same GSP. In such a case, the LLS should provide the same position for all strokes in the same channel (Schulz et al., 2012 [42]). If a flash consists of at least two strokes following the same channel to ground, the LA of the LLS can be analyzed. The location difference between the FI and every SU stroke within the same channel can be calculated with spherical trigonometry by using the stroke locations of the LLS data. It has to be mentioned, that the resulting LA distribution would show the same result if such calculations were performed for two SU strokes following the same channel. Such calculations always lead to a Rayleigh distribution of the LA (see Schulz et al., 2012 [42]). To compare video determined location errors with location errors, determined by using data from instrumented towers, the calculated location differences have to be scaled by using a factor of $1/\sqrt{2}$ (see Schulz et al., 2012 [42]). This was conducted for all analyzed LA values to make a comparison with published values in literature possible.

Figure 12 and Figure 13 show an example of three strokes out of a flash with a total of seven strokes, recorded in the pre-alpine area. The first stroke (FI1) strikes ground in a distance of 1.77 km to the second stroke (FI2). The following five strokes are terminating at the same GSP as FI2.



Figure 12: Second (FI2), forth (SU2) and seventh (SU2) stroke following the same channel to ground (from left to right)

Table 4 shows the LLS data including the LA for this flash (recorded on 4th August 2018 at 13:45:33 UTC). For this case, the LA of the SU2 strokes relative to FI2 is in the range from 0.11 to 0.23 km (calculated by using locations provided by the LLS; only scaled distances are given). Since the real GSPs are not always visible, particularly in mountainous regions, the calculated values show upper limits of the LA (Biagi et al., 2007 [43]).

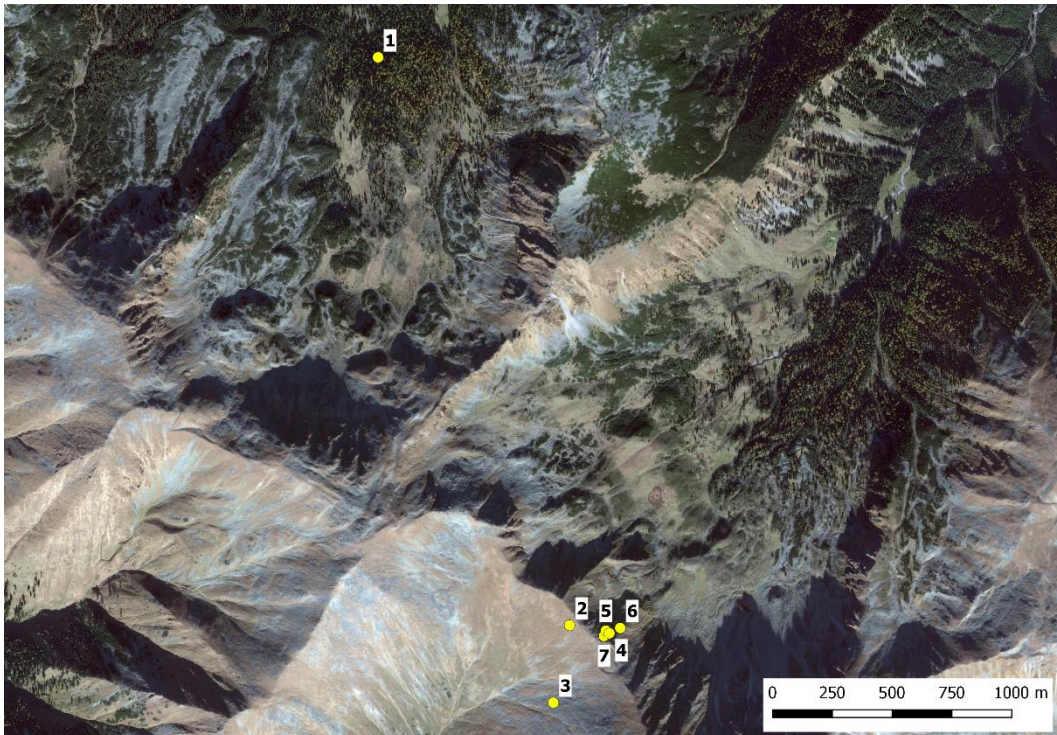


Figure 13: LLS detection of the flash, stroke two to seven struck the same GSP; Google satellite map in the background

Due to the ongoing improvements in the LLS sensor technology, the lightning detection software and the continuous adaption of the LLS, only most recent observations of LA values from national and international literature shall be compared with the calculated LA values of the present analysis (see subsection 6.4.3).

The results of the analyzed LA of the LLS detections and its distribution, the LA for particular leader channel phenomena, reasons for large LLS location errors and the comparison with recent values available in the literature are shown in section 6.4.

Table 4: LLS data with LA calculation in km (Return stroke peak current in kA, sn = stroke number, nbdf = sensor detections, nbdfit = sensors data with sufficient quality, maxis = major axis in km, ki2 = quality criteria, ToS = Type of Stroke, Flx = First stroke to GSP x, SUx = Subsequent stroke to GSP x)

Latitude	Longitude	Return Stroke Peak Current	sn	nbdf	nbdfit	maxis	ki2	ToS	LA
		kA							
47.3655	14.7146	-15.50	1	7	4	1.9	2.2	FI1	
47.3442	14.7252	-4.70	2	5	5	0.1	1.0	FI2	
47.3413	14.7243	-21.20	3	34	26	0.0	6.0	SU2	0.23
47.3439	14.7274	-14.10	4	40	27	0.1	1.3	SU2	0.12
47.3440	14.7272	-9.80	5	22	18	0.1	0.8	SU2	0.11
47.3441	14.7280	-13.30	6	34	26	0.1	1.0	SU2	0.15
47.3438	14.7271	-11.50	7	28	20	0.1	1.4	SU2	0.11

5.2.5 Detection Efficiency (DE)

For analyzes of the DE of a LLS it is necessary to consider two different types of DEs, the flash and the stroke DE. The stroke DE is defined as percentage of detected strokes to really occurred strokes (detected in the video record). In the following we are distinguishing two different categories of detected strokes:

- (1) Completely correctly detected strokes: These are strokes, where every assignment of the LLS detection (e.g. polarity, IC/CG stroke categorization) can be confirmed as correct with the VFRS data
- (2) Detected strokes: These are all strokes which have been detected by the LLS and correlated with the VFRS data (e.g. CG stroke misclassified as IC included)

This strict categorization should give additional insights into the quality of the LLS detections. The flash DE is calculated in the same way but for the strict categorization of correctly detected flashes only (FI1 strokes only have to be classified correctly). All calculations have been carried out for flashes and strokes for the three individual years and for the total data set. Since continuous improvements of the LLS strongly influence the DE values in this case, DE values from more recent publications shall be compared with the calculated DE values of the present investigation. The results of the DE analysis, reasons for different flash and stroke DE values and the comparison with recent values available in the literature are shown in section 6.5.

6 Results

6.1 Negative Single Stroke Flashes

6.1.1 Data of Single Stroke Flashes

For this analysis, correlated VFRS and LLS data of 2015, 2017 and 2018 are analyzed regarding single stroke flash percentage. Figure 14 shows the recorded data for negative CG flashes (multi and single stroke flashes) merged for 2015 until 2018 and the VFRS measurement locations on an elevation map in the background. Table 5 shows the analyzed data for single stroke flashes detected by analyzing VFRS data for the years 2015, 2017 and 2018 and in total.

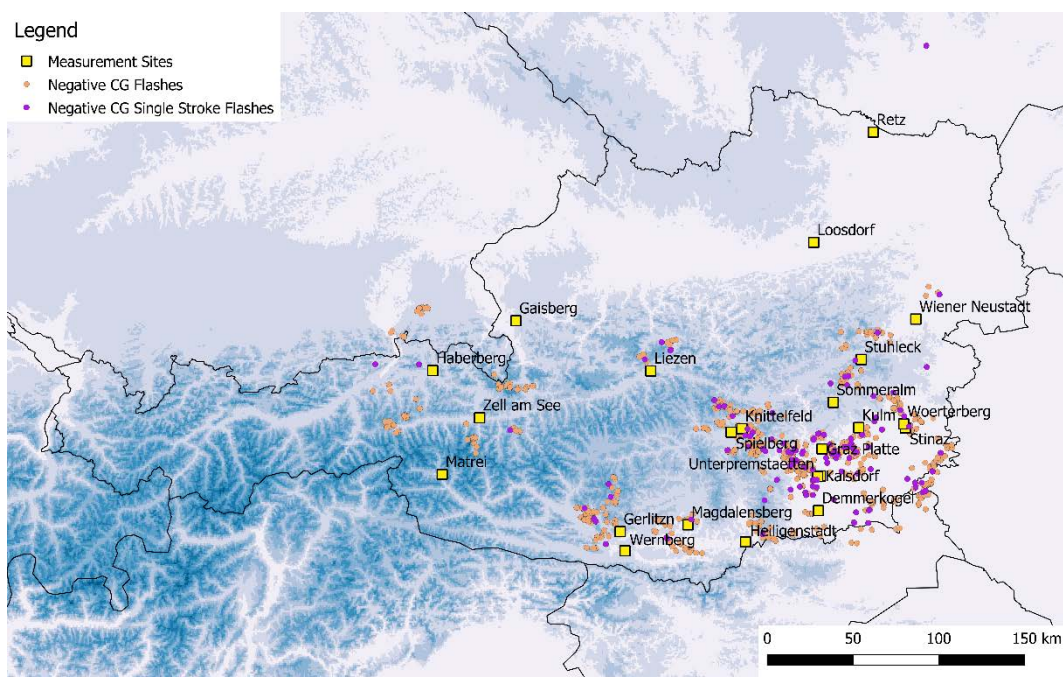


Figure 14: Recorded data for negative CG flashes (multi and single stroke ones) merged for 2015 until 2018 and VFRS measurement locations

Table 5: Analyzed thunderstorms, total negative flashes and negative single stroke flashes for VFRS data for 2015 and 2018

Year	Thunderstorms	Number of Flashes	Single Stroke Flashes
2015	15	153	37
2017	10	94	25
2018	13	217	62
Total	38	464	124

6.1.2 Single Stroke Flashes Detected by VFRS and LLS

In this subsection, single stroke flashes detected by the VFRS and the LLS shall be compared. Over the course of an entire measurement season (May to August), the variability of the percentage of single stroke flashes per year largely levels out to values between 24 % and 29 % for VFRS data and between 22 % and 30 % for LLS data (see Table 6). The described overestimation of single stroke flashes of LLS data in Poelman et al., 2016 [11] does not occur and is not expected for analyses correlated with VFRS measurements, because of the comparison with ground truth data (i.e. LLS misclassified inter/intra-cloud flashes are not included).

Table 6: Negative single stroke flash percentage for VFRS and LLS data from 2015 to 2018; Number of single stroke flashes in parenthesis

Measurement Period	VFRS Total Flashes	Single Stroke Flashes for VFRS data	LLS Total Flashes	Single Stroke Flashes for LLS data
		% (Number)		% (Number)
2015	153	24 (37)	147	22 (32)
2017	94	27 (25)	93	30 (28)
2018	217	29 (62)	206	30 (62)
Total	464	27 (124)	446	27 (122)

Figure 15 shows the percentage of single stroke flashes for measurement days with ten or more recorded flashes of 2015, 2017 and 2018, as example for detection differences between

VFRS and LLS data. The single stroke flash percentage shows a considerable variability for the individual thunderstorm days.

Lowest values for the data are in the range of 0 to 10 %, highest values show a percentage of over 40 % both for VFRS and LLS data (see Figure 15). Similar analyses for measurements in Austria of 2009 to 2015 can be found in Schwalt et al., 2017 [44].

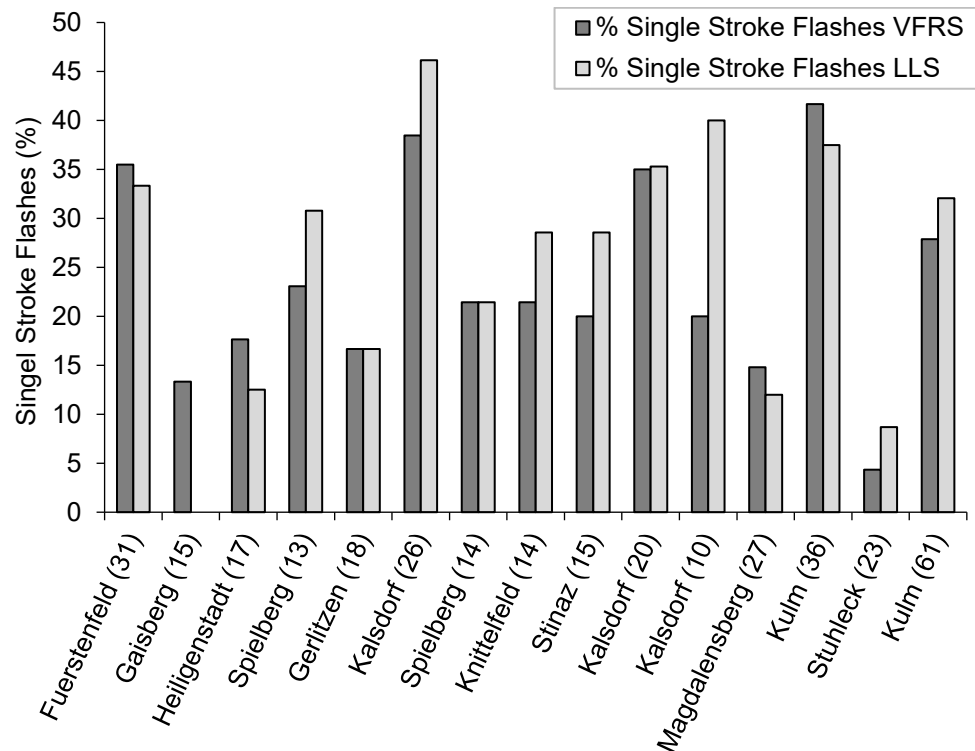


Figure 15: Percentage of negative single stroke flashes of VFRS and LLS data for individual thunderstorm days in 2015, 2017 and 2018; number of VFRS recorded flashes in parenthesis

6.1.3 Analysis of Negative Single Stroke Flashes by Thunderstorm Type for Data from 2009 to 2018

To get a spread view on all different thunderstorm types for this analysis, data of previous VFRS measurements in Austria of 2009, 2010 and 2012 were merged with the present data set (2015, 2017 and 2018). That is necessary because some individual thunderstorm types occurred just a few times during the whole measurement period. The entire data set contains 735 negative CG flashes with 196 single stroke flashes, recorded at 33 different measurement locations on 61 different days. As described in subsection 5.2.2 different thunderstorm types, categorized by the use of radar data (single, multi or supercells as well as lines) or vertical

wind shear (change of the wind vector both in strength and in direction from 0 to 6 km height) are analyzed in this section.

The main difference of the measurement system used during the measurement period from 2009 to 2012 compared to the actually used one was the use of a different camera type. For the measurements from 2009 to 2012, a monochrome camera with a frame rate of 200 fps, 8-bit image depth and VGA resolution (640 x 480 pixels) was used (see Schulz and Saba, 2009 [45]). From 2015 onwards, the camera type described in section 3.1 was in use (2000 fps, resolution 1344 x 400 pixels, image depth 14 bit).

Figure 16 shows the recorded data for negative CG flashes (multi and single stroke flashes) merged for 2009 until 2018 and VFRS measurement locations on an elevation map in the background.

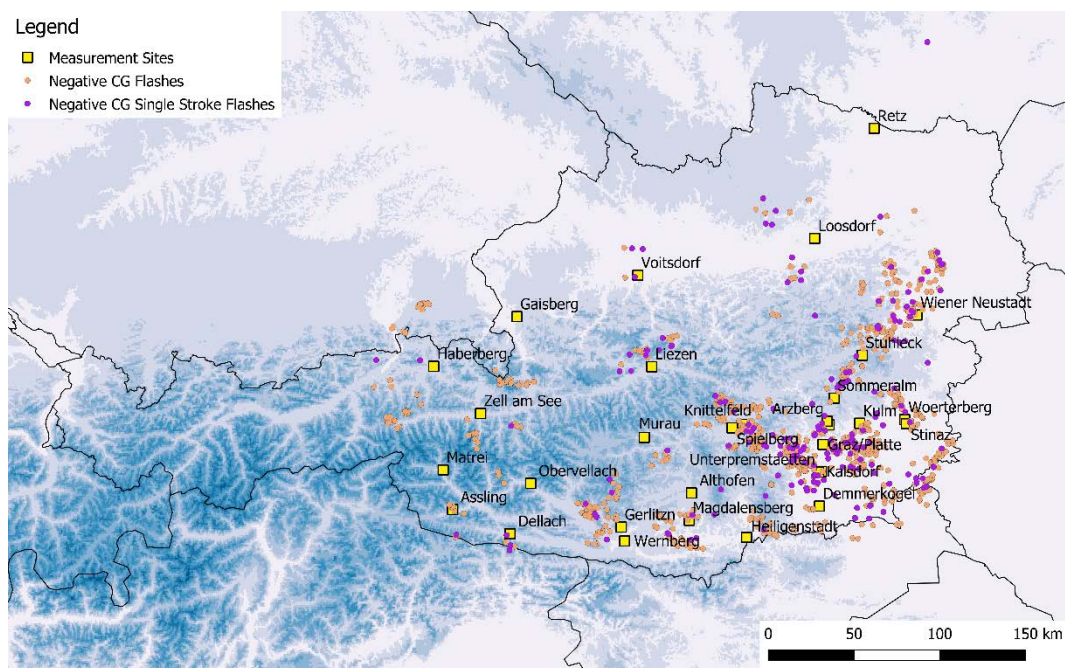


Figure 16: Recorded data for negative CG flashes (multi and single stroke ones) merged for 2009 until 2018 and VFRS measurement locations

Table 7 shows the additionally analyzed data for single stroke flashes detected by analyzing VFRS data for the years 2009, 2010 and 2012. The data set of 2015, 2017 and 2018 is shown in Table 5.

Table 7: Additional data of measurement campaigns in 2009, 2010 and 2012; analyzed thunderstorms, total negative flashes and single stroke flashes for VFRS

Year	Thunderstorms	Total Flashes	Single Stroke Flashes
2009	2	45	9
2010	13	109	33
2012	8	117	30

Table 8 shows the percentage of negative single stroke flashes with respect to the manual thunderstorm classification considering radar data. This classification reveals very similar percentages of negative single stroke flashes in single cells (26 %), multicells (27 %), supercells (28 %) and thunderstorm lines (26 %). To avoid issues related to small sample sizes, the somewhat more sparsely populated classes of multicells, supercells and lines have been merged into a joint category of organized thunderstorms, which yields a value of 27 % as well.

Table 8: Percentage of negative single stroke flashes calculated by thunderstorm type for merged data from 2009 to 2018; Number of single stroke flashes in parenthesis

Number of Thunderstorms	Thunderstorm Type	Flashes	Single Stroke Flashes
			% (Number)
21	Single Cell	234	26 (62)
29	Multicell	379	27 (102)
3	Supercell	43	28 (12)
8	Line	78	26 (20)
32	Multi-, Supercell	422	27 (114)
40	Multi-, Supercell and Line	500	27 (134)

The above presented results can be confirmed with the classification according to vertical wind shear between 0 and 6 km (DLS). Table 9 shows the percentage of negative single stroke flashes with respect to a classification with DLS data. It yields a single stroke flash percentage of 27 % for DLS below 10 m/s, when single cells are most common, 27 % for DLS between

10 and 20 m/s when multicells are the most likely mode, and 32 % for DLS above 20 m/s, when supercells or lines are common. Again, merging all cases with DLS > 10 m/s into a joint category of enhanced vertical wind shear, the resulting single stroke flash percentage value is 26 %. The higher percentage of single stroke flashes in the class of strong DLS (i.e. > 20 m/s) therefore entirely appears to be an artifact of the small sample size of 38 flashes spread over five thunderstorms only.

Table 9: Percentage of negative single stroke flashes for a categorization by vertical wind shear between 0 and 6 km (DLS) for merged data from 2009 to 2018; Number of single stroke flashes in parenthesis

Number of Thunderstorms	Vertical Wind Shear (DLS)	Flashes	Single Stroke Flashes
			% (Number)
24	0 to 10 m/s	273	27 (74)
32	11 to 20 m/s	423	26 (110)
5	> 20 m/s	38	32 (12)
37	> 10 m/s	461	26 (122)

6.1.4 Comparison with Values Available in the Literature

For this analysis, previously published results for different countries shall be compared with the VFRS measurements of 2015, 2017 and 2018. Data of measurements from 2009, 2010 and 2012 were additionally taken into account and an overall single stroke flash percentage for measurements from 2009 to 2018 was calculated (see Table 10).

The previously published results of single stroke flash analyses are based on numerous studies and international publications, conducted in various regions all over the world during the last decades. The 45 % of single stroke flashes, described by Anderson and Eriksson, 1980 [2], still exceeds our highest value and is today seen as an overestimate by a factor of two (see CIGRE TB 549, 2013 [13]). Zhu et al., 2015 [46] published the lowest value in the literature (12 %). They used data of electric field measurements from Florida for their analyses. For the records in New Mexico by Kitagawa et al., 1962 [47], electric field and moving-film camera records were correlated. These measurements showed a single stroke flash percentage of 13 % (Kitagawa et al., 1962 [47]). Measurements in Malaysia, analyzed by Baharudin et al., 2014 [48], showed a percentage of 16 % from electric field measurements.

The analyses of Rakov and Uman, 1990 [49] in Florida showed a percentage of 17 %, the same as the analyses of Balarotti et al., 2012 [50] in Brazil. The measurement data of Rakov and Uman, 1990 [49] is based on electric field records and a multiple-station TV system; measurements of Balarotti et al., 2012 [50] have been conducted with high speed video cameras in correlation with LLS data. For the records in Sweden, done by Cooray and Pérez, 1994 [51], which showed a single stroke flash percentage of 18 %, broadband electric field records were used. The analysis of measurements from Arizona described by Saraiva et al., 2010 [52] showed a percentage of 19 % (high speed video observations). Saba et al., 2006 [6] showed a single stroke percentage of 20 % for high speed video camera records in correlation with LLS data in Brazil. 21 % have been reported for analyses in Belgium (Poelman et al., 2013 [53]) and Sri Lanka (Cooray and Jayaratne, 1994 [54]). For analyses in Belgium (Poelman et al., 2013 [53]) a VFERS data set and LLS data were used and for measurements in Sri Lanka (Cooray and Jayaratne, 1994 [54]) electric field measurements have been analyzed. The result of 24 % of Antunes et al., 2013 [55] in Brazil has been conducted with high speed video cameras in correlation with LLS data. Table 10 shows a summary of all results for the percentage of single stroke flashes of the present and previous studies.

The analyzed ground truth VFERS data for the Austrian Alpine region shows a higher percentage of single stroke flashes than previous studies in other parts of the world (see again Table 10). All analyzed measurement periods as well as the calculated value for the merged data set from 2009 to 2018, show a single stroke flash percentage of 26 or 27 %. The sample sizes of our measurements are in the range of the ones used for other studies in the literature (see Table 10). Qie et al., 2004 [56] reported a number of 40 % single stroke flashes within a data set of 83 negative flashes. These data were recorded in the Chinese Gansu province in 1996 by using a broadband slow antenna system. Rakov et al. (CIGRE TB 549, 2013 [13]) stated that it is presently unknown why the value differs significantly from other values (see Table 10) and indicated that more data from China are needed.

In general, it should be kept in mind that analyses based only on electric field records are mostly based on all flashes recorded up to a certain distance all around the measurement location. If measurements are conducted with a camera system, the recorded data is limited to the field of view of the camera. Therefore, the VFERS recorded data might show just a sample of the total lightning activity for some cases, which occurred during the observed thunderstorm.

For our on-site observations, distances of 15 to 20 km from the measurement location to the center of the thunderstorm were favored because of better observation possibilities and the to lower personnel risk. However, even for such VFERS observations it may happen that a

specific thunderstorm moves in direction of the measurement location and makes the ongoing measurements impossible (e.g. due to heavy rain and/or wind, hail and close lightning strikes).

Table 10: Summary of results for the percentage of negative single stroke flashes of the present and previous studies by various authors

Location	Year	Measurement System	Flash Sample Size	Single Stroke Flashes
				%
New Mexico [47]	1959 - 1960	Video	83	13
Florida [49]	1979	Video	76	17
Sweden [51]	1992 - 1993	Electric Field	137	18
Sri Lanka [54]	1993	Electric Field	81	21
Brazil [6]	2003 - 2004	Video	233	20
Arizona [52]	2007	Video	209	19
Brazil [50]	2003 - 2010	Video	883	17
Austria [57] ¹	2009 - 2010	Video	154	27
Austria [58] ¹	2012	Video	117	26
Belgium [53]	2011	Video	57	21
Brazil [55]	2012 - 2013	Video	357	24
Malaysia [48]	2009	Electric Field	100	16
Florida [46]	2013 - 2014	Electric Field	478	12
Austria (present study)	2015 - 2018	Video	464	27
Austria (present study)	2009 - 2018	Video	735	27

¹ Measurements with a different video camera (200 fps; Schulz and Saba, 2009 [45])

6.2 Mean Multiplicity and Multiplicity Distribution of Negative Flashes

6.2.1 Analysis of the Multiplicity of VFERS and LLS Data

The mean multiplicity was obtained for each year and in total from both the VFERS and the LLS data for the correlated flashes. The results for this analysis are shown in Table 11. The calculated values for the true multiplicity, determined with the VFERS data, are comparable to the results from previous measurements in the Austrian Alps (see Vergeiner et al., 2013 [57]).

The decrease of the mean LLS multiplicity value for 2017 and 2018 is caused by the new LLS IC/CG classification, which was introduced in 2016 (see section 3.2). A lower LLS multiplicity value appears if CG strokes are misclassified as IC strokes. The new IC/CG classification performs worse for negative CG strokes below -15 kA (Kohlmann et al., 2017 [59]). A deeper analysis of these misclassified strokes shows four strokes with return stroke peak currents greater than -15 kA for 2017 (total 35 misclassified) and for 2018 (total 117 misclassified). That led to a percentage of approximately 90 % of misclassified strokes with a negative return stroke peak current below -15 kA for 2017. In 2018, more than 95 % of the misclassified strokes had a return stroke peak current lower than -15 kA.

Two of the misclassified strokes (i.e. CG strokes classified as IC strokes) have been detected as single stroke flashes by the LLS in 2017. They showed a return stroke peak current of -2.9 kA and -5 kA. In 2018, four of the non-correctly detected strokes have been categorized as single stroke flashes (return stroke peak currents in a range from -2.0 kA to -5.6 kA).

Table 11: Mean multiplicity for VFERS and LLS data of negative flashes (2015, 2017, 2018 and total)

Year	Mean VFERS Multiplicity	Mean LLS Multiplicity
2015	3.4	3.6
2017	3.4	2.8
2018	3.2	2.8
Total	3.3	3.1

Compared to all strokes detected by VFRS a percentage of 11.04 % in 2017 (total number of strokes 317 versus 35 non-correctly detected) and 16.88 % (total number of strokes 693 versus 117 non-correctly detected) for 2018 respectively have not been correctly detected (see Table 11).

6.2.2 Multiplicity Distribution of VFRS and LLS Data

To determine the total multiplicity distribution, the VFRS and LLS data of the same events have been analyzed and the distribution of the correlated flashes of the VFRS and LLS data have been compared. Differences in multiplicity distributions for the three investigated measurement periods could be caused by variances in the observed thunderstorm characteristics as well (see Antunes et al., 2015 [60]). Another reason for such differences could be again strokes not detected or misclassified by the LLS. The detected multiplicity maxima of the VFRS data are 14 strokes in one flash for 2015, 13 strokes for 2017 and 14 strokes for 2018, respectively. Figure 17 shows the merged distribution of negative strokes per flash for 2015, 2017 and 2018, respectively.

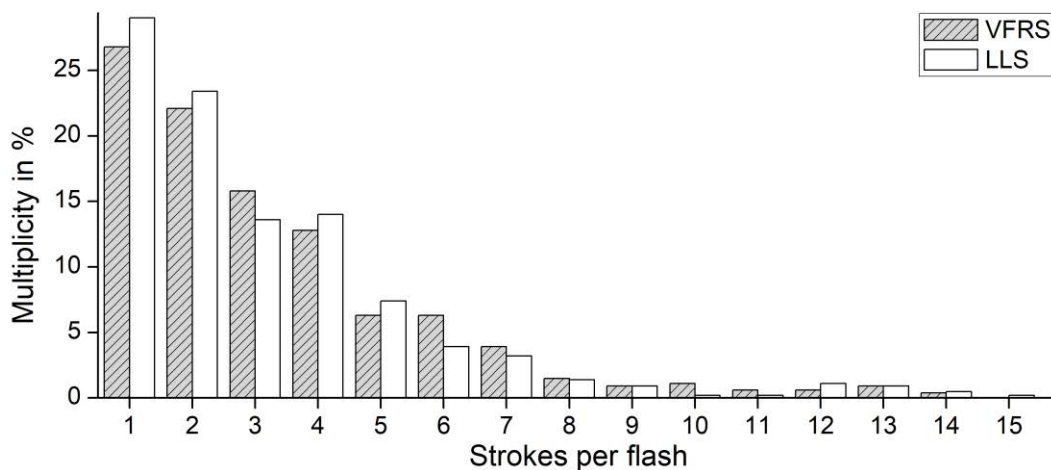


Figure 17: Multiplicity of the VFRS and LLS data of negative flashes (2015, 2017 and 2018)

6.2.3 Comparison with Values Available in the Literature

For the following analysis previously published results for different countries shall be compared with the VFRS measurements of 2015, 2017 and 2018. Data of VFRS

measurements in Austria of 2009 and 2010 by Vergeiner et al., 2013 [57] were additionally taken into account (see Table 12).

The previously published results of multiplicity values are based on numerous studies and international publications, conducted in various regions all over the world during the last decades. The highest multiplicity value of 6.4 was reported from Kitagawa et al., 1962 [47] for their correlated measurements of electric field and moving-film camera records. Rakov et al., 1990 [49] published a multiplicity value of 4.6 for Florida based on electric field records and a multiple-station TV system. The same value of 4.6 was reported by Ballarotti et al., 2012 [50] for its high speed video camera records in correlation with LLS data in Brazil. Zhu et al., 2015 [46] showed again a multiplicity value of 4.6 for Florida. They used data of electric field measurements for their analyses. Cooray and Jayaratne, 1994 [54] have reported a multiplicity value of 4.5 for their electric field measurements in Sri Lanka. The result of 4.2 of Antunes et al., 2013 [55] in Brazil has been conducted with high speed video cameras in correlation with LLS data. Measurements in Malaysia, analyzed by Baharudin et al., 2014 [48], showed a multiplicity value of 4.0 for electric field measurements. The analysis of measurements from Arizona described by Saraiva et al., 2010 [52] showed a multiplicity value of 3.9 (high speed video observations). Qui et al., 2004 [56] (electric field measurements, China) same as Saba et al., 2006 [6] (high speed video camera records in correlation with LLS data, Brazil) reported a multiplicity value of 3.8. Poelman et al., 2013 [53] reported a slightly lower value of 3.7 for analyses in Belgium. For this observations a VFRS data set and LLS data have been used (Poelman, 2013 [53]). For the records in Sweden, done by Cooray and Pérez, 1994 [51], which showed a multiplicity value of 3.4, broadband electric field records were used. Vergeiner et al., 2013 [57] showed a multiplicity value of 3.3 for previous analyses in Austria. They used VFRS measurements (video recording speed 200 fps) in correlation with LLS records (Vergeiner et al., 2013 [57]). Table 12 shows a summary of the analyzed multiplicity values of the present and previous studies.

As already reported in subsection 6.1.4, Qie et al., 2004 [56] showed a mean multiplicity value of 3.8 for a data set of 83 negative flashes, recorded in in the Chinese Gansu province in 1996 by using a broadband slow antenna system including 40 % single stroke flashes (i.e. a number of 33 single stroke flashes). This seem a rather high percentage of single stroke flashes (40 %) having in mind that the mean multiplicity value is 3.8.

Table 12: Summary of results for flash multiplicity of negative flashes from present and previous studies by various authors

Location	Year	Measurement System	Flash Sample Size	Mean Multiplicity
New Mexico [47]	1959 - 1960	Video	83	6.4
Florida [49]	1979	Video	76	4.6
Sweden [51]	1992 - 1993	Electric Field	137	3.4
Sri Lanka [54]	1993	Electric Field	81	4.5
China [56]	1997	Electric Field	83	3.8
Brazil [6]	2003 - 2004	Video	233	3.8
Austria [57] ¹	2009 - 2010	Video ¹	154	3.3
Arizona [52]	2007	Video	209	3.9
Brazil [50]	2003 - 2010	Video	883	4.6
Belgium [53]	2011	Video	57	3.7
Brazil [55]	2012 - 2013	Video	357	4.2
Malaysia [48]	2009	Electric Field	100	4.0
Florida [46]	2013 - 2014	Electric Field	478	4.6
Austria (present study)	2015, 2017, 2018	Video	464	3.3

¹ Measurements with a different video system (200 fps; Schulz and Saba, 2009 [45])

6.3 Negative Return Stroke Peak Currents of LLS Detections

6.3.1 Return Stroke Peak Currents for Flashes, all Strokes, FI and SU Strokes

Table 13 shows the mean, median and 95 % values of LLS return stroke peak currents for all strokes, FI and SU strokes and flashes (FI1) for each investigated period and in total. In total 452 return stroke peak currents for 2015, 204 for 2017 and 591 for 2018, respectively,

have been analyzed. Please note, that the abbreviation FI and SU is related to the GSP and not to the flash.

Table 13: Mean, median and 95 % value for negative return stroke peak currents of the ALDIS LLS detections for all negative strokes, first (FI), subsequent (SU) and FI1 strokes (flash peak current) for the year 2015, 2017 and 2018 and in total

Year	Type of Strokes	Number of Strokes	Mean	Median	95 % Value
			kA	kA	kA
2015	All	452	-13.4	-10.1	-35.3
	FI	248	-16.0	-12.1	-41.6
	SU	186	-9.9	-7.2	-27.3
	FI1	131	-18.1	-12.4	-51.4
2017	All	204	-13.6	-11.2	-31.9
	FI	127	-14.6	-12.1	-31.9
	SU	77	-12.1	-9.1	-29.6
	FI1	75	-16.4	-13.5	-36.1
2018	All	591	-11.3	-8.0	-29.7
	FI	343	-11.8	-8.8	-30.6
	SU	243	-10.6	-7.5	-27.7
	FI1	198	-12.9	-8.4	-35.8
Total	All	1247	-12.4	-9.4	-33.4
	FI	718	-13.9	-10.8	-35.8
	SU	506	-10.6	-7.6	-27.7
	FI1	404	-15.2	-10.7	-42.7

The number of FI and SU strokes for 2015 is 248 and 186, respectively. For first strokes in a flash (FI1) 131 have been analyzed. For 2017, 127 FI (75 FI1 strokes) and 77 SU strokes and for 2018 343 FI (198 FI1 strokes) and 243 SU strokes have been analyzed. The detected minimum and maximum return stroke peak current was -1.8 kA and -90.1 kA for 2015, -1.4 kA

and -83.0 kA for 2017 and -1.1 kA and -84.5 kA for 2018, respectively. The resulting values for negative median return stroke peak currents of all strokes are around 16 % lower for 2015, around 7 % lower for 2017, about 33 % lower for 2018 than results of older VFRS measurement campaigns in the Alps. Schulz et al., 2016 [19] showed a median return stroke peak current of -12 kA for a merged data set of 2009, 2010 and 2012 for all used strokes. The calculated value for all strokes over the whole measurement period (2015, 2017 and 2018) is about 22 % lower compared to the previous value (Schulz et al., 2016 [19]). Values for flash return stroke peak currents (FI1) show as expected higher values than SU return stroke peak currents (abbreviation SU related to the GSP). Maximum, mean and median peak currents for FI strokes are greater compared to SU strokes for all three years.

For all LLS detected strokes, the same field to current conversion factor is used (see section 3.2). Again, it should be kept in mind that the used current conversion factor is validated for negative subsequent strokes, with a return stroke peak current lower than -60 kA only (see section 3.2). A validation for negative first return strokes and positive return strokes is still needed (CIGRE TB 376, 2009 [28]). The variability of the return stroke speed makes a highly accurate field to current conversion for individual strokes difficult. However, it has been shown that a statistical estimation of current parameters out of measured electromagnetic fields is possible (see Rachidi et al., 2004 [29]). The values shown in Table 13 depend on the DE of the LLS because only LLS data correlated with VFRS ground truth data is used for the analysis (see CIGRE TB 376, 2009 [28]). No dependency of the return stroke peak current on the distance between strike point and measurement location was detected for all three years (maximum distances of 50 km analyzed).

Return stroke peak currents for all categories show variances over the three investigated periods (2015, 2017 and 2018). The observation of thunderstorms with variable characteristics for each year can be a reason for that for example (see subsection 2.2). Therefore, a merged data set should be used for comparisons with previous measurements.

6.3.2 Return Stroke Peak Current distribution for all Strokes, FI and SU Strokes and Flashes

The following figures (Figure 18 to Figure 21) show the detected return stroke peak current distributions for all strokes, for FI and SU strokes and flashes for a merged data set of all three years. Attention – the abbreviation FI and SU is again related to the GSP and not to the flash. It should be noted that this analysis shows a statistical estimation of current parameter distributions based on measured peak electromagnetic fields by the LLS sensors. Rachidi et

al., 2004 [29] showed that such statistical analyses are possible for peak current parameters calculated based on electromagnetic fields.

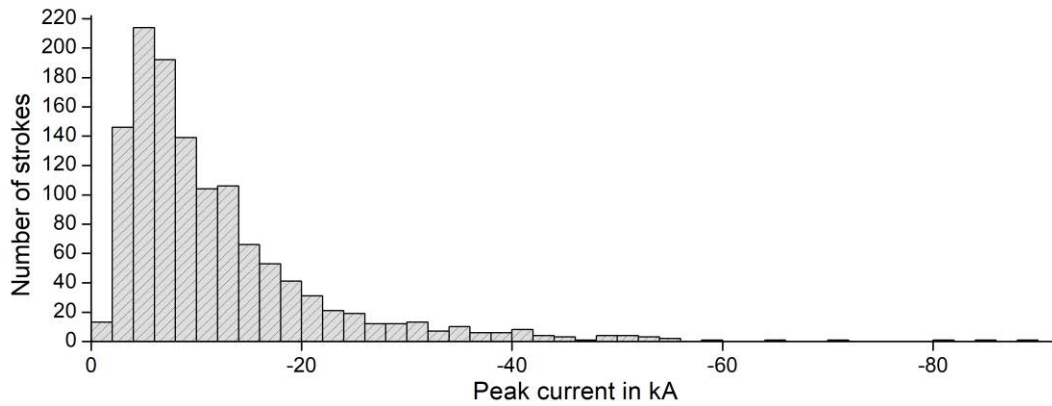


Figure 18: Peak current distribution for all negative return strokes for 2015, 2017 and 2018

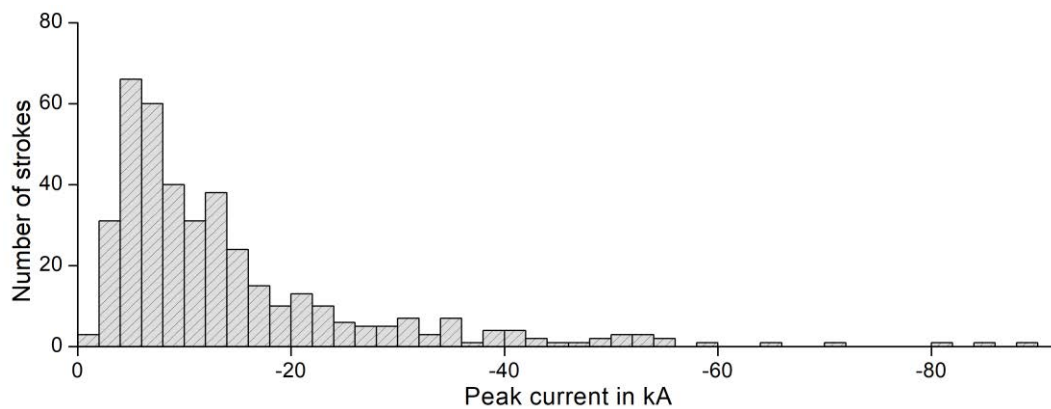


Figure 19: Peak current distribution of negative flashes (F11) for 2015, 2017 and 2018

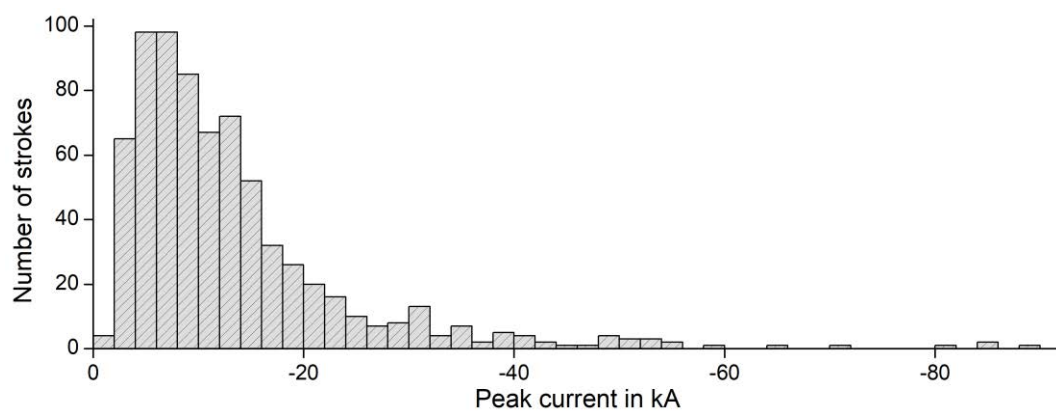


Figure 20: Peak current distribution for negative first return strokes (FI) for 2015, 2017 and 2018

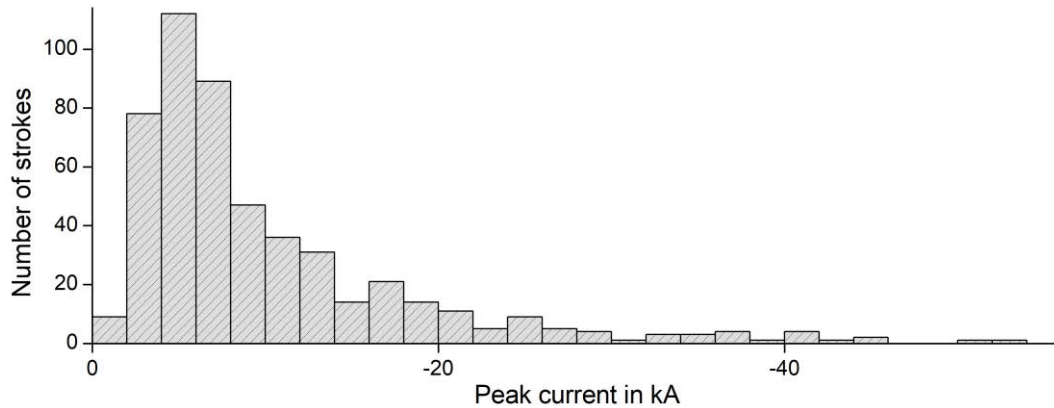


Figure 21: Peak current distribution for negative subsequent return strokes (SU) for 2015, 2017 and 2018

It is known that return stroke peak current distributions should follow lognormal distributions (see Berger et al., 1975 [40], Slyunyaev et al., 2018 [61]). From the visual inspection of Figure 18 to Figure 21, all return stroke peak current analyses seem to show lognormal distributions, even if return stroke peak currents and number of analyzed strokes vary per category (see total number of strokes in Table 13).

For the return stroke peak currents derived by the LLS, it should be kept in mind that the return stroke speed has an influence on the calculated return stroke peak current (see section 3.2). LLS are using the same return stroke speed for first and subsequent strokes. Assuming that the return stroke speed of first strokes is lower than for subsequent strokes the peak currents for first strokes are underestimated by the LLS. Even if the return stroke speed between first and subsequent strokes varies, the difference in speed is not very large (see CIGRE TB 549, 2013 [13]).

6.3.3 Return Stroke Peak Current Analysis for Ground Strike Points

In this subsection, negative peak currents of first return strokes (i.e. LLS flash data FI1) with peak currents of first (FI) strokes in a GSP shall be compared. As described in section 5.2 the GSPs are determined manually by using the video data. All analyzed cases show multiple-stroke flashes or multiple strokes in the same GSP. The relation of FI return stroke peak currents versus SU return stroke peak currents was especially investigated, both for flashes and per GSP. For this investigation, again measurements for all three years were merged. As described in subsection 5.2.3 only flashes with absolute stroke peak currents greater than 2 kA (lower limit in Berger's distribution; Berger et al., 1975 [40] and confirmed in a theoretical way

by Cooray and Rakov, 2012 [41]) are used for this investigation. Additionally, only VFRS data with a maximum distance of 50 km between the observation point and the LLS calculated location of the stroke was analyzed for this investigation, because of visibility issues and the manual GSP definition accuracy.

The analysis of negative peak currents of first return strokes and peak currents of first strokes in a GSP showed the following results:

- In total 241 multiple-stroke flashes were analyzed. 99 flashes exhibited at least one SU stroke with a return stroke peak current greater than the FI1 stroke. This leads to a ratio of 41 %. For this analysis, every stroke except the first stroke (FI1) of the original LLS flash grouping has been counted as SU stroke. Comparing all SU strokes with SU strokes with a higher return stroke peak current than the FI1 in the flash only revealed that 14 % of the total SU strokes have a peak current larger than the first stroke.
- A total of 167 FI strokes with at least one following SU stroke within the same GSP were analyzed for the following investigation. 66 GSPs are counted with at least one SU return stroke peak current greater than the FI stroke peak current. This leads to a ratio of 40 %. For this analysis, only strokes following the same channel to ground were assigned as SU strokes (same GSP visible in the VFRS data). Comparing all SUs per GSP to SU strokes with a higher return stroke peak current than the first stroke in the same GSP only revealed that 15 % of the SU strokes have a peak current larger than the first stroke.

An analysis of the median return stroke peak currents and the multiplicity characteristics for flashes and for strokes per GSP is shown in the following figures. Figure 22 shows the median FI stroke peak current versus multiplicity of a flash (dashed) and versus multiplicity per GSP (grey) for the whole data set of the three measurement periods (return stroke peak currents were rounded to the nearest integer for this analysis). For this analysis, single stroke flashes have also been included to analyze the dependence of the return stroke peak current for the whole multiplicity distribution.

The results show an increase for both analyses leading to higher peak currents for the FI stroke in flashes (FI1) and GSP (FI) with a higher multiplicity. The maximum multiplicity for flashes was 14 and the one for strokes to a single GSP was 13. For both investigations, only a few events had a multiplicity higher than 8 for flashes or strokes per GSP, respectively. This small sample size is responsible for the large increase of the peak current for multiplicity values greater than 8 (number of events shown on top of each bar in Figure 22 and Figure 23).

Figure 22 shows a lower return stroke peak current for single stroke flashes (-7.3 kA) than for flashes with a higher multiplicity, at least for analyses of flashes. This analysis is comparable with findings in the literature (see Nag et al., 2008 [62], Schulz et al., 2005 [12], Orville et al., 2002 [63]). Nag et al., 2008 [62] stated that return stroke peak currents of first strokes in single stroke flashes are on average smaller than first strokes in multiple stroke flashes.

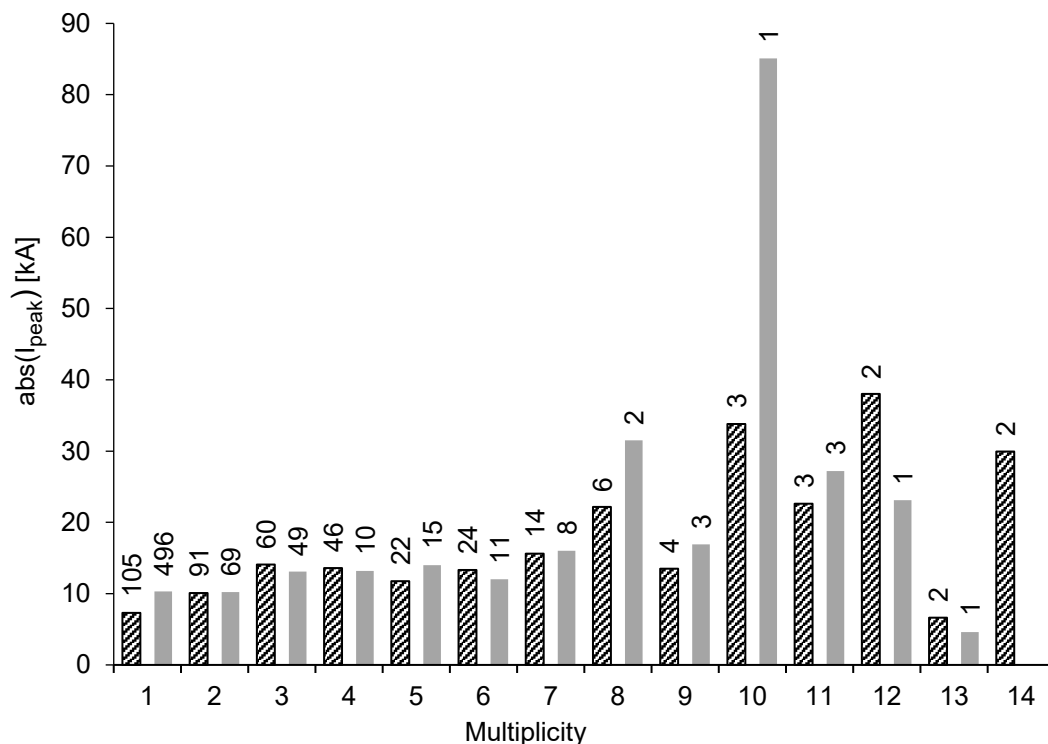


Figure 22: Negative median FI peak current versus multiplicity of a flash (dashed) and versus multiplicity per GSP (grey); Peak current shown as absolute values; Number of events on top of each bar

Figure 23 shows the same analysis for a maximum multiplicity of eight, both for flashes and per GSP. To prove the increase of the peak current of the first stroke in correlation with higher multiplicity, same for flashes and per GSP, a linear regression of the median FI peak current versus multiplicity of a flash and versus multiplicity per GSP was calculated in addition. The given expressions and the shown linear trend lines in Figure 23 confirm the increase of the return stroke peak current of the first stroke in correlation with higher multiplicity, for flashes and per GSP.

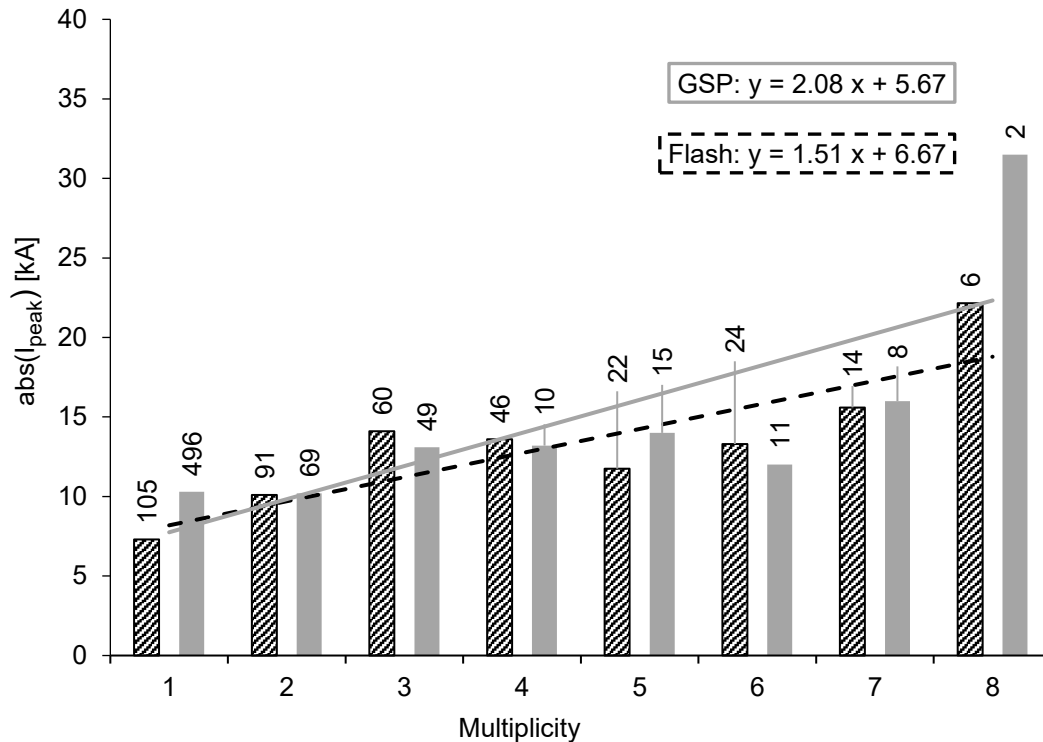


Figure 23: Negative median FI peak current versus multiplicity of a flash (dashed) and versus multiplicity per GSP (grey) with linear trend line for each analysis (trend equations in frames); Maximum multiplicity value of 8; Peak current shown as absolute values; Number of events on top of each bar

6.3.4 Comparison with Values Available in the Literature

Peak current distributions have nowadays been included in all international and national lightning protection standards (e.g. OVE 62305-1, 2012 [64]). Rakov et al. (CIGRE TB 549, 2013 [13]) stated that the direct current measurements by Berger and co-workers (e.g. Berger et al., 1975 [40]) in Switzerland remain the primary reference for both lightning research and lightning protection studies. Berger's peak current distributions have been generally confirmed by direct current measurements in Japan, Austria, and Florida (see CIGRE TB 549, 2013 [13]).

The shown distributions in subsection 6.3.2 have been carried out from return stroke peak currents calculated by the LLS. Previous analyses of median return stroke peak current data from Austria, Belgium and France can be found in Schulz et al., 2016 [19]. A value of -12 kA is obtained for all analyzed median return stroke peak currents for VFRS measurements in Austria from 2009 to 2012. Median stroke peak currents for VFRS measurements correlated to EUCLID LLS return stroke peak currents in Belgium (2011) are in the range of -18 kA and in the range of -16 kA for France (2012 – 2013). The calculated median return stroke peak current for all strokes over the whole measurement period (2015, 2017 and 2018) for this analysis is -9.4 kA (see Table 13). This is again lower (22 %) than the lowest value shown

above for previous measurement campaign in Austria. Compared to the detected values for Belgium, the present median return stroke peak current of -9.4 kA is almost 50 % lower. The same field to current conversion factor was used for all shown LLS data analyses (used current conversion factor is validated for negative subsequent strokes, with a return stroke peak current lower than -60 kA only; see Diendorfer et al., 2007 [23]). Nevertheless all reported values from median return stroke peak currents correlated with ground truth VFRS data show significantly lower values than the reported median peak currents of the direct current measurements of Berger et al., 1975 [40].

Analyses of multiple-stroke flash characteristics reported in different studies are shown in Table 14.

Table 14: Summary of negative multiple-stroke flash characteristics reported in different studies

Location	Year	Total Number of Flashes	Flashes with SU Strokes		Type of records
			at least one SU Stroke Peak greater than the FI	with Field Peaks greater than the FI	
			%	%	
Florida [65]	1979	46	33	13	E-Field and TV
Sweden [51]	1992 -1993	276	24	15	E-Field
Sir Lanka [54]	1993	81	35	12	E-Field
Austria [34]	1996	15905	51	–	LLS
Austria [35]	2015	81	49	32	E-Field
Brazil [66]	2007	259	38	20	E-Field
Sweden [67]	2006	93	32	18	E-Field
Florida [62]	2006	176	24	21	E-Field
Austria (present study) ¹	2015, 2017, 2018	241	41	14	E-Field and Video

¹ LLS peak currents assumed to be proportional to measured field peaks

The present analysis showed a percentage of 41 % of multiple-stroke flashes exhibiting a SU stroke with a peak current larger than the FI stroke and considering all three analyzed measurement periods (2015, 2017 and 2018). For these cases, at least one following SU stroke within the flash showed a higher peak current than the FI stroke. The calculated value is lower than the results shown in previous analyses for Austria (49 % by Schulz and Diendorfer, 2006 [36] to 51 % by Diendorfer et al., 1998 [35]). These relatively high values could, e.g., originate from misclassifications of field pulses from preliminary breakdown as CG strokes. Such misclassified strokes would be classified as FI strokes in a flash, if they fulfill the time and spatial grouping criteria (Cummins et al., 1998 [32]). Rakov et al. (CIGRE TB 549, 2013 [13]) stated that about one third of multi-stroke flashes contain at least one stroke with a higher field peak or peak current than the first stroke. Our results show an even higher percentage of such multi-stroke flashes (41 %). Studies of other countries show similar values but also much lower ones for similar analyses (24 % to 38 %; see Table 14). Comparing all SU strokes with SU strokes with a higher return stroke peak current than the FI1 for flashes and per GSP only revealed that 14 % of the total SU strokes having a peak current larger than the first stroke for flashes. This value is at the lower end of the percentages shown in the literature (12 % to 32 %; see Table 14). The highest percentage was calculated again in one of the previous studies for the Austrian region (Schulz and Diendorfer, 2006 [36]). LLS peak currents have been assumed to be proportional to the measured electric field peaks for this analysis (see Nag et al., 2008 [62]).

6.4 Location Accuracy of the LLS for Negative Flashes

6.4.1 Location Accuracy Distribution

The location accuracy (LA) distribution has been calculated for all three investigated years by calculating the distance of the subsequent stroke location to the first stroke location for all strokes following the same channel to ground (see subsection 5.2.4). Table 15 shows the median LA and 95 % LA for all three years and in total. A bug, fixed by a later update, in the LLS location algorithm caused the relatively large 95 % LA value for 2015 compared to 2017 and 2018.

Table 15: Values for median LA and 95 % LA for 2015, 2017, 2018 and total for negative flashes

Year	Flashes for LA calculation	SU Strokes for LA calculation	Median LA	95 % LA
			m	km
2015	63	163	95	2.8
2017	34	77	130	1.5
2018	87	235	90	0.9
Total	184	475	100	1.6

Figure 24 shows the calculated LA distributions for the merged data set of 2015, 2017 and 2018. Only LA distances up to 3.5 km are shown in this figure. Just for 2015 four values larger than 3.5 km have been observed.

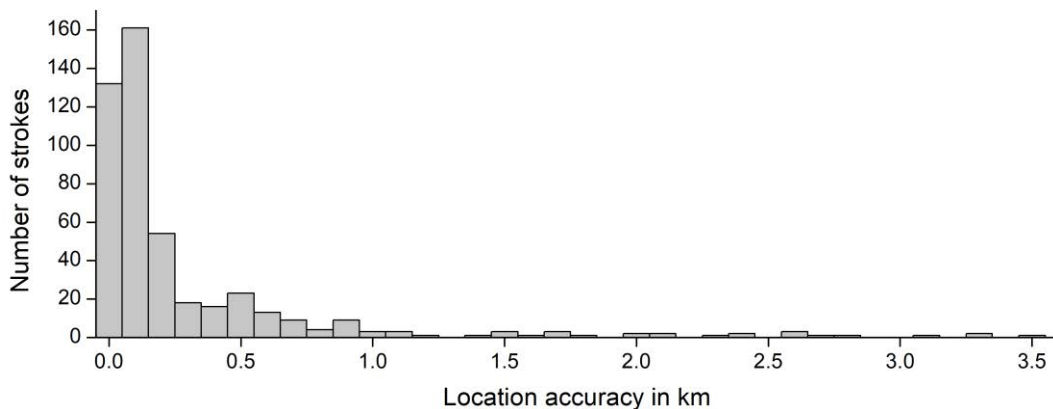


Figure 24: Location accuracy distribution for merged data of 2015, 2017 and 2018 of negative flashes

6.4.2 Location Accuracy for Particular Channel Geometries

For this analysis, all strokes used for the LA calculation have been manually categorized in strokes with a nearly straight or an inclined 2D channel geometry (subjective categorization by the author). This analysis shall show the influence of channel inclination of CG strokes on the detection quality and so even at the LA. After separation in straight and inclined category, a new median LA for each individual category was determined. As described in section 3.2 the calculation of the strike point location by the LLS is nowadays based on a combined method

of MDF and TOA (Diendorfer, 2007 [23]). The location calculation is based on time stamps derived from the measured electromagnetic fields. Those time stamps are related to field onsets, which are related to processes in the lower few hundred meters of the return stroke channel. For that reason, the bottom section of the channel is assumed to be the crucial part of the channel for this analysis. Figure 25 shows an example of strokes categorized as straight (left) and inclined (right) channels of strokes recorded in 2018 (height of cloud base was approximately 3000 to 4000 m above sea level, height of GSP was approximately 1200 to 1500 m above sea level).



Figure 25: Straight (left) and inclined (right) leader channels of strokes recorded in 2018

The results of the new LA calculation after the separation of strokes in straight and inclined leader channel showed almost no difference in the LA analysis. Median LA values of 100 m for straight (369 strokes) and 99 m for inclined channels to ground (58 strokes) have been determined. Also, for the 95 % LA similar values have been calculated (approximately 1.4 km for strokes with straight and 1.5 km for strokes with inclined channels at their bottom section; see Table 16). The more or less identical values of LA for both categories leads to the conclusion, that the inclination of the bottom section of the channel to ground has almost no influence on the LA of the LLS.

It should be kept in mind that analyses with video records from one direction only provide two-dimensional data. This could lead to some inaccuracies in the performed categorization. Because of the very small deviation between LA values obtained for the two categories (straight, inclined) this influencing parameter is insignificant for the preset analysis.

Table 16: Comparison of number of negative strokes used for LA calculation, median LA and 95 % LA for straight and inclined stroke channels for merged data of 2015, 2017 and 2018

	Straight Channels	Inclined Channels
Number of Strokes	369	58
Median LA [m]	100	99
95 % LA [m]	1392	1525

For 2015, 2017 and 2018, LA values larger than 1 km have been caused by strokes to same GSPs but different channels to ground (see Figure 26).

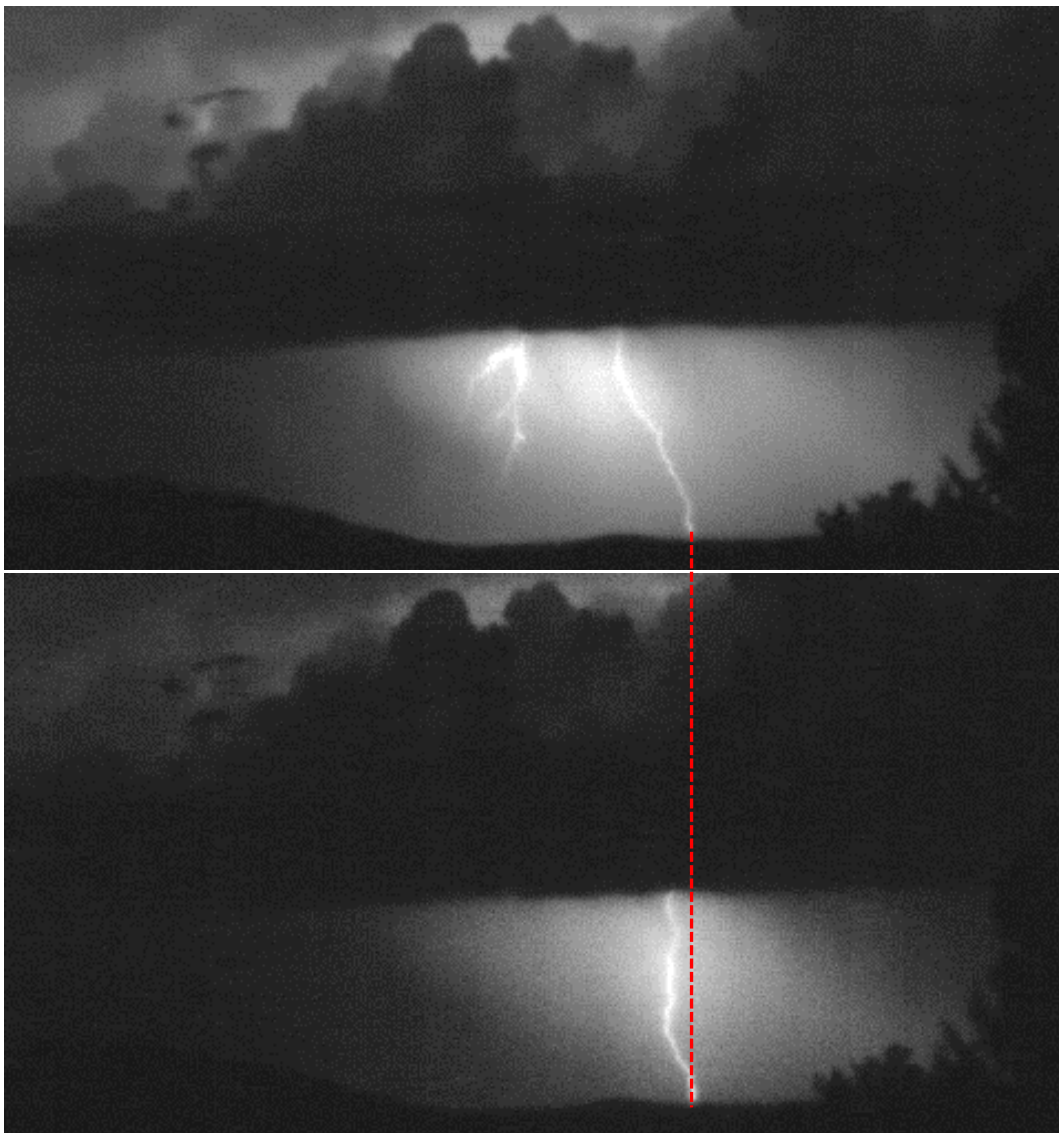


Figure 26: FI and SU stroke appearing as same GSP for this 2D analysis but with different channels to ground; dashed red line indicates the GSP

Two video frames of a FI stroke and a following SU stroke recorded in 2015 are shown in Figure 26 (interstroke interval approximately 77 ms; dashed red line indicates the GSP). For this case a LA of 1.48 km was calculated for the location of the SU strokes relative to the FI stroke location. Again, it should be mentioned that the 2D observation method with only one camera limits the GSP categorization accuracy.

Forked strokes are an additional phenomenon of naturally occurring lightning discharges. If two channel branches start their propagation from the cloud to ground at the same time and propagate with the same speed towards ground until both leader branches connect to ground, those events are called forked strokes (see Figure 27).

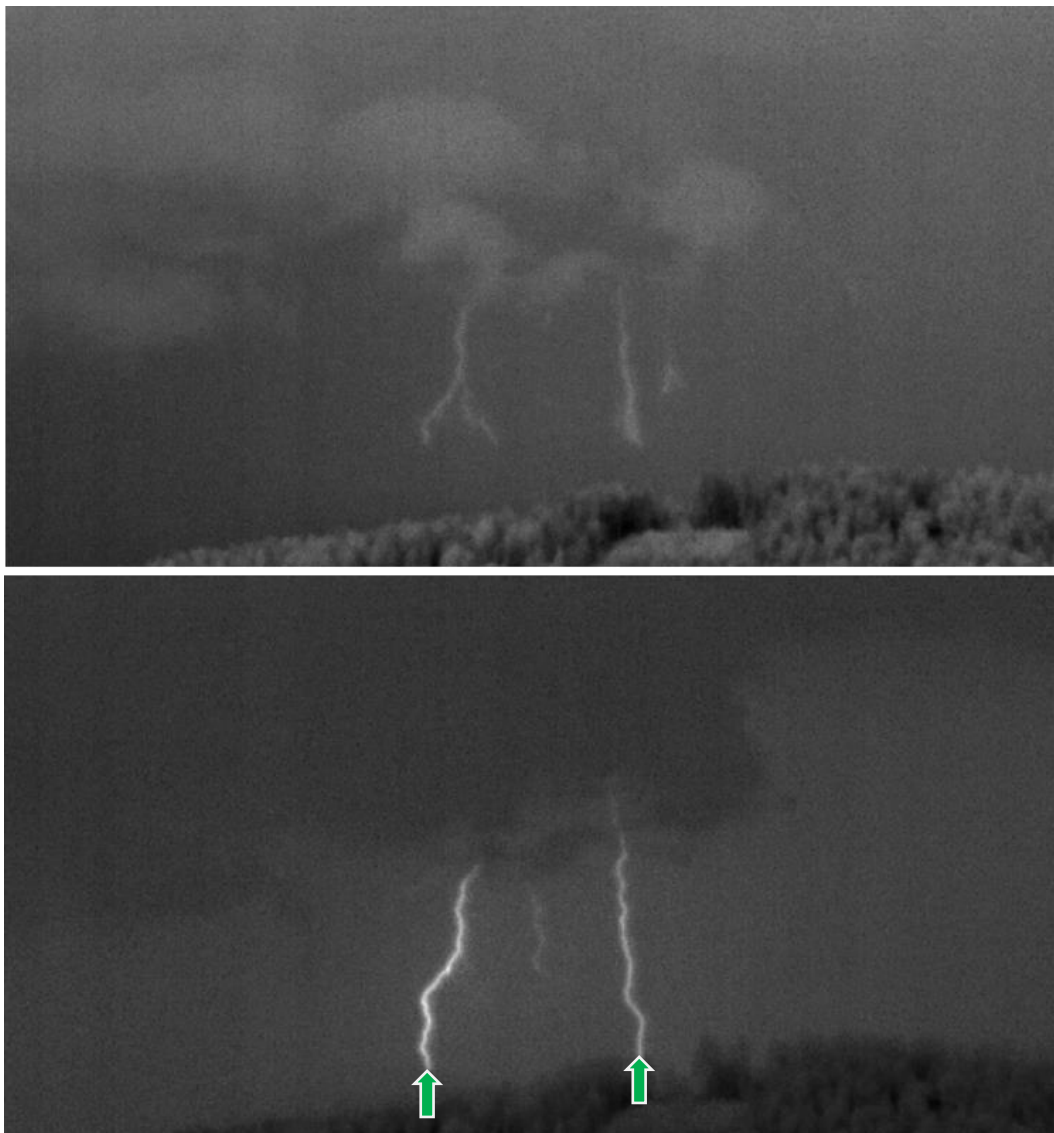


Figure 27: Two successive video frames of a forked stroke stepped leader and its two return strokes from different GSPs (highlighted)

Ballarotti et al., 2005 [68] showed six flashes where two channels remained connected to ground simultaneously. Saraiva et al., 2014 [69] analyzed 22 forked strokes, recorded during observations of the RAMMER project in 2013. The forked strokes are responsible for LA values larger than 1 km too. Such terminations are not easily detectable with VLF/LF LLS because of the quasi-simultaneous strike to ground. Therefore, an improvement of location errors caused by this type of strokes is not easily possible. Figure 27 shows two successive video frames of such a forked stroke recorded in 2018 (FI stroke of a two stroke flash; time interval between video frames 500 μ s). Both leader branches appear at the cloud base at the same time, propagating downward and terminated almost simultaneously in the two GSPs on two different hills (video recording speed limits the time resolution). The electric field record of the forked stroke showed a second field peak after the first stroke caused by the second ground contact (time difference of 46 μ s). Further, the SU stroke of this flash followed the visible right channel in Figure 27 after approximately 50 ms. The LLS detected two strokes and the LA calculation showed a distance of 2.67 km between the FI and the SU stroke in this case.

6.4.3 Comparison with Recent Values Available in the Literature

Due to the ongoing improvements in the sensor technology, the localization algorithm and the continuous adaption of the LLS only recently reported LA value of the ALDIS/EUCLID system shall be analyzed in this subsection. To compare these values with values from other large scale lightning detection networks, LA values of the most recent ground truth data analyses for the U.S. NLDN, the Brazilian LLS RINDAT and Japanese Lightning Detection Network (JLDN) will be shown. LA values of previous VFRS measurements have been shown for the EUCLID system by Schulz et al., 2016 [19]. They showed LA calculations for VFRS data correlated with LLS data of the Austrian region in 2009, 2010 and 2012. In the same publication, also LA values for VFRS measurements in Belgium (2011) and France (2012 and 2013) correlated to LLS data have been presented. LA calculations by using data of the instrumented Gaisberg Tower has been shown by Schulz et al., 2016 [19]. Heidler and Schulz, 2016 [70] compared direct current measurements from the Peissenberg Tower with EUCLID LLS data in 2016. Matsui et al., 2015 [71] compared the JLDN LLS data with findings for large scale LLS like EUCLID and NALDN by correlating LLS data with direct current measurements at a wind turbine equipped with a Rogowski coil. For the U.S. NLDN two publications show recent analyses of LLS LA analyses correlated with rocket triggered lightning events in Florida (Mallick et al., 2014 [72]) and high speed video observations of lightning strikes to wind turbines in Kansas (see Cummins et al., 2014 [73]). Ballarotti et al., 2006 [74] showed recent analyses

for Brazil and analyzed CG strokes recorded during high speed video observations correlated with RINDAT LLS data. Table 17 shows a summary of the median LA values presented in the different studies.

All data should be seen as snapshot of the LA performance of the LLS for the given observation period. As shown in Table 15 already small variations on the system side (e.g. software upgrade) can lead to variance (see 95 % LA value for present analyses of data from 2015).

Table 17: Median LA values, number of negative strokes used for LA calculation and observation methods for different studies

Country	Year	Observation Method	Number of Strokes	Median LA
				m
Brazil [74]	2003 - 2004	Video	26	3400
Austria [19]	2009 - 2010	VFRS	119	326
Belgium [19]	2011	VFRS	25	600
Austria [19]	2012	VFRS	108	157
France [19]	2012	VFRS	14	256
USA (Florida) [72]	2004 - 2013	RTL ¹	292	309
USA (Kansas) [73]	2012 - 2013	Video	85	126
France [19]	2013	VFRS	143	90
Japan [71]	2013 - 2014	Wind Turbine	6	361
Austria [19]	2014	Tower	100	89
Germany [70]	2011 - 2015	Tower	30	144
Austria (present study)	2018	VFRS	235	90

¹ Rocket Triggered Lightning

6.5 Detection Efficiency of the LLS for Negative Flashes

6.5.1 Analysis of the Detection Efficiency

For the analysis of the DE of an LLS two different types of DE have to be considered, the flash DE and the stroke DE. The stroke DE is calculated as percentage of LLS detected strokes out of the total occurred strokes (seen on the video record; see subsection 5.2.5). This category is additionally separated into detected and correctly detected strokes (see Table 18). This additional strict categorization (every assignment of the LLS detection is confirmed as correct with VFRS data; e.g. polarity, categorization as CG stroke) should give additional insights of the quality of the LLS detections. As described in subsection 5.2.5, the flash DE is calculated in the same way but for the strict categorization of correctly detected flashes only (FI1 strokes only have to be classified correctly). Table 18 shows the number of flashes and strokes recorded by the VFRS, the LLS and the results for the flash and stroke DE for the three years and in total.

Table 18: DE of the ALDIS LLS for negative detected strokes, correctly detected strokes and flashes for the year 2015, 2017, 2018 and total

Year	Type	VFRS	ALDIS LLS detected	DE - detected Strokes	ALDIS LLS correctly detected	DE - correctly detected Flashes/ Strokes
				%		%
2015	Flashes	153	—	—	147	96.1
	Strokes	514	452	87.9	440	85.6
2017	Flashes	94	—	—	93	98.5
	Strokes	317	279	88.0	242	76.3
2018	Flashes	217	—	—	214	98.6
	Strokes	693	666	96.1	548	79.1
Total	Flashes	464	—	—	454	97.8
	Strokes	1524	1397	91.7	1230	80.7

6.5.2 Reason for Flash and Stroke Detection Efficiency Variations

Flash DE values show constantly high values for the whole investigated period. The flash DE increased from 96.1 % in 2015 to 98.6 % in 2018 and is comparable to the merged DE value of 98 % for the years 2009 to 2012 (see Schulz et al., 2016 [19]). The merged DE for all three years shows a total value of 97.8 % for this analysis. Percentages for detected and correctly detected strokes show a higher variance over the three years. The stroke DE for correctly detected strokes in 2017 (76.3 %) and 2018 (79.1 %) is lower than the DE for correctly detected strokes for 2015 (85.6 %) and the one for investigations of 2009 until 2012 (84 %; see again Schulz et al., 2016 [19]). For 2018 the stroke DE for correctly detected strokes show an increase of around 3 % compared to 2017. The stroke DE for detected strokes shows a strong increase from 88.0 % in 2017 to 96.1 % in 2018.

The reason for the observed decrease of the stroke DE for the correctly detected strokes in 2017 and 2018 was a new intra-cloud/could-to-ground (IC/CG) classification algorithm provided by the LLS manufacturer, which was implemented by ALDIS in 2016 and performed worse for negative CG strokes below -15 kA. Kohlmann et al., 2017 [59] showed a more detailed analysis about the IC/CG classification performance in 2017. In the analyzed data, approximately 90 % of the negative stroke peak currents of non-correctly detected (misclassified) strokes of 2017 are below -15 kA. In 2018, more than 95 % of the non-correctly detected strokes had a peak current lower than -15 kA (see subsection 6.2.1). The misclassified strokes below -15 kA showed a distribution of 30 % FI1, 30 % SU1, 15 % FI2 and 15 % SU2 strokes for the merged data set (2017 and 2018). The remaining 10 % are distributed among FI and SU strokes of higher stroke order.

6.5.3 Comparison with Recent Values Available in the Literature

Nag et al., 2015 [9] showed a summary of expected performance ranges of LLS. For medium range LLS (up to 400 km of sensor distance) an expected DE of 70 % to 90 % for strokes and 85 % to more than 95 % for flashes is expected. Since continuous LLS improvements also strongly influence the DE values in this case, only data from current publications will be compared in this section. Flash and stroke DE values of recent studies based on ground truth data for the ALDIS/EUCLID, U.S. NLDN, and the Brazilian LLS RINDAT are shown in Table 19.

Table 19: DE values for negative flashes and strokes as well as observation methods for different studies

Country	Year	Observation Method	Type	Data set	DE
					%
Brazil [74]	2003 - 2004	Video	Flashes	206	87.4
			Strokes	413	54.7
Belgium [19]	2011	VFRS	Flashes	—	—
			Strokes	928	84
Austria [19]	2009 - 2012	VFRS	Flashes	—	—
			Strokes	210	84
USA (Kansas) [73] ⁴	2012	Video	Flashes	190	96.3
			Strokes	529	88.5
USA (Florida) [72]	2004 - 2013	Rocket Triggered Lightning	Flashes	90	94
			Strokes	388	75
France [19]	2012 - 2013	VFRS	Flashes	259	93
			Strokes	833	89
USA (Kansas) [73] ⁴	2013	Video	Flashes	103	96.1
			Strokes	208	69.2
Austria [19] ⁵	2005 - 2014	Tower	Flashes	—	96
			Strokes	—	70
Germany [70]	2011 - 2015	Tower	Flashes	11	100
			Strokes	37	81
Austria (present study) ⁶	2015, 2017, 2018	VFRS	Flashes	454	97.8
			Strokes	1230	80.7

DE values of previous VFRS measurements have been presented for the EUCLID system by Schulz et al., 2016 [19]. They showed flash and stroke DE calculations for VFRS data

⁴ No definition about polarities of the analyzed flashes and strokes

⁵ For strokes with a return stroke peak current larger than 2 kA

⁶ Only correctly detected flashes and strokes (see subsection 5.2.5)

correlated with LLS data of the Austrian region in 2009, 2010 and 2012. In the same publication, also DE values for VFRS measurements in Belgium (2011) and France (2012 and 2013) correlated to LLS data have been presented. DE estimates by using data of the instrumented Gaisberg Tower has been shown by Schulz et al., 2016 [19]. Heidler and Schulz, 2016 [70] obtained DE values for direct lightning current measurements at the Peissenberg Tower correlated with EUCLID LLS data in 2016. For the U.S. NLDN two publications show recent analyses of LLS DE analyses correlated with rocket triggered lightning events in Florida (Mallick et al., 2014 [72]) and high speed video observations of lightning strikes to wind turbines in Kansas (see Cummins et al., 2014 [73]). Ballarotti et al., 2006 [74] showed recent analyses for Brazil and analyzed negative CG strokes recorded during high speed video observations correlated with RINDAT LLS data. Table 19 shows a summary of flash and stroke DE values for the different studies. Note – Measurements at the Gaisberg Tower (Schulz et al., 2016 [19]) and the Peissenberg Tower (Heidler and Schulz, 2016 [70]) include mostly strokes in upward initiated flashes. Those type of flashes (same for triggered lightning) do not contain a first stroke, which in general exhibits a larger peak current. Therefore, this type of measurement underestimates the DE.

6.6 Analyses of Positive Flashes

6.6.1 Single Stroke Flashes

In this section, positive single stroke flashes, detected by the VFRS and the LLS, shall be compared. 59 positive CG flashes and 71 positive CG strokes are analyzed in total (see Table 2 and Table 20). The total sample size of the present analysis is situated at the lower end of the ones stated in the literature. Table 20 shows the calculated percentage of single stroke flashes in 2015, 2017 and 2018 as well as in total for VFRS and LLS data. The calculated percentage for LLS data shows lower values in 2015 and 2018 compared to VFRS analyses. The lower number of single stroke flashes of the LLS in 2015 originate from double detections of the same stroke by the LLS (detected by the LLS as multiple stroke flashes). The two missing single stroke flashes in the LLS data in 2018 (20 for LLS data versus 22 for VFRS data; see Table 20) are caused by the misclassification of an initial breakdown pulse as CG stroke and the grouping of an IC stroke with a CG single stroke flash to a multiple stroke flash by the LLS.

Results for VFRS data in 2015 and 2018 are in a similar range like the one calculated for the total data set. They range from 81 to 82 % (see Table 20). This small variation could originate from inter annual differences of thunderstorm behavior over the two years. A comparison on an annual basis is just reasonable for the measurements of 2015 and 2018 because of the small data set in 2017. Calculated values for these two years are in the range of previously published values (see Table 21).

Table 20: Positive single stroke flash percentage for VFRS and LLS data from 2015 to 2018; Number of single stroke flashes in parenthesis

Measurement Period	VFRS Total Flashes	Single Stroke Flashes for VFRS data	LLS Total Flashes	Single Stroke Flashes for LLS data
		% (Number)		% (Number)
2015	28	82 (23)	28	71 (20)
2017	4	100 (4)	4	100 (4)
2018	27	81 (22)	27	74 (20)
Total	59	83 (49)	59	75 (44)

The previously published results of single stroke flash analyses are based on numerous studies and international publications, conducted in various regions all over the world during the last decades. Baharudin et al., 2016 [75] published the lowest value in the literature for measurements in 2010 and 2011 (63 %). For their analyses, they used data of electric field measurements from Sweden. Measurement analyses for Florida (Nag and Rakov, 2012 [76]) and for the merged data set from Austria, Brazil and the U.S. (Arizona and South Dakota) of Saba et al., 2010 [77] show a percentage of 81 %. Nag and Rakov, 2012 [76] used electric field records for their analyses in the U.S. (Florida), measurements of Saba et al., 2010 [77] have been conducted with high speed video cameras correlated with LLS data. Recent measurements from Hazim et al., 2017 [78] in Indonesia showed the same percentage of 83 % for positive single stroke flashes like the present analyses for Austria (merged data set for 2015, 2017 and 2018). Analyses in Indonesia have been conducted by using electric field measurements. VFRS data has been correlated again with LLS data for the present analyses.

Table 21: Summary of results for the percentage of positive single stroke flashes of the present and previous analyses by various authors

Location	Year	Measurement system	Sample size	Positive Single Stroke Flashes
				%
USA [79]	2005	Video	204	96
Austria, Brazil and USA [77]	n.s.	Video	103	81
Florida [76]	2007 - 2008	Electric Field	53	81
China [80]	2009 - 2010	Electric Field	185	95
Sweden [75]	2010 – 2011	Electric Field	107	63
Indonesia [78]	2014	Electric Field	77	83
Austria (present study)	2015, 2017, 2018	Video	59	83

The highest percentages of positive single stroke flashes have been reported by Fleenor et al., 2009 [79] (96 %) and Qui et al., 2013 (Qie et al. 2013) (95 %). Fleenor et al., 2009 [79] used data of high speed video records from central Great Plains in correlation with LLS data too, whereas Qui et al., 2013 (Qie et al. 2013) used data of a VLF/LF lightning detection network for their analyses in northeastern China.

6.6.2 Multiplicity

To calculate the mean multiplicity for positive flashes for each year and in total, the VFRS and LLS data of the same events have been compared. The results for this analysis are shown in Table 11. The calculated values for the true multiplicity, determined with the VFRS data, are higher than the results from previous measurements in the Austrian Alps (1.2 for the present analyses versus 1.1 for analyses of VFRS data from 2008 to 2012 respectively (Schulz et al., 2013 [81])). The analyzed LLS data for 2015 shows a multiplicity of 1.6 compared to the ground truth VFRS data of 1.2 for the same year. That implies a number of multiple stroke flashes of

57 % (at least two strokes per flash included) for the LLS data set of 2015. This difference is mainly caused by misclassified IC pulses as CG strokes (four flashes; e.g. one stroke visible in the video was grouped with eight IC strokes wrongly classified as CG strokes in the LLS data). Multiplicity parameters for 2015 and 2018 show the same results. Nevertheless, the relatively small data set for 2017 (four flashes; see Table 22) should be noticed.

Table 22: Mean multiplicity of positive flashes for VFRS and LLS data (2015, 2017, 2018 and total)

Year	Mean VFRS Multiplicity	Mean LLS Multiplicity
2015	1.21	1.57
2017	1.00	1.00
2018	1.22	1.22
Total	1.20	1.37

6.6.3 Positive Return Stroke Peak Currents of LLS Detections

Table 23 shows the mean, median and 95 % values of LLS return stroke peak currents for all correctly detected positive strokes for each investigated period and in total. A total of 27 return stroke peak currents have been analyzed in 2015, 4 in 2017, and 28 in 2018. The number of strokes is by incidence the same as for flashes shown in Table 20 because of the usage of the correctly detected strokes only.

Table 23: Mean, median and 95 % value for return stroke peak currents of the ALDIS LLS detections for all positive strokes for the year 2015, 2017 and 2018 and in total

Year	Number of Strokes	Mean	Median	95 % Value
		kA	kA	kA
2015	27	59.4	43.7	163.0
2017	4	40.7	47.6	57.9
2018	28	54.4	41.8	120.6
Total	59	55.8	43.8	145.1

For this analysis, no discrimination of FI and SU strokes was carried out because of the small data set of multiple stroke flashes. The detected minimum and maximum return stroke peak current for all strokes was 8.1 kA and 331.9 kA for 2015, 8.1 kA and 59.5 kA for 2017, and 8.6 kA and 202.2 kA for 2018, respectively. Compared to results of older VFRS measurement campaigns in the Alps reported by Schulz et al., 2013 [81], the resulting values in this study for positive median return stroke peak currents of all strokes show around 29 % higher values for 2015, around 40 % higher values for 2017, about 23 % higher values for 2018. Schulz et al., 2013 [81] showed a median return stroke peak current of 34 kA for a merged data set of 2008 to 2010 and 2012 for all used strokes. The median return stroke peak current for the merged data set is again about 29 % higher than the value reported by Schulz et al., 2013 [81]. The median return stroke peak current is about 11 % lower than reported for similar observations for a merged data set from Austria, Brazil and the U.S. too (39.4 kA; see Saba et al., 2010 [77]). Saba et al., 2010 [77] showed a minimum and maximum return stroke peak current value of 4.8 kA and 142 kA, respectively.

For the present and the previous analyses by Schulz et al., 2013 [81], and Saba et al., 2010 [77] the same field to current conversion factor was used for all detected strokes (see section 3.2). Especially for an analysis of flashes with positive polarity, it should be kept in mind that the used current conversion factor is validated for negative subsequent strokes, with a return stroke peak current lower than -60 kA only (see section 3.2). A validation for positive return strokes is still needed (CIGRE TB 376, 2009 [28]) therefore the shown return stroke peak currents have to be seen as rough estimates.

6.6.4 Detection Efficiency

For analyzes of the DE of the LLS again two different types of DE have been considered, the flash DE and the stroke DE. An additional strict separation into detected and correctly detected strokes (every assignment of the LLS detection confirmed as correct with VFRS data; e.g. polarity, categorization as CG stroke; see subsection 5.2.5 and Table 24) shall give additional information about the quality of the analyzed LLS data for positive flash data.

Table 24: DE of the ALDIS LLS for positive flashes, detected strokes and correctly detected strokes for the year 2015, 2017, 2018 and total

Year	Type	VFRS	ALDIS LLS detected	DE - detected Strokes	ALDIS LLS correctly detected	DE - correctly detected Flashes/ Strokes
				%		%
2015	Flashes	28	—	—	26	92.9
	Strokes	34	31	91.2	27	79.4
2017	Flashes	4	—	—	4	100
	Strokes	4	4	100	4	100
2018	Flashes	27	—	—	26	96.3
	Strokes	33	32	97.0	28	84.8
Total	Flashes	59	—	—	56	94.9
	Strokes	71	67	94.4	59	83.1

The flash DE is again calculated in the same way but for the strict categorization of correctly detected flashes only (FI1 strokes only have to be classified correctly). Table 24 shows the number of positive flashes and strokes recorded by the VFRS, the LLS and the results for the flash and stroke DE for the three years and in total.

In 2018, the stroke DE of detected strokes shows a higher percentage than the ones for correctly detected flashes (97.0 % compared to 96.3 % for detected strokes and correctly detected flashes respectively). The analysis of correctly detected flashes only (see subsection 5.2.5) causes this lower value for the flash DE compared to the DE of detected strokes.

6.7 Direct Impact of Lightning Discharges on Power Generation and Transmission Systems

6.7.1 Lightning Strikes to two Wind Turbines

During the measurement campaign of 2018 a flash that directly struck two wind turbines has been recorded on the 8th August 2018 at 15:45:20 UTC (see Figure 28). All four strokes of this flash can be clearly identified as downward strokes by analyzing the high speed video record. Montanyà et al., 2016 [82] stated that downward lightning to high buildings, such as wind turbines, are more likely during deep convective situations (e.g. warm season thunderstorms) and, in addition, downward lightning strokes are the most frequent type of lightning in general. The exposure and the regional ground flash density are the two key parameters for the overall number of downward lightning strikes to a wind turbine (see again Montanyà et al., 2016 [82]). A percentage of 30.3 % is given as an average outage rate for wind turbines in low mountain (pre-alpine) areas of Europe caused by direct strikes. It is noted by the members of the working group that the shown percentage is based on statistics obtained in late 1990 and that in the meanwhile wind turbines have doubled their total height but no data for those turbines were available at that time (see CIGRE TB 578, 2014 [83]).

The wind turbines that were struck by this flash are part of a wind farm comprised of 21 generators situated on a mountain ridge at a height of about 1450 m above sea level (see Figure 28). Each of these three-bladed wind turbines has a maximum height of around 120 m and a nominal power of 2.3 MW.

The recorded flash consists of four strokes. Three strokes struck turbine #1 (first stroke (F11) and two subsequent strokes (SU1) within the same channel) and the fourth stroke (F12) followed a new channel and struck turbine #2 in Figure 28. A downward stepped leader is visible in the video before the first return stroke. For the fourth stroke, a downward stepping process is visible too. A correlation of the VFRS data and the LLS data is possible because of the used GPS time. The installed protection relays in each wind turbine are synchronized to server time (time resolution: seconds) but no other event was recorded at the wind farm on that day. For that reason, a correlation of VFRS and LLS data with the network fault protocol of the wind park operator was possible.

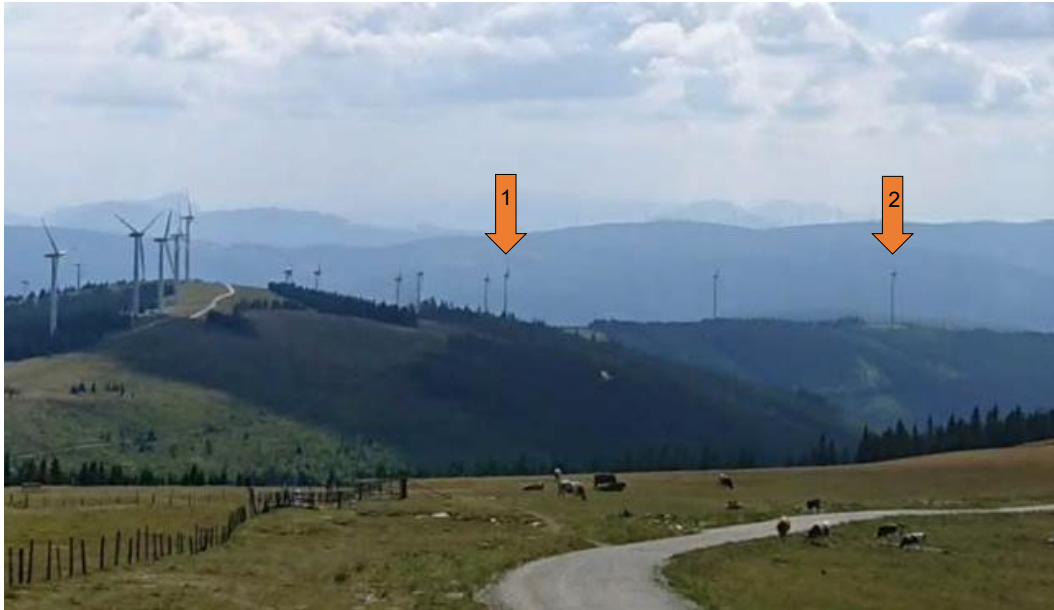


Figure 28: Wind farm on pre-alpine mountain ridge (ca. 1450 m a.s.l.); Stroked wind turbines #1 and #2 highlighted⁷

The LLS data and the distances between the wind turbine and the LLS provided locations are given in Table 25. Six frames of the high speed video of this case are shown in Figure 29. The negative flash, including all four strokes, was correctly detected by the LLS. The strikes to the first wind turbine triggered the installed earth-fault detection relay of this wind turbine. Stroke one to three had LLS estimated return stroke peak currents in the range of -6 kA to -23 kA (see Table 25).

The strike points of the three strokes were located at distances ranging from 65 to 140 m to the first turbine (first stroke one (FI1) and two subsequent strokes (SU1) within the same channel; see Table 25). The GSP of stroke four (first stroke two (FI2); new GSP) was detected by the LLS in a distance of 775 m to the second wind turbine. This stroke had a very low return stroke peak current of -3 kA and did not trigger the earth-fault detection relay of turbine two. The high speed video shows a direct strike of stroke FI2 to the second wind turbine followed by a continuing current with a duration of 117 ms.

⁷ © Google Maps

Table 25: LLS data with distance to wind turbine #1 and #2 in m (Return stroke peak current in kA, sn = stroke number, nbdf = sensor detections, nbdfit = sensors data with sufficient quality, maxis = major axis, ki2 = quality criteria, ToS = type of stroke, Flx = first stroke to GSP x, SUx = subsequent stroke to GSP x)

Latitude	Longitude	Return Stroke Peak Current	sn	nbdf	nbdfit	maxis	ki2	ToS	Distance
		kA				km			m
47.5316	15.7050	-23.2	1	56	19	0.1	0.30	F11	64
47.5314	15.7054	-6.3	2	9	8	0.1	0.60	SU1	99
47.5317	15.7060	-9.9	3	15	12	0.1	0.50	SU1	137
47.5403	15.7009	-2.9	4	5	3	0.1	0.20	F12	775

Figure 29 shows the frames of the high speed video for the stepped leader of F11, first return stroke (F11), subsequent strokes 2 and 3 (SU1), stepped leader of F12 and the second return stroke (F12).

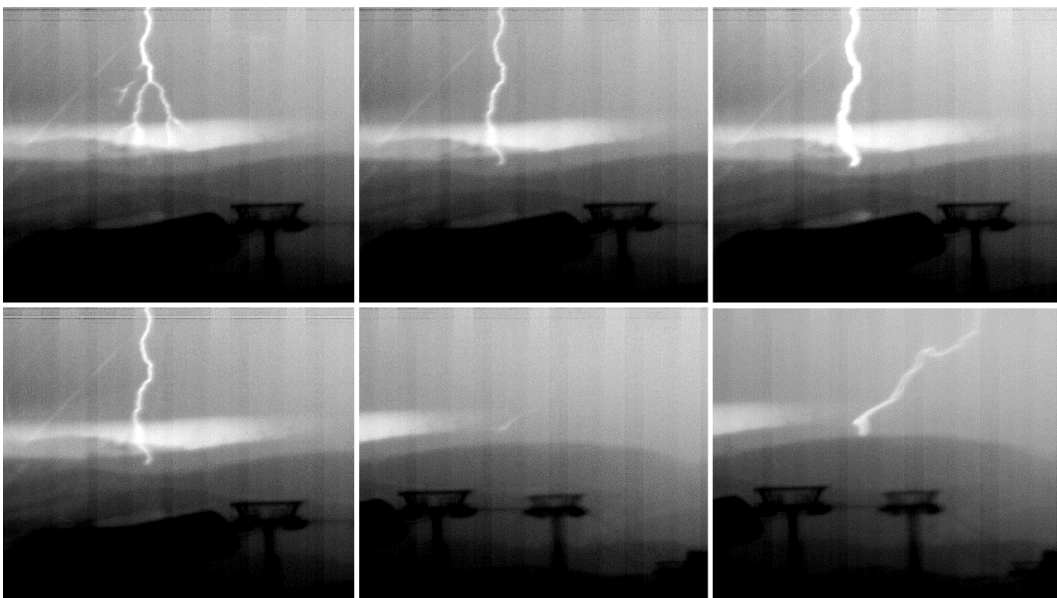


Figure 29: Stepped leader of F11, first return stroke (F11), subsequent strokes 2 and 3 (SU1), stepped leader of F12 and second return stroke (F12) from top left to bottom right

The locations of the wind turbines, LLS detections and 50 % confidence ellipses of the located strokes are shown in Figure 30.

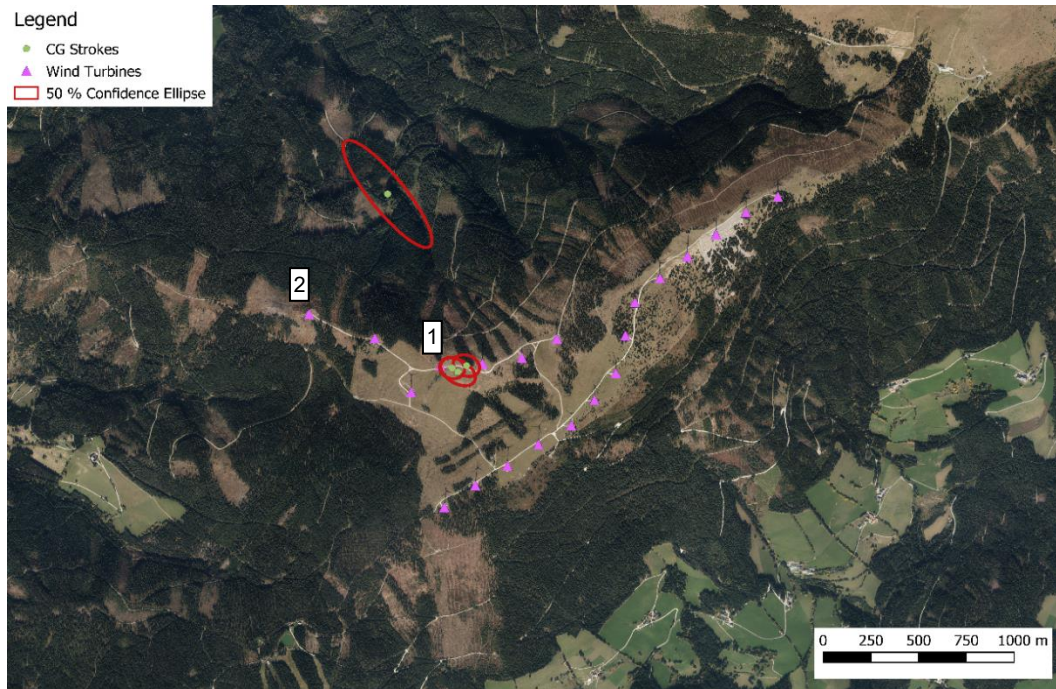


Figure 30: Locations of the wind turbines, LLS detections and 50 % confidence ellipses of the strokes; Strokes 1 to 3 struck wind turbine #1, stroke 4 struck wind turbine #2; ESRI satellite map in the background

6.7.2 Lightning Strike to a Railway Overhead Line

As a second case of direct strikes to infrastructures, a lightning strike to a railway overhead line shall be analyzed in this subsection. This flash, consisting of three strokes was recorded on 3rd July 2018 at 16:47:49 UTC. All three strokes of this flash can be clearly identified as downward strokes by analyzing the high speed video record. The railway overhead line in the analyzed section consists of a phase wire, mounted on top of concrete towers, and the feeder at the height of the pantograph. The Austrian railway system is operated as a single-phase system and the railway tracks are used as return conductors. The line, operated at a voltage level of 15 kV and a frequency of 16.66 Hz, is connected to two substations. Digital protection relays and inductive instrument transformers are installed in both substations. Figure 31 shows the section of the analyzed track. No train was on the track section at the moment of the lightning strike.



Figure 31: Railway overhead line in the analyzed track section; tower structure highlighted⁸

The recorded flash consists of three strokes, a first stroke (FI1), with a prior visible stepping process from cloud to ground, and two subsequent strokes (SU1). The digital protection relays recorded a fault record for this case. A correlation of the VFRS data and the LLS data is possible because of the used GPS time. Appendix 0 shows the analysis of the electric field and video record by using the available software analysis tools (see section 3.1) for this specific case. The installed relays in the substation are synchronized to server time (time resolution: milliseconds) but no other event was recorded for this day. For that reason, a correlation of VFRS and LLS data with distance protection relay fault records of the Austrian railway operator was possible.

The data of the LLS and the distances between the tower and the LLS provided locations are given in Table 26. The negative flash, including all three strokes, was correctly detected by the LLS. The start time of the short circuit in the digital fault record correlates with the LLS time of the first stroke (time stamp accuracy of distance protection relay in milliseconds). Stroke one to three had an LLS estimated return stroke peak current of -4 kA to -10 kA, respectively. All three strokes struck the same tower (same GSP visible in the video). These three strokes were located at distances ranging from 81 to 1424 m from this tower.

⁸ © Markus Hipfl, bahnbilder.warumdenn.net

Table 26: LLS data for with distance to the railway transmission line tower in m (Return stroke peak current in kA, sn = stroke number, nbdif = sensor detections, nbdfit = sensors data with sufficient quality, maxis = major axis, ki2 = quality criteria, ToS = type of stroke, Flx = first stroke to GSP x, SUx = subsequent stroke to GSP x)

Latitude	Longitude	Return Stroke Peak Current	sn	nbdif	nbdfit	maxis	ki2	ToS	Distance
		kA				km			m
46.7217	14.2894	-10.2	1	16	13	0.1	1.6	F11	1424
46.7330	14.2871	-3.9	2	6	6	0.1	1.2	SU1	160
46.7337	14.2870	-5.5	3	10	10	0.1	1.0	SU1	81

Six frames of the high speed video of this case are shown in Figure 32. The first stroke caused a flashover, visible in the video for a duration of 79 ms, on the affected tower and on two other towers. For this reason, a direct hit to the overhead line can be assumed (see second picture in the bottom row of Figure 32).



Figure 32: Stepped leader, first return stroke (F11), flashover on two towers, subsequent stroke 2 (SU1), flashover on three towers and subsequent stroke 3 (SU1) from top left to bottom right

After 46 ms the line was tripped and after 123 ms the whole fault handling was closed by the distance protection relay. No transient signal changes, caused by lightning discharges, were detected in the digital fault records because of the low sampling rate of the protection relay (20 samples per 16.66 Hz period) and the used inductive instrument transformers. They are installed to generate an image of the 16.66 Hz component for measurement and protection purposes and not for recording transient signals.

The location of the railway track, the affected tower, LLS detections and 50 % confidence ellipses of the strokes are shown in Figure 33.

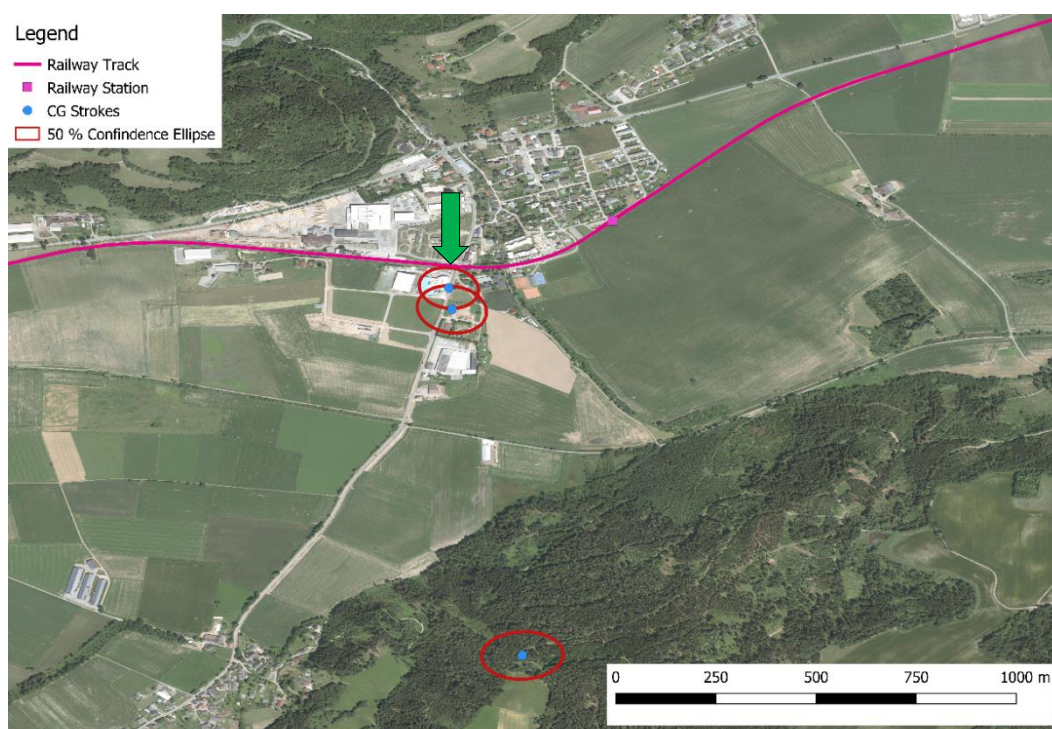


Figure 33: Railway track, locations of the LLS detections and 50 % confidence ellipses of the three strokes; all strokes struck the same tower (highlighted); ESRI satellite map in the background

7 Discussion

7.1 Negative Single Stroke Flashes

Due to the analysis of ground truth data of on-site VFRS measurements, every stroke can be correctly assigned to a flash and insights in real flash distributions can be gathered. The analyzed ground truth measurements of lightning in the Alpine region of Austria show the highest amount of negative single stroke flashes (27 % for the merged data set of 2015, 2017 and 2018) compared to values of other international publications (12 to 24 %, see Table 10). This high percentage of single stroke flashes has a direct influence to flash multiplicity statistics (i.e. the number of strokes per flash). The multiplicity parameter is one of the main characteristics of lightning discharges and is linked to the protection principles of transmission lines for example (Anderson and Eriksson, 1980 [2]).

The percentages of single stroke flashes show considerable variations for the individual thunderstorm days. A range of 4 to 42 % single stroke flashes for VFRS measurements and 0 to 46 % for LLS data has been determined for individual thunderstorm days of 2015, 2017 and 2018 (see Figure 15). The range is comparable with the analysis of Diendorfer et al., 1998 [34]. Similar analyses for measurements in Austria between 2009 to 2015 can be found in Schwalt et al., 2017 [44].

For the performed measurements, annual percentages of single stroke flashes show variations for both, LLS and VFRS data (see Table 6). This varying percentages of single stroke flashes can be caused by the different spectrum of thunderstorm characteristics for individual years. In addition, the different number of measurements over the years can influence each result. The sample sizes of our measurements for negative flashes by year are comparable to sample sizes of other measurements in the literature (see Table 5 and Table 10). The increase of the percentage of single stroke flashes up to 30 % for LLS data for 2017 and 2018 (see Table 6) could be caused, at least in part, by the new IC/CG classification algorithm, which was implemented by ALDIS in 2016. The detected overestimation of single stroke flashes by the LLS described by Poelman et al., 2016 [11] does not occur and is not expected for analyses correlated with VFRS measurements, because of the comparison with ground truth data (i.e. misclassified inter/intra-cloud flashes are not included).

For the analysis of negative single stroke flashes per thunderstorm type, the present data sets of 2015, 2017 and 2018 were merged with data of previous VFRS measurements in Austria of 2009, 2010 and 2012. That is necessary because of the rare occurrence of some

individual thunderstorm types during the whole measurement period. As described in subsection 5.2.2 different thunderstorm types, categorized by the use of radar data (single-, multi- or supercells as well as lines) or vertical wind shear (change of the wind vector both in strength and in direction from 0 to 6 km height) are analyzed.

The analysis of single stroke flashes for different thunderstorm types (manual classification of thunderstorms by using radar data) in subsection 6.1.3 showed similar percentages as for the categorizations by different values of vertical wind shear between 0 and 6 km height (see Table 8 and Table 9). For the calculated single stroke flash percentage of 32 % for a DLS in excess of 20 m/s, it has to be kept in mind that these events are less common (five analyzed thunderstorms; see Table 5). After the combination of all storms with wind shear regimes favoring higher storm organization (DLS > 10 m/s 26 %; see Table 9) into one category, the percentage of single stroke flashes is again similar to the category under weak vertical wind shear (DLS < 10 m/s 27 %; see Table 9).

Two possible hypotheses for the distribution of single stroke flashes for different thunderstorms have been pointed out in Schwalt et al., 2017 [44]. First, organized storms could indeed be more common in the Alpine region than in many other parts of the world. Second, the possibility that the measurements are subject to a sampling bias for the short-lived nature of single cells cannot be discounted. Both hypotheses cannot be confirmed for the present analysis. First, the analyzed data set shows a uniform distribution between the number of analyzed single cells (i.e. DLS < 10 m/s) and organized storms (i.e. DLS > 10 m/s), even if the short-lived nature of single cells makes them often elusive for measurements with a mobile system (see Table 9). Of course the longer lifetime of better-organized thunderstorms enhances the planning and preparation time and makes them more attractive for lightning discharge recordings with a mobile system, but this fact is not reasonable for our measurements over six years (24 thunderstorms at a DLS < 10 m/s versus 37 thunderstorms at a DLS > 10 m/s; see Table 9). Second, in Table 9 the percentages of negative single stroke flashes for classified single cells, or alternatively for thunderstorms under weak vertical wind shear (DLS < 10 m/s), do not show any significant differences to the merged category of multicells, supercells and lines or their equivalent of storms with enhanced vertical wind shear (DLS > 10 m/s).

The review of previous studies showed lower values for the percentage of negative single stroke flashes than the one calculated for the Austrian region in this study. Nevertheless, even analyses performed in the same country resulted in different percentages of single stroke flashes (see Table 10). The different results for Florida could be caused by the use of two different measurement techniques. Zhu et al., 2015 [46] (12 % single stroke flashes) used

electric field measurements for their analysis, whereas the records of Rakov and Uman, 1990 [49] (17 % single stroke flashes) are based on electric field records in correlation with a multiple-station TV system. The total number of analyzed flashes could also be a reason for this deviation (478 flashes for Zhu et al., 2015 [46] versus 76 flashes for Rakov and Uman, 1990 [49]). As already mentioned in subsection 6.1.4, the recorded data are limited to the field of view of the camera for measurements with a camera system or a VFRS. In contrast, every occurring CG flash striking around the recording system within a certain distance can be detected by using electric field records. Therefore, the recorded video data represent for some cases just a fraction of the complete lightning activity, which occurred during the observed thunderstorm. This can be a possible reason for the annual variations obtained for single stroke flash percentages of VFRS and LLS data in the present study using data from 2015 to 2018 (see Table 6).

Results of 24 % single stroke flashes for five thunderstorm days shown by Antunes et al., 2013 [55] and 17 % for 109 storms of Ballarotti et al., 2012 [50] represent again data of the same area (southern Brazil). The records of both studies have been conducted with high speed video cameras in correlation with LLS data (see Ballarotti et al., 2012 [50] and Antunes et al., 2013 [55]). However, the larger percentage of single stroke flashes reported by Antunes et al., 2013 [55] could be related to the limited number of thunderstorm days (random measurement of storms with a higher amount of single stroke flashes) but also by the different spectrum of thunderstorm characteristics in general. Antunes et al., 2013 [55] also found different lightning characteristics with different thunderstorm types, but could not find a direct relation between lightning frequency and thunderstorm type.

Results of almost all previous studies regarding single stroke flashes show data of one particular area in each country (see Table 10). For such analyses, variances of the single stroke flash occurrence across the country cannot be determined.

Rakov et al. (CIGRE TB 549, 2013 [13]) stated that there is no evidence of a dependence of negative CG lightning parameters on geographical location in the literature, except for return stroke peak current intensity. However, there is a strong indication that the higher percentages of negative single stroke flashes of the present analyses might be caused (at least partly) by meteorological aspects in the Alpine region of Austria (e.g. total thunderstorm height and charge distributions in the clouds).

7.2 Mean Multiplicity and Multiplicity Distribution of Negative Flashes

Differences regarding the multiplicity values for negative flashes of the three measurement periods can be caused by variances in the observed thunderstorm characteristics, but could be also related to not detected or misclassified strokes. Day-to-day variances of thunderstorm characteristics have been observed by Antunes et al., 2015 [60] too. Analyses in the present thesis showed mean flash multiplicity values for VFRS data ranging from 3.2 to 3.4 for 2015, 2017 and 2018. Mean flash multiplicity values determined with the VFRS data are comparable to the results for measurements in the Austrian Alps in 2009 and 2010 (3.3 for the mean multiplicity of merged data; see Vergeiner et al., 2013 [57]). Analyzing the LLS data, the mean multiplicity values for 2017 and 2018 (both 2.8) are at least 21 % lower than the one for 2015 (3.6). This decrease of the mean LLS multiplicity value for 2017 and 2018 is caused by the new IC/CG classification, which was implemented by ALDIS in 2016.

Previously published results of flash multiplicity values are based on numerous studies conducted in various regions all over the world during the last decades. These values show a variation from 3.3 to 6.4 strokes per flash. The lowest value was reported by Vergeiner et al., 2013 [57] for previous VFRS studies in Austria. The highest value was reported by Kitagawa et al., 1962 [47] for correlated measurements of electric field and moving-film camera records in New Mexico. Several analyses for different countries and conducted with different measurement systems showed multiplicity values in the range from 3.7 to 4.6. Rakov et al. (electric field records and a multiple-station TV system; see Rakov and Uman, 1990 [49]) and Zhu et al., 2015 [46] (electric field measurements) both published a multiplicity value of 4.6 for observations in Florida. Ballarotti et al., 2012 [50] (high speed video camera records in correlation with LLS data) showed the same value for observations in Brazil. Cooray and Jayaratne, 1994 [54] have reported a similar multiplicity value of 4.5 for their electric field measurements in Sri Lanka and also the result of 4.2 of Antunes et al., 2013 [55] in Brazil is in the same range (high speed video cameras in correlation with LLS data). Baharudin et al., 2014 [48], Saraiva et al., 2010 [52], Qui et al., 2004 [56] and Saba et al., 2006 [6] showed multiplicity values of 3.8 to 4.0 for their measurements. In Malaysia and China they conducted electric field measurements (see Baharudin et al., 2014 [48] for Malaysia and Qie et al., 2004 [56] for China). In the U.S. they used data from high speed video observations (Arizona; see Saraiva et al., 2010 [52]) and in Brazil high speed video camera records have been correlated with LLS data (Brazil; see Saba et al., 2006 [6]). Poelman et al., 2013 [53] (VFRS data set and LLS data, Belgium) reported a slightly lower multiplicity of 3.7. The records in Sweden, done by Cooray and Pérez, 1994 [51], which showed a multiplicity value of 3.4 (broadband electric

field records) are comparable to previous (see Vergeiner et al., 2013 [57]) and present findings for the Austrian region (multiplicity of 3.3). VFRS measurements (video recording speed 200 fps for Vergeiner et al., 2013 [57] and 2000 fps for the present analyzed data set) in correlation with LLS records have been used for both analyses in Austria. The single stroke flash percentage of 27 % has a direct impact on the multiplicity and influences the multiplicity towards lower values. The analyses in Sweden showed a single stroke flash percentage of 18 % (Cooray, 1994 [51]) which should have a lower impact on the multiplicity value.

A mean multiplicity value of 3.8 obtained from a data set of 83 negative flashes, recorded in the Chinese Gansu province in 1996 by using a broadband slow antenna system, was reported by Qie et al., 2004 [56]. Their data include 40 % single stroke flashes (i.e. a number of 33 single stroke flashes). Compared to the shown values for most of the other analyses those seems to be a rather high mean multiplicity considering the detection of 40 % single stroke flashes. Rakov et al. (CIGRE TB 549, 2013 [13]) stated that more data from China are needed.

Baharudin et al., 2014 [48] stated that it may appear that the number of strokes per flash does not vary significantly from one geographical region to another. Findings by Kitagawa et al., 1962 [47], Rakov et al., 1994 [84] (analysis based on data from Rakov and Uman, 1990 [49]) and Saba et al., 2006 [6] have been reviewed. Nevertheless, findings for the European region show the lowest values compared to findings from other parts in the world (see above description and Table 12).

Additionally to the multiplicity also the GSPs per flash have been analysed. Table 27 shows the results for this analysis for each year and in total. Data of all FI strokes per GSP were related to all flashes (F11) for this analysis.

Table 27: Analysis of GSPs per flash for 2015, 2017 and 2018 and in total

Year	F11 Strokes	FI Strokes	GSP per Flash
2015	131	248	1.89
2017	75	127	1.69
2018	198	343	1.73
Total	404	718	1.78

The results for GSP per flash of the present thesis are comparable with results from Saraiva et al., 2010 [52] who used high speed video observations in Arizona and São Paulo and calculated an average number of ground contacts of 1.7 for both locations. Rakov et al., 1994 [84] showed similar findings for TV-records in Florida and New Mexico.

7.3 Negative Return Stroke Peak Currents of LLS Detections

To estimate the negative return stroke peak current the same field to current conversion factor is used for all LLS detected strokes. This current conversion factor is only validated for negative subsequent strokes, with a return stroke peak current lower than -60 kA (see section 3.2). A validation for negative first return strokes and for positive return strokes is still needed (CIGRE TB 376, 2009 [28]). The variability of the return stroke speed makes a highly accurate field to current conversion for individual strokes difficult. However, it has been shown that a statistical estimation of current parameters out of measured electromagnetic fields is possible (see Rachidi et al., 2004 [29]).

Return stroke peak currents for all shown categories in subsection 6.3.1, show variances over the three investigated periods (2015, 2017 and 2018). The observation of thunderstorms with variable characteristics for each year can be a reason for that (see subsection 2.2). The median values for all negative return stroke peak currents are around 16 % lower for 2015 (-10.1 kA), around 9 % lower for 2017 (-11.2 kA) and about 30 % lower for 2018 (-8.0 kA), respectively, than for detections of older VFERS measurements in the Alps (-12 kA for measurements from 2009 to 2012; see Schulz et al., 2016 [19]). Reasons for these differences can be variances of the observed thunderstorms per measurement period (see Antunes et al., 2015 [60]) or among the analyzed years in general. As expected values of median return stroke peak currents for FI strokes are higher than the ones for SU strokes (-10.8 kA for all FI strokes and -7.6 kA for all SU strokes, respectively; see Table 13). Maximum and mean values of FI strokes compared to SU show the same characteristic.

The hypothesis that SU strokes with larger return stroke peak currents than FI1 strokes of the flash originate from strokes to new GSP was analyzed in subsection 6.3.3 by using the present ground truth data.

A percentage of 42 % of multiple-stroke flashes exhibit a SU stroke with a return stroke peak current larger than the FI1 stroke (first return stroke in a flash), considering all three analyzed measurement periods. For these cases, at least one following SU stroke within the flash showed a higher return stroke peak current than the FI1 stroke. The calculated value is

lower than the results shown in previous analyses for Austria (49 % by Schulz and Diendorfer, 2006 [35] and 51 % by Diendorfer et al., 1998 [34]). These relatively high values could, e.g., originate from misclassifications of preliminary breakdowns as CG strokes. Such misclassified strokes would be classified as FI strokes in a flash, if they fulfill the time and spatial grouping criteria (Cummins et al., 1998 [31]). The expectation of Rakov et al., (CIGRE TB 549 2013 [13]) that about one third of multi-stroke flashes contain at least one stroke with a higher field peak, or return stroke peak current respectively, than the first stroke is exceeded in this study. Studies of other countries show similar values but also much lower ones for the same analyses (24 % to 38 %, see Table 14). Comparing all SU strokes with SU strokes with a higher return stroke peak current than the FI1 in the flash only revealed that 14 % of the total SU strokes have a peak current larger than the first stroke. This value is situated at the lower end of the percentages shown in the literature (12 % to 32 %; see again Table 14). The highest percentage was obtained again in one of the previous studies for the Austrian region by Schulz and Diendorfer, 2006 [35].

The separation of the LLS flash to strokes per individual GSP leads to a new distribution regarding FI and SU return stroke peak currents. 37 % of the GSPs exhibit a SU stroke with a return stroke peak current greater than the FI stroke in the GSP, considering the whole data set. For this analysis, only strokes striking the same GSP were assigned as SU strokes by using the VFRS data. Comparing all SUs per GSP to SU strokes with a higher return stroke peak current than the first stroke in the same GSP only revealed that 15 % of the SU strokes have a peak current larger than the first stroke. Comparing SUs per GSP only revealed 15 % of the SU strokes having a return stroke peak current larger than the first stroke. This result leads to the conclusion that the larger SU return stroke peak currents within LLS grouped flashes are unlikely to originate from FI strokes to a new GSP (42 % for flashes versus 37 % per GSP). The median peak currents for both FI1 strokes of multiple-stroke flashes and FI strokes of multiple-strokes per GSP show similar values (-14 kA versus -13 kA respectively).

Berger et al., 1975 [85] obtained a median peak current for FI1 strokes of -30 kA, based on tower measurements. Such significant differences between these direct current measurements and the shown LLS peak current estimations of the present analysis (see subsection 6.3.1 and Table 13) have already been reported for FI1 strokes in Austria (-10 kA inferred by the EUCLID network; see CIGRE TB 376, 2009 [28]). The reason for the large difference between peak currents based on LLS data and peak currents from Berger et al., 1975 [85] is up to now unknown. The difference between the LLS data reports mentioned above and our analysis could be that our data are based on ground truth CG data and no misclassified intracloud pulses (e.g. preliminary breakdowns) are included. The data set for

the present analysis of FI1 strokes of flashes contains multiple-stroke flashes only, which in general exhibit higher first stroke peak currents compared to single stroke flashes (Nag et al., 2008 [62], Orville et al., 2002 [63]) and therefore bias the distribution towards higher values (see Figure 22).

Because of the use of LLS data to determine the individual stroke peak current, the SU strokes with higher peak currents than FI1 strokes for flashes and for the FI strokes per GSP could be caused, at least in part, by variances of SU return stroke speed for individual strokes. The occurrence of these SU strokes of larger return stroke peak current than FI strokes can vary for different locations or for different types of storms too (Nag et al., 2008 [62]).

Regarding the analyses of FI peak currents versus the multiplicity of a flash and versus the multiplicity per GSP, the results are shown in Figure 22. An increase of FI return stroke peak current with multiplicity is observed for both cases. The relatively small sample size for multiplicity values greater than 8 should be considered both for flashes and for strokes per GSP, when interpreting the results shown in Figure 22. For that reason, a linear trend line was calculated for a multiplicity up to 8 strokes per flash and per GSP only (see Figure 23). This linear trend line accentuates the findings of the increase leading to higher peak currents for the FI strokes with increasing multiplicity for both cases mentioned above. Such increases for FI stroke peak currents as a function of multiplicity have already been reported in the literature (Cummins et al., 1998 [31], W. Schulz et al., 2005 [12], Orville et al., 2002 [63]).

For all return stroke peak current distributions in international and national lightning protections standards direct current measurements by Berger and co-workers (e.g. Berger et al., 1975 [40]) in Switzerland remain the primary reference for both lightning research and lightning protection (e.g. OVE 62305-1, 2012 [64]). Rakov et al. (CIGRE TB 549, 2013 [13]) stated that Berger's peak current distributions have been generally confirmed by direct current measurements in Japan, Austria, and Florida.

Previous analyses of return stroke peak current data for Austria from 2009 to 2012 show a median of -12 kA. Median stroke peak currents determined with VFRS measurements correlated to EUCLID LLS return stroke peak currents are in the range from -16 kA (France, 2012 – 2013; Schulz et al., 2016 [19]) to -18 kA (Belgium, 2011; Schulz et al., 2016 [19]). The median return stroke peak current for all strokes during the whole measurement period (2015, 2017 and 2018; see Table 13) is -9.4 kA. This value is 22 % lower than the lowest stated value in previous literature for Austria. Compared to the detected median return stroke peak current for Belgium (-18 kA; Schulz et al., 2016 [19]), the present median return stroke peak current is almost 50 % lower. Such a decrease for the median return stroke peak current of all strokes could indicate an increase of the percentage of detected strokes with low lightning peak

currents. No dependency of the return stroke peak current on the distance between strike point and measurement location was detected for all three years (maximum distances of 50 km analyzed). A direct comparison of return stroke peak current parameters of different LLS is not reasonable because of the dependency of the estimated currents on the DE of each system (see CIGRE TB 376, 2009 [28]).

Median return stroke peak currents correlated with ground truth VFRS data show significantly lower values than the median peak currents reported for direct current measurements of Berger et al., 1975 [40]. Diendorfer, 2016 [16] stated that it is not clear if the lower values reported by the LLS are correct and the -30 kA need to be revised or vice versa. Diendorfer, 2016 [16] pointed out that LLS first stroke data could be contaminated by lower current subsequent strokes or by misclassified IC discharges and that the used equation (1) (see section 3.2) is not applicable for CG first strokes. A validation of the current conversion factor for negative first return strokes and positive return strokes is still needed (Gerhard Diendorfer, 2016 [16]). If equation (1) indeed is valid, Diendorfer, 2016 [16] proposes that a smaller value for the return stroke velocity needs to be used for first strokes. A misclassification of IC discharges can be neglected for all analyses of VFRS data (misclassified intercloud pulses, e.g., preliminary breakdowns, are not included) in correlation with LLS data because only video confirmed return strokes have been used for the analysis.

7.4 Location Accuracy of the LLS for Negative Flashes

Results of calculated LA values for negative flashes of 2015, 2017 and 2018 show slightly higher values than reported for strokes recorded at the Gaisberg Tower. The calculated median LLS LA of 95 m in 2015, of 130 m in 2017 and of 90 m in 2018 are slightly higher than the LA value of 89 m calculated for the Gaisberg Tower location for measurements in 2014 (Schulz et al., 2016 [19]). This is most likely related to the fact that the radiation field waveforms from lightning strikes to such a vertical metallic structures make a location calculation by the LLS easier, than for natural CG lightning attaching to ground (Nag et al., 2015 [9]). The resulting LA values of this analysis show an ongoing improvement compared to the median LA values in 2009 – 2010 (326 m) and in 2012 (157 m) in Austria (see Schulz et al., 2016 [19]). This is caused by the fact, that LLS calculations, prior to 2011, have been performed without the implementation of the sensor-based onset time corrections and prior to 2013 no propagation corrections were used (see Schulz et al., 2016 [19]).

The 95 % LA obtained in this study shows a higher value in 2015 (2.8 km) and similar ones in 2017 (1.7 km) compared to previous analyses of 2009 – 2010 (1.6 km) and 2012 (1.5 km) in Austria (Schulz et al., 2016 [19]). A bug in the location algorithm caused this larger 95 % LA in 2015. The 95 % LA analysis in 2018 showed developments towards a lower value of 0.9 km. This reduction could be caused, at least partly, by updates of sensor technology (e.g. Vaisala Inc. LS7002) around Austria. The Italian LLS operator changed the sensors to a newer version during 2015. The operator of the German and the Czech Republic LLS did the same in 2016. The new sensors are equipped with an antenna board of higher sensitivity. The higher sensitivity allows a detection of signals with lower amplitudes, in the case of an adequate signal-to-noise ratio and this affects the number of sensors reporting per stroke. Buck et al., 2014 [25] reported that the signal-to-noise ratio should also have been improved for the newer sensor technology. This affects the number of sensors reporting for strokes in the Austrian region. An analysis of the strokes with LA values larger than 1 km showed that almost all of these location errors are caused by locations calculated with data of two sensors only. All data should be seen as a snapshot of the LA performance of the LLS for the given observation period.

In 2017 and 2018, LA values larger than 1 km have been caused additionally by FI and SU strokes to the same GSPs showing different channels to ground (at least as far it could be resolved from the 2D video record, see Figure 26). Further, forked strokes are responsible for LA values larger than 1 km too, but such simultaneous terminations are not detectable with LLS sensors. Figure 27 shows two successive video frames of such a forked stroke. Both channels terminated almost simultaneously in the two GSPs (video recording speed limits the time resolution). Processes of forked strokes have already been analyzed and published previously by Ballarotti et al., 2005 [68] (six flashes with two channels connected to ground simultaneously) and Saraiva et al., 2014 [69] (analysis of 22 forked strokes).

A categorization of all analyzed strokes in strokes with a straight or with an inclined channel from cloud to ground showed almost no difference in the LA analysis (see Table 16). Median LA values of 100 m for straight (369 strokes) and 99 m for inclined channels to ground (58 strokes) have been determined. Also for the 95 % LA similar values have been calculated (1.4 km for strokes with straight and 1.5 km for strokes with inclined channels from cloud to ground). This leads to the conclusion, that the inclination of the channel to ground has not any significant influence on the LA. It should be kept in mind that videos recorded for one direction show two-dimensional data only. This will lead to a certain inaccuracy for such categorizations.

The results for the LLS LA determined by video data have to be considered as upper limits because of potential visibility problems of the lightning channel close to ground, particularly in

mountainous areas. Rakov et al., 1994 [84] stated this too and indicated that distinguishing between GSP separated by some ten meters only is not possible because of obscuration of the channel GSP by trees for example.

The resulting LA distribution calculated for distances of SU strokes to FI strokes that followed the same channel would show the same result if such calculations were performed for two SU strokes following the same channel because such calculations always lead to a Rayleigh distribution of the LA (Schulz et al., 2012 [42]). To compare the video determined LA with LA determined by using data of instrumented towers, the calculated location differences from the video analysis have been scaled by using a factor of $1/\sqrt{2}$ (Schulz et al., 2012 [42]).

Comparisons of recent LA analyses for ALDIS/EUCLID show further ongoing improvements towards lower location errors (LA of 326 m for VFRS in Austria 2009 - 2010 to LA of 90 m for VFRS measurements of 2018; see Table 17) due to continuous adaptations in the sensor technology and the LLS software. The comparison of LA analyses for ALDIS/EUCLID with other large scale LLS showed higher LA values for analyses performed in Florida (Mallick et al. 2014 (Mallick et al. 2014)) but also comparable median LA values for analyses done in Kansas (Cummins et al. 2014 (Cummins et al. 2014)) for data of the U.S. NLDN (see Table 17). Median LA values calculated for Japan (JLDN) for data from 2013 and 2014 (Matsui et al., 2015 [71]) are comparable with former VFRS data analyses in Austria for data from 2009 and 2010 (361 m compared to 326 m respectively; see Table 17). Analyses in Brazil (Ballarotti et al., 2006 [74]) show the highest median LA value (3400 m). These analyses have been conducted for data from 2003 and 2004. For the actual LA performance of the RINDAT network, improvements towards lower values can be expected if similar adaptations of the LLS have been realized as for the EUCLID system for example.

7.5 Detection Efficiency of the LLS for Negative Flashes

For the analyses of the DE of ALDIS in correlation with ground truth measurements for flashes and strokes with a negative polarity, DE calculations for detected strokes and correctly detected strokes have been carried out (see definition in subsection 5.2.5 and analyses in section 6.5). The flash DE for correctly detected flashes increased from 96.1 % in 2015 to 98.6 % in 2018 and is comparable to the DE value of 98 % for the merged data of the years 2009 to 2012 (Schulz et al., 2016 [19]) (see Table 19). The stroke DE for correctly detected strokes in 2017 (76.3 %) and in 2018 (79.1 %) is lower than the stroke DE in 2015 (85.6 %)

and the one for investigations of data from 2009 to 2012 (Schulz et al., 2016 [19]) (DE of 84 % for correctly detected strokes) although the “standard” stroke DE is higher. The reason for the decrease of the stroke DE for correctly detected strokes is a new IC/CG classification algorithm used in 2017 and 2018, which performed worse for negative CG strokes of peak currents below -15 kA (Kohlmann et al., 2017 [59]). As described in subsection 6.5.2 approximately 90 % of the negative stroke peak currents of non-correctly detected (misclassified) strokes of 2017 are below -15 kA. In 2018, more than 95 % of the non-correctly detected strokes had a peak current lower than -15 kA.

The DE values given in recent publications have been analyzed and compared to expected DE values for medium range LLS, with a sensor distance up to 400 km (mid-range LLS) given by Nag et al., 2015 [9]. The DE values in literature should be compared to “standard” DE values in this thesis and not to the stroke DE of correctly detected strokes. Nag et al., 2015 [9] stated a DE of 70 % to 90 % for strokes and 85 % to more than 95 % for flashes for such networks.

Flash DE values show results in the range of the stated DE of 85 % to more than 95 % by Nag et al., 2015 [9] for all compared studies (see Table 19). Stroke DE values for Brazil (Ballarotti et al., 2006 [74]) from 2003 to 2004 show lower values (54.7 %) than stated by Nag et al., 2015 [9] (70 to 90 % for mid-range LLS). The used IMPACT and various LPATS type sensors (see Ballarotti et al., 2006 [74]) could cause the low values for the stroke DE in Brazil. Distances between the sensor locations will affect the detections of individual strokes for this type of sensors in particular, especially for strokes with low return stroke peak currents (see section 3.2). As stated by Buck et al., 2014 [25] improvements of the sensors software and the central processing unit to latest releases will affect the DE value towards higher DE values (higher sensitivity of the sensor to low amplitudes, additional provided waveform parameter for each stroke and digital filtering or better signal-to-noise ratio). Mallick et al., 2014 [72] showed a stroke DE value of 75 % for rocket triggered lightning observations from 2004 to 2013 in Florida. Stroke DE values at the Gaisberg Tower for measurements from 2005 to 2014 and for observations in Kansas (Cummins et al., 2014 [73]) for 2013 show stroke DE values at the lower edge of 70 % (see again Table 19). This low DE values are mainly caused by the missing of first strokes for measurements at the Gaisberg Tower (same as for rocket triggered lightning) and can be a reason for low DE values in Kansas because of the observations of strikes to wind turbines, where similar phenomena as for strikes to towers are expected. Further, for video observations of strikes to towers, initial continuing currents including initial continuing current pulses can bias the DE results towards lower values.

7.6 Analyses of Positive Flashes

The data set of positive flashes was analyzed regarding the percentage of single stroke flashes, multiplicity, return stroke peak currents of all strokes and the DE of the LLS data. The overall data set for the three investigated years showed 59 flashes comprised of 71 strokes (see section 4.2). Due to the lack of data from strokes following the same channel for positive CG strokes, the LA could not be obtained for positive strokes in this thesis.

The percentages of single stroke flashes for the VFRS data and the LLS data are 83 % and 75 %, respectively, for the merged data set (2015, 2017 and 2018). The values for the VFRS data are rather low compared to previous analyses for VFRS data from Austria (91 % for data of 2008 to 2010 and 2012; see Schulz et al., 2013 [81]). The single stroke flash percentages of the present analysis (83 %) are situated within the range of previously published values in the literature (63 % to 96 %; see Table 21).

The mean multiplicity is 1.2 and 1.1 in the present analysis and the previous analysis by Schulz et al., 2013 [81], respectively, for VFRS data from Austria. Saba et al. reported a multiplicity of 1.2 for data from Brazil but also for a merged data set from Austria, Brazil and the U.S. They all used high speed video observation correlated with LLS data for their analyses.

The analyzed return stroke peak currents of the LLS data show variances over the three investigated periods (2015, 2017 and 2018; see Table 23). These annual variations can be caused, at least partly, by variable lightning characteristics. The shown return stroke peak current analyses for all strokes in Austria (median of 43.8 kA for the merged data set; see Table 23) are higher than the values reported by Berger et al., 1975 [85] (median of 35 kA) for their direct current measurements. The present median return stroke peak current of the merged data set is also higher compared to previous analysis of VFRS data by Schulz et al., 2013 [81] for Austria and by Saba et al., 2010 [77] for a merged data set from Austria, Brazil and the U.S. They showed median return stroke peak currents in the range of 34 kA (Schulz et al., 2013 [81]) and 39.4 kA (Saba et al., 2010 [77]) for all strokes. The same field to current conversion factor was used for all detected strokes for the present and previous analyses of LLS data (Schulz et al., 2013 [81] and Saba et al., 2010 [77]). As described in section 3.2, the used current conversion factor is validated for negative subsequent strokes with a return stroke peak current lower than -60 kA only. A validation for positive return strokes is still needed (CIGRE TB 376, 2009 [28]) therefore the shown return stroke peak currents have to be seen as roughly estimated values. Rakov et al. (CIGRE TB 549, 2013 [13]) stated that it is still recommended to use the peak current distribution for engineering applications shown by

Berger et al., 1975 [85] because of the absence of other direct current measurements for return strokes with positive polarity. The uncertainty that not all analyzed cases of Berger et al. are of return strokes type should be kept in mind (CIGRE TB 549, 2013 [13]).

The DE for positive flashes is somewhat lower than the one for negative flashes for 2015, 2018 and in total (93.2 % compared to 97.8 %). The DE for positive flashes and strokes in 2017 is 100 %, but in this year only 4 flashes containing 4 strokes have been analyzed (minimum peak current of 8.1 kA). The stroke DE of detected and correctly detected strokes for the merged data set is slightly higher for positive flashes compared to negative ones (94.4 % and 83.1 % for positive strokes and 91.7 % and 80.7 % for negative strokes). A comparison of the DE for positive and negative strokes shows not significantly higher values even though the median return stroke peak current of positive strokes for all strokes is higher (43.8 kA compared to -9.4 kA for positive and negative strokes respectively).

Schulz et al., 2013 [81] obtained a DE of 97 % for flashes and 92 % for correctly detected strokes for data from Austria. They used VFRS data in correlation with LLS data recorded from 2008 to 2010 and in 2012. The flash DE is in the range of the presented analysis of the merged data set (94.4 %; see Table 24). The stroke DE of correctly detected strokes of Schulz et al., 2013 [81] is about 10 % higher than the one of the present analysis (92 % compared to 83.1 %). The new IC/CG classification algorithm implemented in 2016 causes this difference.

Fleenor et al., 2009 [79] analyzed data of the NLDN in correlation with high speed videos from 2009 recorded in the U.S. (central Great Plains). They showed a DE for flashes and strokes of 89 % and 88 %, respectively. The lower value for the flash DE is caused by the higher average distance between neighboring sensors in the US compared to Austria (Schulz et al., 2013 [81]).

7.7 Direct Impact of Lightning Discharges on Power Generation and Transmission Systems

The two analyzed cases show recent records of lightning discharges in the Austrian Alpine region. Ground truth measurements give an insight to lightning strikes to power generation and transmission systems in the observed area, both for buildings on mountainous and flat terrain. The data set of the Video and Field Recording System (VFRS) measurements and corresponding LLS data are synchronized to GPS-time. This is a key factor for such correlations. System protection and detection relays are synchronized to server time in both

cases. A fault within the same second when the VFRS recorded a lightning strike was detected by the fault detection relay of the wind turbine and within the same millisecond by the protection relay of the railway system. In addition, no other event triggered the relays during that day. This made a precise correlation of VFRS and LLS data possible, even if no synchronization to GPS-time was available for the additional data sets.

For the lightning strike to two wind turbines, two downward stepped leaders are visible in the video for stroke 1 and 4 (top left picture and bottom right picture in Figure 29). Three strokes followed the first channel, which struck the first wind turbine (first GSP). Due to limitations of the video quality because of heavy rain and hail, it was not visible in the video, if the strokes struck the lightning diverter on the blade tip, the lightning receptor, the blade structure or the tower top. One of the three strokes triggered the earth-fault detection relay. Because of the LLS estimated return stroke peak current of about -23 kA for the first stroke (FI1; see Table 25), it is most likely that this stroke already triggered the earth-fault detection relay. The high speed video shows a direct strike to the second wind turbine (second GSP) followed by a continuing current with a duration of 117 ms for stroke 4 (FI2; see Figure 29).

The deviation of 775 m of the calculated strike point for FI2 to wind turbine two is caused by poor LLS detections (see Figure 30 and Table 25). Five LLS sensors detected FI2 and only the data of three sensors were used to process the location. A detailed analysis of the raw data of the sensor signals showed a signal shape for FI2 with a larger width and two field peaks making it difficult to define the correct start time of the event and this leads to location inaccuracy (personal information provided by ALDIS). The relatively low return stroke peak current of FI2 (-2.9 kA) makes a correct location calculation of this stroke even more difficult. LLS location calculations for the other strokes show strike points at distances of 64 m and 137 m from the first wind turbine. These distances are comparable to values of the median location accuracy of the ALDIS LLS (see section 6.4). The operator of the wind farm reported no lasting damage of the wind turbines, which were struck by the strokes.

For the lightning strike to a railway overhead line, again a downward stepped leader is visible in the video (top left picture in Figure 32). All three strokes followed the same channel to the same GSP (second picture in the top section and first and third picture in the lower section of Figure 32). The railway overhead line is not directly visible in the video but a flashover on the insulator of the tower at the GSP and two nearby towers are visible (top right and second picture in the lower section of Figure 32). For that reason, a direct strike of the overhead line is most likely. The flashover was visible in the video for 79 ms, on the affected tower and on two other towers. The analysis of the digital fault record of the distance protection relay shows that the line was tripped after 46 ms. After 123 ms the whole fault handling was

closed by the distance protection relay. A mechanical breaker closing response time and an eventual time shift between the tripping times of the two substations can cause the difference of 33 ms between the tripping time of the line and expired flashover in the video. The installed distance protection relay⁹ operates with a sampling rate of 20 samples per period and the used inductive instrument transformer is built to generate an image of the sinusoidal 16.66 Hz signal, for measurement and protection purposes. For that reason, no transient signal changes, caused by lightning discharges, can be observed in the digital fault records. To detect such transient signals on the line a resistive-capacitive voltage divider and a transient measurement system is needed (see Schwalt et al., 2017 [86]).

The large deviation of the calculated strike point of stroke 1 (F11) to the tower (1424 m) is again caused by poor LLS detections. The analysis of the raw data of the sensor signals for F11 showed a signal shape with a larger width and two field peaks too. This causes the same problems as described for the lightning strike to the wind turbines. Location calculations for the other two strokes show strike points at a distance of 81 m and 160 m to the tower of the overhead line. These values are comparable to values of the median LA of the ALDIS LLS (see section 6.4). The Austrian railway operator reported no lasting damage along the transmission line, which could be correlated to this lightning strike.

To easily correlate lightning strikes, detected by the VFRS and the LLS, with fault records in the transmission system or strikes to wind turbines, a time synchronization to GPS-time has to be implemented in these systems in the future.

⁹ Numerical Overhead Contact-Line Protection, type 7SA517 by Siemens

8 Conclusion

Subsequently, the main conclusions regarding the investigated field of research for the present thesis (see section 1.4) are addressed and will be discussed:

(1) Analysis of lightning phenomena in the Alpine region of Austria based on video and electric field recordings of cloud-to-ground lightning discharges.

To gather the needed ground-truth-data for analyses of lightning phenomena in Austria recordings of CG flashes have been carried out in 2015, 2017 and 2018. In the present thesis, key parameters for CG flashes in general and for the Austrian Alpine region in specific were analyzed. Ground truth measurements for the thunderstorm periods in 2015, 2017 and 2018 give an insight into lightning activity in the observed area. Since the measurement days as well as the measurement locations varied over the investigated periods, a unique insight into lightning parameters in mountainous regions as well as for flat terrain was achieved. The presented VFRS measurement data were recorded with a high speed video camera (2000 frames per second) and an electric field recording system (see section 3.1). For the analyses of single stroke flashes by thunderstorm type additional measurements from the years 2009, 2010 and 2012 have been taken into account (different camera system with a recording speed of 200 fps; see subsection 6.1.3). Each data set of the VFRS measurements and corresponding LLS data was only used if both measurements were of high quality (e.g. GSP visible in the video record, every stroke detected by the LLS).

To illustrate the effort to gather the measurement data in the following the total days of measurements and number of thunderstorms are presented. In 2015 data of 24 thunderstorms have been analyzed. This data set was recorded during 30 measurement days. For 2017 data of 13 thunderstorms have been analyzed, gathered during 20 measurement days and for 2018 the relation was 14 thunderstorms in 23 measurement days, respectively. This leads to an overall efficiency of about 70 % of recording a thunderstorm on a measurement day successfully.

As described in subsection 6.1.4, a distance of 15 to 20 km from the measurement location to the center of the thunderstorm was favored for VFRS measurements because of better observation possibilities and to maintain a low personnel risk. In addition to misleading weather forecasts, it sometimes occurred that the predicted thunderstorm

changed its direction during VFRS measurements, heading towards the measurement location. Such events made it necessary to stop the measurements (e.g. due to heavy rain or/and wind, hail and close lightning strikes).

Three years of ground truth measurements in the Alpine region, conducted at several locations over the country, have been carried out for the first time and an exclusive data set was collected. The overall VFRS data set of 2015, 2017 and 2018 includes 531 CG flashes and 1639 CG strokes recorded during 51 different thunderstorm days. The recorded data showed a polarity distribution of 87.2 % negative, 11.1 % positive and 1.7 % bipolar CG flashes. A high quality and integrity of the present data set can be concluded, since these distributions are in line with findings by Rakov et al., 2003 [87], who pointed out that around 10 % of all flashes show a positive return stroke current.

(2) Correlation of VFRS and LLS data and analysis of characteristic parameters for cloud-to-ground flashes. Comparison with values from the literature and similar older investigations.

Further analyses of single stroke flash percentages, multiplicities and return stroke peak currents have been chosen as parameters of interest. Furthermore, variations of the described parameters over the years and comparisons to similar previous measurements in Austria and other countries have been analyzed. By means of the on-site VFRS measurements, the location data provided by the ALDIS LLS were analyzed regarding location accuracy (LA) and detection efficiency (DE). The analyzed LLS data and the obtained ALDIS performance characteristics have been compared with data from international literature as well. First, a conclusion about analyses of the data set for flashes with a negative polarity and second for analyses of flashes with a positive polarity were given.

Occurrence statistics of single stroke flashes was of special interest for this thesis, since the analyzed ground truth measurements for the Alpine region of Austria show a particularly high percentage of negative single stroke flashes (27 % for the merged data set of 2015, 2017 and 2018) compared to values published for other regions of the world (12 % to 24 %; see subsection 6.1.4). The annual percentage of single stroke flashes largely levels out to values between 24 % and 29 % for VFRS data (see Table 6) and reassures the high percentage of negative single stroke flashes for the investigated region. Annual percentages for LLS data are between 22 % and 30 % (see Table 6). These variations are most likely due to different spectra of thunderstorm characteristics for individual years. The sample sizes of the analyzed measurements for negative

flashes per year are in the range of the ones used by other authors in previous investigations.

The multiplicity distribution and the mean multiplicity were obtained for each year and in total from both the VFRS and the LLS data for the correlated flashes. The calculated VFRS multiplicity values for negative flashes have been compared additionally with values from former national and international analyses. Analyses for the present thesis showed mean multiplicity values for VFRS data from 3.2 to 3.4 for 2015, 2017 and 2018. Mean multiplicity values determined from the present VFRS data are comparable to the results obtained from VFRS measurements of 2009 and 2010 in Austria (mean multiplicity of 3.3).

For analyses regarding the return stroke peak current, estimated peak currents of correlated ALDIS LLS data of each analyzed return stroke have been used. Analyses for all negative return stroke peak currents showed median return stroke peak currents ranging from -8.0 kA to -11.2 kA between 2015 and 2018. Additionally, return stroke peak currents of first return strokes in multiple stroke flashes based on LLS flash data have been compared with return stroke peak currents of the first strokes in a GSP in case of multiple strokes to a GSP (GSP were determined manually by using the video data; procedure see subsection 6.3.3). In this respect, the relation between FI initial return stroke peak currents versus SU return stroke peak currents was especially considered. For 42 % of the LLS grouped flashes, at least one SU return stroke peak current in a flash showing a greater value compared to the FI1 stroke in this flash. Checking the peak currents within individual GSPs reveals 37 % with at least one SU stroke with a larger peak current than the FI stroke in the same GSP. Comparing all SU strokes with SU strokes with a higher return stroke peak current than the FI for flashes and per GSP only revealed that 14 % of the total SU strokes having a peak current larger than the first stroke for flashes and 15 % for analyses per GSP. For the analysis of FI return stroke peak currents versus the multiplicity, the results show an increase for both analyses (flashes and GSPs) leading to higher return stroke peak currents for the FI strokes exhibiting a larger multiplicity.

Furthermore, values for LLS LA and DE for the available ground truth data of negative flashes and strokes have been analyzed. LLS LA values are in the range of 90 m to 130 m for the three years. The total LLS DEs for correctly detected flashes showed 97.8 % and the stroke detection efficiencies showed 80.7 % and 91.7 % considering correctly detected strokes and detected strokes, respectively. Overall, the values for LA and DE are within the expected range, even if the thunderstorm activities and especially

the measurement days and measurement locations varied between the three investigated periods. Comparisons of recent LA analyses for ALDIS/EUCLID show ongoing improvements towards lower (better) LA values due to continuous improvements in sensor technology and ongoing adaption of the LLS. Compared to other large scale LLS operated in the U.S., Japan and Brazil, ALDIS/EUCLID data exhibited the lowest (best) LA. Here it should be mentioned that for actual LA performance analyses for the LLS of other countries improvements towards lower (better) values are to be expected, if similar adaptations of the LLS were realized as for the EUCLID system for example. LLS performance estimations based on VFRS measurements, recorded in a certain area, can be rated as superior compared to any locally restricted approaches to determine the LLS performance, since the results are valid for a larger region. The same statements apply to the compared DE analyses of previous investigations for other countries and LLS.

The data set of positive flashes was analyzed regarding percentage of single stroke flashes, multiplicity, return stroke peak currents of all strokes and the DE of the correlated LLS data. For the merged data set (2015, 2017 and 2018) the percentage of positive single stroke flashes for the VFRS data and the LLS data is 83 % and 75 %, respectively. The mean multiplicity is 1.2 for the present analysis of VFRS data from Austria. The return stroke peak current analyses for all strokes in Austria revealed a median return stroke peak current of 43.8 kA for the merged data set (2015, 2017 and 2018). The obtained DE for the merged data set of positive flashes is 93.2 % and 83.1 % for correctly detected flashes and strokes, respectively. The median return stroke peak current for the merged data set is around 11 % to 29 % higher than the values reported for previous analyses for Austria (Schulz et al., 2013 [81]) and for a merged data set from Austria, Brazil and the U.S. (Saba et al., 2010 [77]).

(3) Analysis of single stroke flashes and their occurrence regarding different thunderstorm types.

A classification of the gathered data set into storm types (single cell, multicell, supercell and line) by using radar data of the individual measurement days was carried out in the first place. The vertical wind shear (DLS) as the change of the wind vector both in strength and in direction from 0 to 6 km height, is analyzed additionally as an alternative and more objective classification, which is related to the atmospheric background conditions on a given day instead of each individual thunderstorm's behavior. Both categorizations have been carried out by the Meteorologist Mag. Georg

Pistotnik (Meteorological Service ZAMG). Single cells usually dominate with a DLS below 10 m/s, multicells between 10 and 20 m/s and supercells above 20 m/s. To get enough data for all different thunderstorm types this data set (2015, 2017 and 2018) was merged with data from 2009, 2010 and 2012. This was necessary, because some thunderstorm types occurred just a few times during the whole measurement period. The analysis showed a similar single stroke flash percentage of 26 % for thunderstorms with low level of organization (single cells) and 27 % for higher organized ones (merged category of multi-, supercells and lines) same as for thunderstorms under weak vertical shear (DLS < 10 m/s) and enhanced vertical wind shear (DLS > 10 m/s). The present analysis gives no evidence regarding a correlation between single stroke flash occurrence and individual thunderstorm types.

(4) Observation of processes and impacts of lightning discharges on power generation and transmission systems.

High speed video data of direct lightning strikes on power generation and transmission systems are rare but such data helps to get a better understanding of such processes and deliver proper information about the impacts. Fortunately, two special cases of direct strikes to two wind turbines and a railway overhead line have been recorded in the pre-alpine area during warm season thunderstorms of 2018. For both cases supplementary information from the wind farm and railway operator have been successfully correlated. The first analyzed flash consists of four downward strokes striking two different wind turbines, which are part of a wind farm comprising 21 generators on a mountain ridge on 1450 m above sea level. The protocol data provided by the wind farm operator were correlated with VFRS and LLS data for this case. The three strokes of the second flash all struck the same tower of a railway overhead line situated in build-up terrain and caused flashovers on the insulators of three towers. The network protocol data provided by the Austrian railway operator and the related digital fault record of the installed distance protection relay were again successfully correlated to VFRS and LLS data. The analyses of the ground truth measurements gave insight into lightning strikes to power generation and transmission systems in the observed area, both for buildings on mountainous and flat terrain. Neither operator reported any lasting damage on their infrastructure, which could be attributed to the observed lightning strikes. To correlate lightning strikes, detected by the VFRS and the LLS, to impacts on infrastructure like power generation and transmission systems, it is advisable to synchronize network protection systems to GPS-time in the future.

9 Summary

In the present thesis, the carried out research about CG lightning phenomena in the Alpine region of Austria and the associated analyzes of the recorded Video and Field Recording System (VFRS) data is described. To perform this analyses, on-site VFRS measurements of real occurring lightning flashes have been conducted during 2015, 2017 and 2018.

The motivation for this work was to gather lightning ground truth data for the major part of Austria out of measurements from on-site VFRS data, because this region shows high lightning activity, especially in the southeastern part of the country. Analyses of this exclusive data set provide insights about lightning characteristics for the Alpine region. A contribution to a better understanding of lightning discharges in the future is established by the results obtained from this data set.

The method of investigation for the present thesis can be split up in two parts: the on-site measurements of ground truth CG lightning for the Austrian Alpine region, recorded with the VFRS at the different measurement locations and the correlation of the recorded VFRS data with LLS data. This correlated data set represents unique ground truth measurements of lightning flashes in general and for the Austrian Alpine region in specific. Analyses regarding characteristic parameters of CG lightning in the investigated area and regarding performance parameters of the LLS have been carried out for that reason.

The VFRS measurements have been conducted during warm season thunderstorms (May to August) at 21 different measurement locations in total, to observe individual thunderstorms and its lightning characteristics over a large area. Each measurement location was pre-selected under the requirements of good visibility (necessary for high speed video observations; distance of 15 to 20 km from the measurement location to the center of the thunderstorm favored), low electric interference and road access. Furthermore an active exchange about weather forecast and thunderstorm prediction with the national meteorological service ZAMG was highly necessary before heading to a measurement location. VFRS observations at measurement sites distributed all over Austria can only be carried out when perfectly adapted thunderstorm predictions for the planned measurements are available.

The used VFRS consists of two main components: a high speed video camera and an electric field measurement system. The high speed video camera was parametrized to record videos with a recording speed of 2000 frames per second, to observe the optical properties of lightning discharges. The electric field recording system consists of a flat plate antenna as a sensor and an integrator circuit, an amplifier, a fiber optic link, a digitizer and a PXI system as

processing unit, to record the transient electric field. First VFRS measurements have been conducted in 2015. From 2017 on, the research project “Lightning Observation in the Alps (LiOn)” was established at Graz University of Technology to enhance the research in this field.

The conducted measurements resulted in a total data set of 531 CG flashes including 1639 CG strokes (87.2 % negative, 11.1 % positive and 1.7 % bipolar polarity), recorded during 51 days spread over the whole measurement period. This VFRS ground truth data were correlated with data of the LLS ALDIS for all records to complement the data set of each lightning flash (e.g. strike point location and return stroke peak current).

The analyzed data for the Alpine region of Austria show a high percentage of negative single stroke flashes compared to published values in the literature. The analysis of the single stroke flash percentage of different thunderstorm types, classified first by using radar data and second by using data of vertical wind shear, did not show any significant differences in the percentage of single stroke flashes for the different thunderstorm types. Analyses of the positive flash data revealed a rather low single stroke flash percentage compared to previous analyses for Austria but the percentage is situated within the range of previously published values for other countries.

The mean multiplicity values for negative flashes determined with the VFRS data are comparable to the results obtained for measurements performed in Austria in 2009 and 2010 and are still situated at the lower end compared to published results from other international studies. Mean multiplicity values for positive flashes show similar results than for previous studies.

For the analyses regarding peak currents of return strokes, the ALDIS LLS estimated peak currents of the time correlated strokes have been used. Median negative first return stroke peak current estimations by the LLS show a significant difference compared to direct current measurements used in standards (e.g. lightning strikes to instrumented towers) whereas the LLS median return stroke peak current of all positive strokes show a comparatively high value compared to previous investigations. Return stroke peak currents of negative first return strokes of LLS grouped flashes have been compared with return stroke peak currents obtained of first strokes in a GSP when GSPs were determined manually by using the video data. The relation of first (FI) initial return stroke peak currents versus subsequent return stroke peak currents was especially considered, however, the hypothesis that larger return stroke peak currents of subsequent strokes than the first stroke of LLS grouped flashes are resulting from first strokes to a new GSP cannot be confirmed. Regarding the analyses of FI return stroke peak currents versus the multiplicity of a flash and versus the multiplicity per GSP the results

show an increase for both cases leading to higher return stroke peak currents for the FI strokes with increasing multiplicity.

The analysis of the LLS LA and DE parameters for each year and in total have been chosen as secondary goal for the present work. Values of the LLS LA analysis for negative flashes are in the range of 90 m to 130 m for the three years. The merged flash DE values for the analysis of negative flashes is comparable to the merged DE value for the years of 2009 to 2012. The stroke DE for correctly detected strokes in 2017 and 2018 is lower than the DE for correctly detected strokes in 2015 and also lower than the one for investigations between 2009 and 2012. Former investigations on the DE for positive flashes resulted in higher values for data from Austria whereas results for data from the U.S. show lower values for the flash DE but higher values for the stroke DE compared to present findings.

A stepwise analysis of two rare VFRS measurements, a direct strike to two wind turbines and to a railway transmission line concludes this work. The analysis of the strikes to two different wind turbines of a wind farm located on a mountain ridge exhibited a flash consisting of four downward strokes. The second case exhibited a flash consisting of three strokes, which struck a railway overhead line tower, situated in flat terrain. The strokes caused flashovers on the insulator of the tower at the GSP and on two towers next to the striking point. The protocol data of the wind farm provided by the operator as well as the network protocol data and the related digital fault recorder data of the installed distance protection relay provided by the Austrian railway operator were correlated successfully to VFRS and LLS data. These ground truth measurement analyses offered the possibility to observe processes of direct lightning strikes to power generation and transmission systems in the investigated area, both for buildings on mountainous and flat terrain. None of the two operators reported any lasting damage, which could be attributed to the observed lightning strikes. It is advisable for operators of such technical infrastructures to synchronize their network protection systems to GPS-time for future analyses of such processes.

10 Abbreviations

ALDIS	Austrian Lightning Detection and Information System
CG	Cloud-to-Ground
DE	Detection Efficiency
DLS	Deep-Layer Shear
EUCLID	EUropean Cooperation for LIghtning Detection
FI	First Stroke
GPS	Global Positioning System
GSP	Ground Strike Point
IC	Inter Cloud
kA	Kilo Ampere
ki2	Quality criteria
LA	Location Accuracy
LF	Low Frequency
LiOn	Lightning Observation in the Alps
LLS	Lightning Location System
maxis	Major axis
n.s.	Not specified
NALDN	North American Lightning Detection Network
nbd	Sensor detections
nbdfit	Sensor data with sufficient quality
NLDN	National Lightning Detection Network
sn	Stroke number
SU	Subsequent Stroke
ToS	Type of Stroke
UTC	Coordinated Universal Time
VFRS	Video and Field Recording System
VLF	Very Low Frequency
ZAMG	Zentralanstalt für Meteorologie und Geodynamik

11 References

- [1] V. A. Rakov, "The physics of lightning," *Surv. Geophys.*, vol. 534, no. 4, pp. 147–241, 2014.
- [2] A. J. Anderson, R. B., Eriksson, "Lightning Parameters for Engineering Application," *CIGRE Electra*, vol. 69, 1980.
- [3] V. A. Rakov and M. A. Uman, *Lightning: Physics and Effects*. Cambridge University Press, 2003.
- [4] J. R. Dwyer and M. A. Uman, "The physics of lightning," *Phys. Rep.*, vol. 534, no. 4, pp. 147–241, 2014.
- [5] V. Cooray, *The Lightning Flash 2nd Edition*. Institution of Engineering and Technology, 2014.
- [6] M. M. F. Saba, M. G. Ballarotti, and J. Pinto, "Negative cloud-to-ground lightning properties from high-speed video observations," *J. Geophys. Res. Atmos.*, vol. 111, no. 3, pp. 1–9, 2006.
- [7] V. A. Rakov, "Lightning electromagnetic environment: from continuing- current fields to x-rays," in *International Conference on Grounding and Earthing & 3rd International Conference on Lightning Physics and Effects*, 2008.
- [8] G. Diendorfer, K. L. Cummins, and W. Schulz, "EUCLID – State of the Art Lightning Detection," in *EUMETNET Lightning Task Force*, 2010.
- [9] A. Nag, M. J. Murphy, W. Schulz, and K. L. Cummins, "Lightning locating systems: Insights on characteristics and validation techniques," *Earth Sp. Sci.*, vol. 2, no. 4, pp. 65–93, 2015.
- [10] R. B. Anderson, Van Niekerk H. R., S. A. Prentice, and D. Mackerras, "Improved Lightning Flash Counters," *CIGRE Electra*, vol. 66, 1979.
- [11] D. R. Poelman, W. Schulz, G. Diendorfer, and M. Bernardi, "The European lightning location system EUCLID - Part 2: Observations," *Nat. Hazards Earth Syst. Sci.*, vol. 16, no. 2, pp. 607–616, 2016.
- [12] W. Schulz, K. Cummins, G. Diendorfer, and M. Dorninger, "Cloud-to-ground lightning in Austria: A 10-year study using data from a lightning location system," *J. Geophys. Res. D Atmos.*, vol. 110, no. 9, pp. 1–20, 2005.

- [13] V. Rakov *et al.*, “TB 549 Lightning Parameters for Engineering Applications,” in *CIGRE WG C4.407*, 2013.
- [14] C. Vergeiner, S. Pack, W. Schulz, and G. Diendorfer, “Negative Cloud-to-Ground Lightning in the Alpine Region A new Approach,” in *CIGRE C4 International Colloquium on EMC, Lightning and Power Quality Considerations for Renewable Energy Systems*, 2016.
- [15] M. Mair, “Elektromagnetisches Fernfeld von Blitzenladungen in Zusammenhang mit der Blitzortung,” Technische Universität Wien, 2000.
- [16] G. Diendorfer, “A Review of 25 Years of Lightning Research in Austria from 1991-2015,” *World Meet. Light.*, 2016.
- [17] G. Diendorfer, R. Thottappillil, H. Pichler, and M. Mair, “Simultaneous current and electric field observations of upward negative leaders initiated from the Gaisberg Tower (LLS Austrian lightning detection system ALDIS),” *2010 Asia-Pacific Int. Symp. Electromagn. Compat.*, pp. 1174–1177, 2010.
- [18] G. Diendorfer, H. Zhou, and H. Pichler, “Review of 10 years of lightning measurement at the Gaisberg Tower in Austria,” *Int. Symp. Winter Light.*, pp. 185–190, 2011.
- [19] W. Schulz, G. Diendorfer, S. Pedebay, and D. Roel Poelman, “The European lightning location system EUCLID - Part 1: Performance analysis and validation,” *Nat. Hazards Earth Syst. Sci.*, vol. 16, no. 2, pp. 595–605, 2016.
- [20] E. T. Pierce, “Some techniques for locating thunderstorms from a single observing station,” *Vistas Astron.*, vol. 2, pp. 850–855, Jan. 1956.
- [21] M. A. Uman, L. Brantely, J. Tiller, E. P. Krider, and K. McLain, “Correlated electric and magnetic fields from lightning return strokes,” *J. Geophys. Res.*, vol. 80, no. 3, pp. 1–2, 1975.
- [22] K. L. Cummins and M. J. Murphy, “An Overview of Lightning Locating Systems : History , Techniques , and Data Uses , With an In-Depth Look at the U.S. NLDN,” *October*, vol. 51, no. 3, pp. 499–518, 2009.
- [23] G. Diendorfer, “Lightning Location Systems (LLS),” in *IX International Symposium on Lightning Protection (SIPDA)*, 2007.
- [24] W. Schulz, “Location Accuracy Improvements of the Austrian Lightning Location System During the Last 10 Years,” *Asia-Pacific Int. Conf. Light.*, pp. 1–5, 2015.

- [25] T. L. Buck, A. Nag, and M. J. Murphy, "Improved Cloud-to-Ground and Intracloud Lightning Detection with the LS7002 Advanced Total Lightning Sensor," *WMO Tech. Conf. Meteorol. Environ. Instruments Methods Obs.*, pp. 1–8, 2014.
- [26] N. Honma, K. L. Cummins, M. J. Murphy, A. E. Pifer, and T. Rogers, "Improved Lightning Locations in the Tohoku Region of Japan using Propagation and Waveform Onset Corrections," *IEEJ Trans. Power Energy*, vol. 133, no. 2, pp. 195–202, 2013.
- [27] M. A. Uman, D. K. McLain, and E. P. Krider, "Electromagnetic Radiation from a finite antenna," *Am. J. Phys.*, vol. 43, no. 33, 1975.
- [28] G. Diendorfer *et al.*, "TB 376 Cloud-to-ground lightning parameters derived from lightning detection systems: the effects of system performance," in *CIGRE WG C4.404*, 2009.
- [29] F. Rachidi, J. L. Bermudez, M. Rubinstein, and V. A. Rakov, "On the estimation of lightning peak currents from measured fields using lightning location systems," *J. Electrostat.*, vol. 60, no. 2–4, pp. 121–129, 2004.
- [30] S. Mallick *et al.*, "On remote measurements of lightning return stroke peak currents," *Atmos. Res.*, vol. 135–136, pp. 306–313, 2014.
- [31] K. L. Cummins, M. J. Murphy, E. A. Bardo, W. L. Hiscox, R. B. Pyle, and A. E. Pifer, "A combined TOA/MDF technology upgrade of the US National Lightning Detection Network," *J. Geophys. Res. Atmos.*, vol. 103, no. D8, pp. 9035–9044, 1998.
- [32] G. Diendorfer, H. Pichler, and W. Schulz, "EUCLID Located Strokes to the Gaisberg Tower – Accuracy of Location and its assigned Confidence Ellipse," *Int. Conf. Light. Detect.*, 2014.
- [33] L. Schwalt, S. Pack, and W. Schulz, "LiOn ground truth data in correlation with ALDIS LLS detections," *34th Int. Conf. Light. Prot. ICLP 2018*, pp. 1–6, 2018.
- [34] G. Diendorfer, W. Schulz, and V. A. Rakov, "Lightning characteristics based on data from the Austrian lightning locating system," *IEEE Trans. Electromagn. Compat.*, vol. 40, no. 4 PART 2, pp. 452–464, 1998.
- [35] W. Schulz and G. Diendorfer, "Flash Multiplicity and Interstroke Intervals in Austria," *Light. Prot. (ICLP), 2006 Int. Conf.*, pp. 402–404, 2006.
- [36] D. R. Poelman, W. Schulz, G. Diendorfer, and M. Bernardi, "European cloud-to-ground lightning characteristics," *2014 Int. Conf. Light. Prot. ICLP 2014*, pp. 24–29, 2014.

- [37] V. A. Rakov, "Lightning flashes transporting both negative and positive charges to ground," *Res. Signpost*, vol. 661, no. 2, pp. 9–21, 2005.
- [38] P. Markowski and Y. Richardson, *Mesoscale Meteorology in Midlatitudes*. Wiley Blackwell, 2010.
- [39] J. P. Craven and H. E. Brooks, "Baseline climatology of sounding derived parameters associated with deep, moist convection," *Natl. Weather Dig.*, vol. 28, pp. 13–24, 2004.
- [40] K. Berger, R. B. Anderson, and H. Kroninger, "Parameters of Lightning Flashes," *Electra*, vol. 41, pp. 23–37, 1975.
- [41] V. Cooray and V. Rakov, "On the upper and lower limits of peak current of first return strokes in negative lightning flashes," *Atmos. Res.*, vol. 117, pp. 12–17, 2012.
- [42] W. Schulz, C. Vergeiner, H. Pichler, G. Diendorfer, and K. L. Cummins, "Location Accuracy Evaluation of the Austrian Lightning Location Systems ALDIS," in *International Lightning Detection Conference and International Lightning Meteorology Conference (ILDC/ILMC)*, 2012.
- [43] C. J. Biagi, K. L. Cummins, K. E. Kehoe, and E. P. Krider, "National Lightning Detection Network (NLDN) performance in southern Arizona, Texas, and Oklahoma in 2003–2004," *J. Geophys. Res. Atmos.*, vol. 112, no. 5, pp. 1–17, 2007.
- [44] L. Schwalt, S. Pack, W. Schulz, G. Diendorfer, and G. Pistotnik, "Number of single-stroke flashes in the alpine region determined with a video and field recording system," in *CIGRE International Colloquium on Lightning and Power systems (ICLPS)*, 2017.
- [45] W. Schulz and M. M. F. Saba, "First Results of Correlated Lightning Video Images and Electric Field Measurements in Austria," *Light. Prot. (X SIPDA), 2009 Int. Symp.*, pp. 2005–2007, 2009.
- [46] Y. Zhu, V. A. Rakov, S. Mallick, and M. D. Tran, "Characterization of negative cloud-to-ground lightning in Florida," *J. Atmos. Solar-Terrestrial Phys.*, vol. 136, pp. 8–15, 2015.
- [47] N. Kitagawa, M. Brook, and E. J. Workman, "Continuing currents in cloud-to-ground lightning discharges," *J. Geophys. Res.*, vol. 67, no. 2, pp. 637–647, 1962.
- [48] Z. A. Baharudin, N. A. Ahmad, J. S. Mäkelä, M. Fernando, and V. Cooray, "Negative cloud-to-ground lightning flashes in Malaysia," *J. Atmos. Solar-Terrestrial Phys.*, vol. 108, pp. 61–67, 2014.

- [49] V. A. Rakov and M. A. Uman, "Some properties of negative cloud-to-ground lightning flashes versus stroke order," *J. Geophys. Res.*, vol. 95, no. D5, pp. 5447–5453, Apr. 1990.
- [50] M. G. Ballarotti, C. Medeiros, M. M. F. Saba, W. Schulz, and O. Pinto, "Frequency distributions of some parameters of negative downward lightning flashes based on accurate-stroke-count studies," *J. Geophys. Res. Atmos.*, vol. 117, no. 6, pp. 1–8, 2012.
- [51] V. Cooray and H. Pérez, "Some features of lightning flashes observed in Sweden," *J. Geophys. Res.*, vol. 99, 1994.
- [52] A. C. V. Saraiva, M. M. F. Saba, O. Pinto, K. L. Cummins, E. P. Krider, and L. Z. S. Campos, "A comparative study of negative cloud-to-ground lightning characteristics in São Paulo (Brazil) and Arizona (United States) based on high-speed video observations," *J. Geophys. Res. Atmos.*, vol. 115, no. 11, pp. 1–9, 2010.
- [53] D. R. Poelman, W. Schulz, and C. Vergeiner, "Performance characteristics of distinct lightning detection networks covering Belgium," *J. Atmos. Ocean. Technol.*, vol. 30, no. 5, pp. 942–951, 2013.
- [54] V. Cooray and K. P. S. C. Jayaratne, "Characteristics of lightning flashes observed in Sri Lanka in the tropics," *J. Geophys. Res. Atmos.*, vol. 99, no. D10, pp. 21051–21056, 1994.
- [55] L. Antunes *et al.*, "Characterization of lightning observed by multiple high-speed cameras," *2013 Int. Symp. Light. Prot. SIPDA 2013*, no. March 2016, pp. 17–25, 2013.
- [56] X. QIE, Y. YU, D. WANG, H. WANG, and R. CHU, "Characteristics of Cloud-to-Ground Lightning in Chinese Inland Plateau," *J. Meteorol. Soc. Japan*, vol. 80, no. 4, pp. 745–754, 2004.
- [57] C. Vergeiner, W. Schulz, and S. Pack, "On the Performance of the Austrian Lightning Detection and Information System (ALDIS)," *Hofler's Days*, no. November, pp. 5–11, 2013.
- [58] L. Schwalt, S. Pack, W. Schulz, and G. Pistotnik, "Number of Single Stroke Flashes in the Alpine Region of Austria," in *International Symposium on Lightning Protection (XV SIPDA)*, 2019.
- [59] H. Kohlmann, W. Schulz, and S. Pedebay, "Evaluation of EUCLID IC/CG classification performance based on ground-truth data," *2017 Int. Symp. Light. Prot. XIV SIPDA 2017*, no. October, pp. 35–41, 2017.

- [60] L. S. Antunes *et al.*, “Day-to-day differences in the characterization of lightning observed by multiple high-speed cameras,” *Electr. Power Syst. Res.*, vol. 118, pp. 93–100, 2015.
- [61] N. N. Slyunyaev, E. A. Mareev, V. A. Rakov, and G. S. Golitsyn, “Statistical Distributions of Lightning Peak Currents: Why Do They Appear to Be Lognormal?,” *J. Geophys. Res. Atmos.*, vol. 123, no. 10, pp. 5070–5089, 2018.
- [62] A. Nag *et al.*, “First versus subsequent return-stroke current and field peaks in negative cloud-to-ground lightning discharges,” *J. Geophys. Res. Atmos.*, vol. 113, no. 19, 2008.
- [63] R. E. Orville, G. R. Huffines, W. R. Burrows, R. L. Holle, and K. L. Cummins, “The North American Lightning Detection Network (NALDN)—First Results: 1998–2000,” *Mon. Weather Rev.*, vol. 130, no. 8, pp. 2098–2109, 2002.
- [64] ÖVE Österreichischer Verband für Elektrotechnik, “ÖVE/ÖNORM EN 62305-1:2012-07 Blitzschutz Teil 1: Allgemeine Grundsätze,” 2012.
- [65] R. Thottappillil, V. A. Rakov, M. A. Uman, W. H. Beasley, M. J. Master, and D. V. Shelukhin, “Lightning subsequent-stroke electric field peak greater than the first stroke peak and multiple ground terminations,” *J. Geophys. Res.*, vol. 97, no. D7, pp. 7503–7509, May 1992.
- [66] A. O. Filho, W. Schulz, M. M. F. Saba, O. J. Pinto, and M. G. Ballarotti, “The relationship between first and subsequent stroke electric field peak in negative cloud-to-ground lightning,” in *13th International Conference on Atmospheric Electricity*, 2007.
- [67] W. Schulz, S. Sindelar, A. Kafri, T. Götschl, N. Theethayi, and R. Thottappillil, “The Ratio Between first and Subsequent Lightning Return Stroke Electric Field Peaks in Sweden,” in *Lightning Protection (ICLP), 2008 International Conference on*, 2008, no. June, pp. 2006–2009.
- [68] M. G. Ballarotti, M. M. F. Saba, and J. Pinto, “High-speed camera observations of negative ground flashes on a millisecond-scale,” *Geophys. Res. Lett.*, vol. 32, no. 23, pp. 1–4, 2005.
- [69] A. C. V Saraiva, L. Z. S. Campos, L. Antunes, O. P. Jr, and K. L. Cummins, “Analysis of Forked Strokes Characteristics over Southeastern Brasil During the Summer Season of 2013,” *23rd Int. Light. Detect. Conf.*, p. 15, 2014.
- [70] F. Heidler and W. Schulz, “Lightning Current Measurements Compared to Data from the Lightning Location System BLIDS,” in *International Colloquium on Lightning and Power Systems*, 2016.

- [71] M. Matsui, K. Michishita, and S. Kurihara, "Comparison of location accuracy of the Japanese lightning detection network with large scale lightning detection networks," in *2015 International Conference on Lightning and Static Electricity*, 2015.
- [72] S. Mallick *et al.*, "An update on the performance characteristics of the NLDN," in *23rd International Lightning Detection Conference/5th International Lightning Meteorology Conference*, 2014.
- [73] K. L. Cummins, D. Zhang, M. G. Quick, A. Candela Garolera, and J. Myers, "Performance of the U.S. NLDN during the Kansas Windfarm 2012 and 2013 Field Programs," in *International Lightning Detection Conference*, 2014, no. April 2016.
- [74] M. G. Ballarotti, M. M. F. Saba, and O. J. Pinto, "A new Performance Evaluation of the Brazilian Lightning Location System (RINDAT) based on High-Speed Camera Observations of Natural Negative Ground Flashes," *19th Int. Light. Detect. Conf.*, vol. 122, pp. 1–4, 2006.
- [75] Z. A. Baharudin, V. Cooray, M. Rahman, P. Hettiarachchi, and N. A. Ahmad, "On the characteristics of positive lightning ground flashes in Sweden," *J. Atmos. Solar-Terrestrial Phys.*, vol. 138–139, pp. 106–111, 2016.
- [76] A. Nag and V. A. Rakov, "Positive lightning: An overview, new observations, and inferences," *J. Geophys. Res. Atmos.*, vol. 117, no. 8, pp. 1–20, 2012.
- [77] M. M. F. Saba *et al.*, "High-speed video observations of positive lightning flashes to ground," *J. Geophys. Res. Atmos.*, vol. 115, no. 24, pp. 1–9, 2010.
- [78] A. Hazmi, P. Emeraldi, M. I. Hamid, N. Takagi, and D. Wang, "Characterization of positive cloud to ground flashes observed in Indonesia," *Atmosphere (Basel)*, vol. 8, no. 1, 2017.
- [79] S. A. Fleenor, C. J. Biagi, K. L. Cummins, E. P. Krider, and X. M. Shao, "Characteristics of cloud-to-ground lightning in warm-season thunderstorms in the Central Great Plains," *Atmos. Res.*, vol. 91, no. 2–4, pp. 333–352, 2009.
- [80] X. Qie, Z. Wang, D. Wang, and M. Liu, "Characteristics of positive cloud-to-ground lightning in da Hinggan Ling forest region at relatively high latitude, northeastern China," *J. Geophys. Res. Atmos.*, vol. 118, no. 24, pp. 13393–13404, 2013.
- [81] W. Schulz, H. Pichler, G. Diendorfer, C. Vergeiner, and S. Pack, "Validation of detection of positive flashes by the austrian lightning location system ALDIS," *2013 Int. Symp. Light. Prot. SIPDA 2013*, pp. 47–51, 2013.

- [82] J. Montanyà *et al.*, “Global distribution of winter lightning: A threat to wind turbines and aircraft,” *Nat. Hazards Earth Syst. Sci.*, vol. 16, no. 6, pp. 1465–1472, 2016.
- [83] Y. Yokoyama *et al.*, “TB 578 Lightning Protection of Wind Turbine Blades,” in *CIGRE WG C4.409*, 2014.
- [84] V. A. Rakov, M. A. Uman, and R. Thottappillil, “Review of lightning properties from electric field and TV observations,” *J. Geophys. Res.*, vol. 99, no. D5, p. 10745, 1994.
- [85] K. Berger, R. B. Anderson, and H. Kroninger, “Parameters of Lightning Flashes,” *CIGRE Electra*, vol. 41, pp. 23–37, 1975.
- [86] L. Schwalt, J. Plesch, S. Pack, W. Schulz, and G. Achleitner, “Transient measurements in the Austrian high voltage transmission system,” in *International Symposium on Lightning Protection, XIV SIPDA 2017*, 2017.
- [87] V. A. Rakov, “A review of positive and bipolar lightning discharges,” *Bull. Am. Meteorol. Soc.*, vol. 84, no. 6, pp. 767–776, 2003.

12 List of Figures

Figure 1: VFRS measurement locations of the research project and sensor locations of ALDIS/EUCLID on an elevation map	2
Figure 2: Charge structure of two thunderclouds and lightning types (Dwyer and Uman, 2014 [4]).....	8
Figure 3: Process of CG flash comprising two strokes; processes of main interest for the present thesis are highlighted; adapted from (Rakov and Uman, 2003 [3]).....	10
Figure 4: Flash density map for political districts of Austria calculated from ALDIS/EUCLID data of 2010 to 2018 for flashes per square km per year; deep grey coloured areas show the districts with highest flash density.....	11
Figure 5: Mean monthly number of flashes with bars representing a ± 1 standard deviation based on ALDIS data from 1992 to 2001 for Austria shown by Schulz et al., 2005 [12]	12
Figure 6: High speed video camera (left) and flat plate antenna (right).....	16
Figure 7: Components of the electric field measurement system.....	17
Figure 8: General measurement setup and components (GPS antenna 1 for E-field system, GPS antenna 2 for camera system).....	23
Figure 9: VFRS measurement sites, recorded data for negative, positive and bipolar CG flashes for 2015, 2017 and 2018; elevation map in the background	25
Figure 10: First (FI1), second (FI2), third (FI3) and fourth (FI4) stroke terminating in a different GSP (from left to right).....	33
Figure 11: LLS detection of the four strokes in the flash. Position 1 to 4 for each GSP (FI1 to FI4); ESRI satellite map in the background.....	33
Figure 12: Second (FI2), forth (SU2) and seventh (SU2) stroke following the same channel to ground (from left to right)	34
Figure 13: LLS detection of the flash, stroke two to seven struck the same GSP; Google satellite map in the background	35

Figure 14: Recorded data for negative CG flashes (multi and single stroke ones) merged for 2015 until 2018 and VFRS measurement locations37

Figure 15: Percentage of negative single stroke flashes of VFRS and LLS data for individual thunderstorm days in 2015, 2017 and 2018; number of VFRS recorded flashes in parenthesis39

Figure 16: Recorded data for negative CG flashes (multi and single stroke ones) merged for 2009 until 2018 and VFRS measurement locations40

Figure 17: Multiplicity of the VFRS and LLS data of negative flashes (2015, 2017 and 2018)46

Figure 18: Peak current distribution for all negative return strokes for 2015, 2017 and 2018 51

Figure 19: Peak current distribution of negative flashes (FI1) for 2015, 2017 and 2018.....51

Figure 20: Peak current distribution for negative first return strokes (FI) for 2015, 2017 and 201851

Figure 21: Peak current distribution for negative subsequent return strokes (SU) for 2015, 2017 and 201852

Figure 22: Negative median FI peak current versus multiplicity of a flash (dashed) and versus multiplicity per GSP (grey); Peak current shown as absolute values; Number of events on top of each bar54

Figure 23: Negative median FI peak current versus multiplicity of a flash (dashed) and versus multiplicity per GSP (grey) with linear trend line for each analysis (trend equations in frames); Maximum multiplicity value of 8; Peak current shown as absolute values; Number of events on top of each bar55

Figure 24: Location accuracy distribution for merged data of 2015, 2017 and 2018 of negative flashes.....58

Figure 25: Straight (left) and inclined (right) leader channels of strokes recorded in 201859

Figure 26: FI and SU stroke appearing as same GSP for this 2D analysis but with different channels to ground; dashed red line indicates the GSP.....60

Figure 27: Two successive video frames of a forked stroke stepped leader and its two return strokes from different GSPs (highlighted)	61
Figure 28: Wind farm on pre-alpine mountain ridge (ca. 1450 m a.s.l.); Stroked wind turbines #1 and #2 highlighted	74
Figure 29: Stepped leader of FI1, first return stroke (FI1), subsequent strokes 2 and 3 (SU1), stepped leader of FI2 and second return stroke (FI2) from top left to bottom right	75
Figure 30: Locations of the wind turbines, LLS detections and 50 % confidence ellipses of the strokes; Strokes 1 to 3 struck wind turbine #1, stroke 4 struck wind turbine #2; ESRI satellite map in the background	76
Figure 31: Railway overhead line in the analyzed track section; tower structure highlighted.	77
Figure 32: Stepped leader, first return stroke (FI1), flashover on two towers, subsequent stroke 2 (SU1), flashover on three towers and subsequent stroke 3 (SU1) from top left to bottom right	78
Figure 33: Railway track, locations of the LLS detections and 50 % confidence ellipses of the three strokes; all strokes struck the same tower (highlighted); ESRI satellite map in the background	79
Figure 34: LLS data correlated to VFRS electric field measurement record (DataViewer 1.5); analyzed flash comprising three strokes highlighted in blue	129
Figure 35: One second VFRS electric field record showing all three detected strokes of the analysed flash (DataViewer).....	130
Figure 36: Detailed VFRS electric field record of stroke #1 (vertical blue line shows LLS time stamp) and time correlated video frame for stroke #1 (FI1)	131
Figure 37: Detailed VFRS electric field record of stroke #2 (vertical blue line shows LLS time stamp) and time correlated video frame for stroke #2 (SU1).....	132
Figure 38: Detailed VFRS electric field record of stroke #3 (vertical blue line shows LLS time stamp) and time correlated video frame for stroke #3 (SU1).....	133

13 List of Tables

Table 1: Analyzed thunderstorms, total flashes and strokes for each year and in total for negative CG flashes in the VFRS data	26
Table 2: Analyzed thunderstorms, total flashes and strokes for each year and in total for positive CG flashes in the VFRS data.....	27
Table 3: Thunderstorms, total flashes and strokes for each year and in total for bipolar CG flashes in the VFRS data	27
Table 4: LLS data with LA calculation in km (Return stroke peak current in kA, sn = stroke number, nbdf = sensor detections, nbdfit = sensors data with sufficient quality, maxis = major axis in km, ki2 = quality criteria, ToS = Type of Stroke, Flx = First Stroke to GSP x, SUx = Subsequent Stroke to GSP x).....	36
Table 5: Analyzed thunderstorms, total negative flashes and negative single stroke flashes for VFRS data for 2015 and 2018	38
Table 6: Negative single stroke flash percentage for VFRS and LLS data from 2015 to 2018; Number of single stroke flashes in parenthesis	38
Table 7: Additional data of measurement campaigns in 2009, 2010 and 2012; analyzed thunderstorms, total negative flashes and single stroke flashes for VFRS	41
Table 8: Percentage of negative single stroke flashes calculated by thunderstorm type for merged data from 2009 to 2018; Number of single stroke flashes in parenthesis	41
Table 9: Percentage of negative single stroke flashes for a categorization by vertical wind shear between 0 and 6 km (DLS) for merged data from 2009 to 2018; Number of single stroke flashes in parenthesis.....	42
Table 10: Summary of results for the percentage of negative single stroke flashes of the present and previous studies by various authors	44
Table 11: Mean multiplicity for VFRS and LLS data of negative flashes (2015, 2017, 2018 and total).....	45

Table 12: Summary of results for flash multiplicity of negative flashes from present and previous studies by various authors.....	48
Table 13: Mean, median and 95 % value for negative return stroke peak currents of the ALDIS LLS detections for all negative strokes, first (FI), subsequent (SU) and FI1 strokes (flash peak current) for the year 2015, 2017 and 2018 and in total	49
Table 14: Summary of negative multiple-stroke flash characteristics reported in different studies.....	56
Table 15: Values for median LA and 95 % LA for 2015, 2017, 2018 and total for negative flashes.....	58
Table 16: Comparison of number of negative strokes used for LA calculation, median LA and 95 % LA for straight and inclined stroke channels for merged data of 2015, 2017 and 2018	60
Table 17: Median LA values, number of negative strokes used for LA calculation and observation methods for different studies	63
Table 18: DE of the ALDIS LLS for negative flashes, detected strokes and correctly detected strokes for the year 2015, 2017, 2018 and total.....	64
Table 19: DE values for negative flashes and strokes as well as observation methods for different studies	66
Table 20: Positive single stroke flash percentage for VFRS and LLS data from 2015 to 2018; Number of single stroke flashes in parenthesis	68
Table 21: Summary of results for the percentage of positive single stroke flashes of the present and previous analyses by various authors.....	69
Table 22: Mean multiplicity of positive flashes for VFRS and LLS data (2015, 2017, 2018 and total).....	70
Table 23: Mean, median and 95 % value for return stroke peak currents of the ALDIS LLS detections for all positive strokes for the year 2015, 2017 and 2018 and in total	70
Table 24: DE of the ALDIS LLS for positive flashes, detected strokes and correctly detected strokes for the year 2015, 2017, 2018 and total.....	72

Table 25: LLS data with distance to wind turbine #1 and #2 in m (Return stroke peak current in kA, sn = stroke number, nbdf = sensor detections, nbdfit = sensors data with sufficient quality, maxis = major axis, ki2 = quality criteria, ToS = type of stroke, Flx = first stroke to GSP x, SUx = subsequent stroke to GSP x)75

Table 26: LLS data for with distance to the railway transmission line tower in m (Return stroke peak current in kA, sn = stroke number, nbdf = sensor detections, nbdfit = sensors data with sufficient quality, maxis = major axis, ki2 = quality criteria, ToS = type of stroke, Flx = first stroke to GSP x, SUx = subsequent stroke to GSP x)78

Table 27: Analysis of GSPs per flash for 2015, 2017 and 2018 and in total.....85

14 Publications by the Author

14.1 Publications with Scientific Relation to the Present Thesis

L. Schwalt, S. Pack, W. Schulz, "Ground truth Data of Atmospheric Discharges in Correlation with LLS Detections", *Electric Power Systems Research*, vol.: ? pp: ?, 2019 (accepted for publication).

L. Schwalt, S. Pack, W. Schulz, G. Pistotnik, "*Number of Single Stroke Flashes in the Alpine Region of Austria*", *International Symposium on Lightning Protection (XV SIPDA) 2019*, 2019.

L. Schwalt, S. Pack, W. Schulz, "Recent Observations of Lightning Strikes to Wind Turbines and Railway Overhead Lines", *International Colloquium on Lightning and Power Systems (ICLPS)*, 2019.

L. Schwalt, S. Pack, W. Schulz, "LiOn Return Stroke Peak Current Analysis for Ground Strike Points in the Austrian Alps", *11th Asia-Pacific International Conference on Lightning, APL*, 2019.

L. Schwalt, S. Pack, W. Schulz, "LiOn ground truth data in correlation with ALDIS LLS detections", *34th International Conference on Lightning Protection (ICLP)* (pp. 1-6), IEEE, 2018¹⁰.

L. Schwalt, S. Pack, W. Schulz, G. Diendorfer, G. Pistotnik, "Number of Single-Stroke Flashes in the Alpine Region Determined with a Video and Field Recording System", *International Colloquium on Lightning and Power Systems (ICLPS)*, 2017.

¹⁰ Awarded with the ICLP Young Scientist Award 2018

14.2 Other Publications by the Author

L. Schwalt, S. Pack, „Blitzforschung LiOn – Erfassung von atmosphärischen Entladungen im österreichischen Alpenraum“, 13. VDE|ABB-Blitzschutztagung, 2019.

L. Schwalt, J. Plesch, S. Pack, „Verhalten von Freileitungen unter Einfluss atmosphärischer Entladungen“, VDE-Fachtagung Hochspannungstechnik 2018, 2018.

J. Plesch, L. Schwalt, S. Pack, „Hochspannungssysteme unter transients Beanspruchung – Korrelationsmethodik“, EnInnov 2018 - 15. Symposium Energieinnovation: Neue Energie für unser bewegtes Europa, S. 236-237, 2018.

L. Schwalt, S. Pack, J. Plesch, W. Schulz, G. Achleitner, „Transient Measurements in the Austrian High Voltage Transmission System“, International Symposium on Lightning Protection (XIV SIPDA) 2017, 2017.

S. Pack, J. Plesch, L. Schwalt, „Blitzphänomene im österreichischen Hoch- und Höchstspannungsnetz – transient erfasst“, e&i - Elektrotechnik und Informationstechnik, 134(8), 2017.

15 Appendix

A. Video and Field Recording System – Technical Data

This section shows the technical data of the used components of the Video and Field Recording System (VFRS). Hereinafter the system specifications and the selected settings of the high speed video camera system are listed:

System specifications:

Model	Vision Research	Phantom v9.1
Maximum frame rate		153.846 fps
Sensor		CMOS (1632 x 1200 pixel)
Image depth		14 bit
Memory		6 GB RAM
Timing ¹¹		External GPS-clock (IRIG-B standard)
Lens	Nikon	AF-S NIKKOR 24 mm, 1:1.4G ED
Red filter	Hoya	HMC 25A
Trigger		Manual
Control Software		Phantom PCC 1.3

Selected settings:

Resolution	1344 x 400 pixel
Framerate	2000 fps
Image depth	14 bit
Record length	1.6 s
Maximum exposure time	500 μ s

The overall electric field measurement system is composed of the flat plate antenna (25 cm in diameter, distance from plate to ground 5 cm; see Figure 6 and Figure 7), an integrator circuit and an amplifier, a fiber optic link, a digitizer and a PXI system as processing unit. This PXI system includes a Windows based computer system and two additional hardware modules, a GPS time receiver and a digitizer module. To avoid influences of the power generator and the measurement systems on the electric field measurements, the flat plate

¹¹ Synchronization to GPS-time in universal time (UTC) offers nanoseconds time resolution and allows a correct time correlation for all strokes within microseconds.

antenna was placed in a distance of 20 m to the measurement vehicle. Measurement locations with low electric field interferences have been selected for that reason only. Hereinafter the system specifications of the electric field measurement system are listed:

PXI System:

Controller		PXI Express
Digitizer	ADLINK	PXI-9816H/512
	Sampling Rate	10 MS/s
	Resolution	16 bit
GPS time receiver ¹²	National Instruments	NI PXI-6683H GPS
Trigger		Manual

Fiber Optic Link:

Terahertz Technologies Inc.	LTX-5515
Analog Signal Bandwidth	DC to 25 MHz
Input Voltage Range	±5 V (adapted to ±10 V for ALDIS)
Resolution	12 bit
Transfer Accuracy	±0.1 % Full Scale, ±20 mV offset
Sampling Rate	100 MS/s
Digital Outputs	LVTTL (0 – 3.3 V)
Optical Transmission Rate	2.0 Gb/s
Fiber Optic Cable	20 m (62.5/125 micron fiber)

Analog Amplifier/Integrator:

Manufacturer	ALDIS (H. Pichler)
Analog Signal Bandwidth	300 Hz to ~1.0 MHz
Input Voltage Range	±15 V

¹² Synchronization to GPS-time in universal time (UTC) offers nanoseconds time resolution and allows a correct time correlation for all strokes within microseconds.

B. Software Tools used for the VFRS Data Analysis and LLS Data Correlation

The following figures show the correlation and analysis process of VFRS and LLS data. The correlation process starts with a request of LLS data for a specific time slot (defined by the VFRS record; 5 s for the present analysis) and a radius around the measurement location (100 km) by using the DataView tool (software version 1.5), provided by ALDIS. Figure 34 shows the output window of such a request for the measurement record of the lightning strike to the railway transmission line on the 3rd July 2018 at 16:48:32 UTC. The LLS detected five events for the requested time and area. Three of the detected events were categorized as cloud to ground strokes (icloud = 0; see Figure 34) and have been grouped to a flash. The other two events have been categorized as cloud pulses (icloud = 1; see Figure 34). This can be confirmed by analyzing the video data.

date	nano	latitude	longitude	amplitude	distance	nbloc	numloc	calcul	nbdf	nbdfit	icloud	maxis	ki2
20180703_164832	304317440	46.7217	14.2894	-10.2	10.6	3	1	114	16	13	0	0.1	1.6
20180703_164832	334404352	46.7330	14.2871	-3.9	10.8	3	2	114	6	6	0	0.1	1.2
20180703_164832	361373952	46.7337	14.2870	-5.5	10.8	3	3	114	10	10	0	0.1	1.0
20180703_164832	491631360	46.5103	14.1562	1.5	31.9	2	1	114	2	2	1	2.2	2.1
20180703_164832	527166976	46.4714	14.0319	0.8	41.6	2	2	114	2	2	1	1.7	0.9

Figure 34: LLS data correlated to VFRS electric field measurement record (DataViewer 1.5); analyzed flash comprising three strokes highlighted in blue

The LLS polarity categorization can now be analyzed by the analysis of the VFRS electric field record. Figure 35 shows the electric field record of all three CG strokes (record length 1 s). Strokes can also be analyzed in detail by clicking on a specific line in the table shown in Figure 34 (box “Zoom to flash” has to be checked).

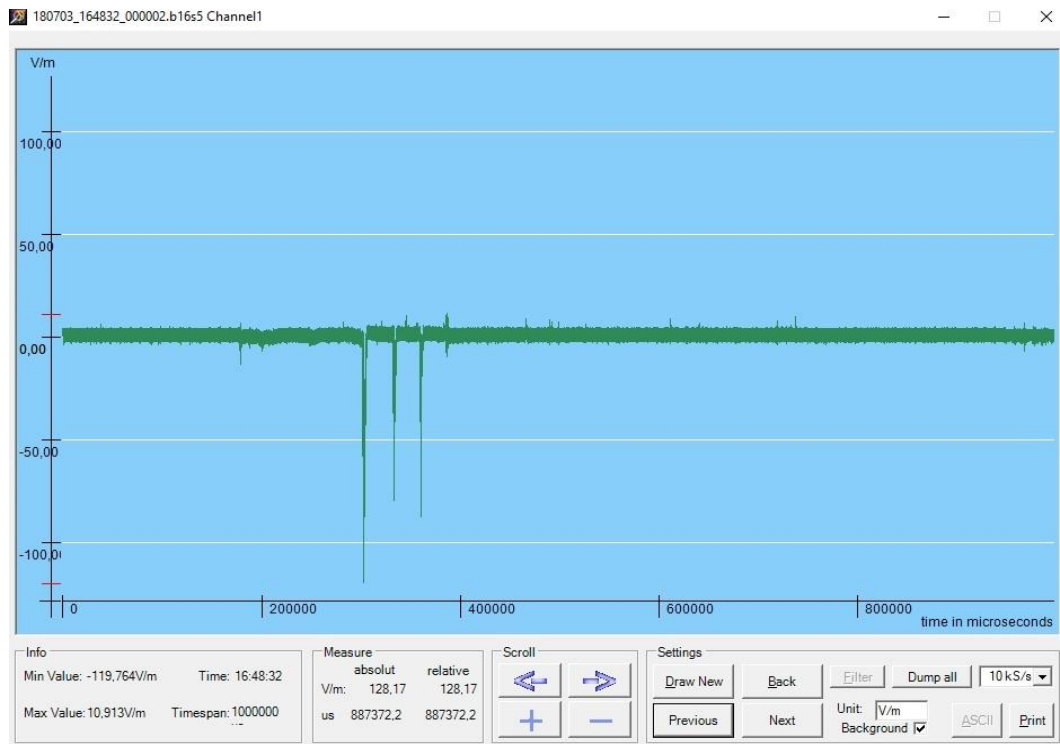


Figure 35: One second VFRS electric field record showing all three detected strokes of the analysed flash (DataViewer)

Figure 36 to Figure 38 show detailed analyses for the first return stroke and the two subsequent strokes. The vertical blue line shows the LLS time stamp and allows a direct examination of the agreement of the time stamps of VFRS and LLS data for the analyzed electric field of the stroke. Furthermore a correlation of the VFRS video data can be carried out by using the LLS provided time stamp for each stroke (see Figure 34). Categorizations of the strokes in strokes following the same channel (e.g. FI1 and SU1) or strokes to new GSP can be withdrawn from this video analysis for example. The synchronisation of the VFRS and LLS system to GPS-time makes such correlations possible.

Figure 36 shows the detailed VFRS electric field record and the time correlated video frame for stroke #1 (FI1).

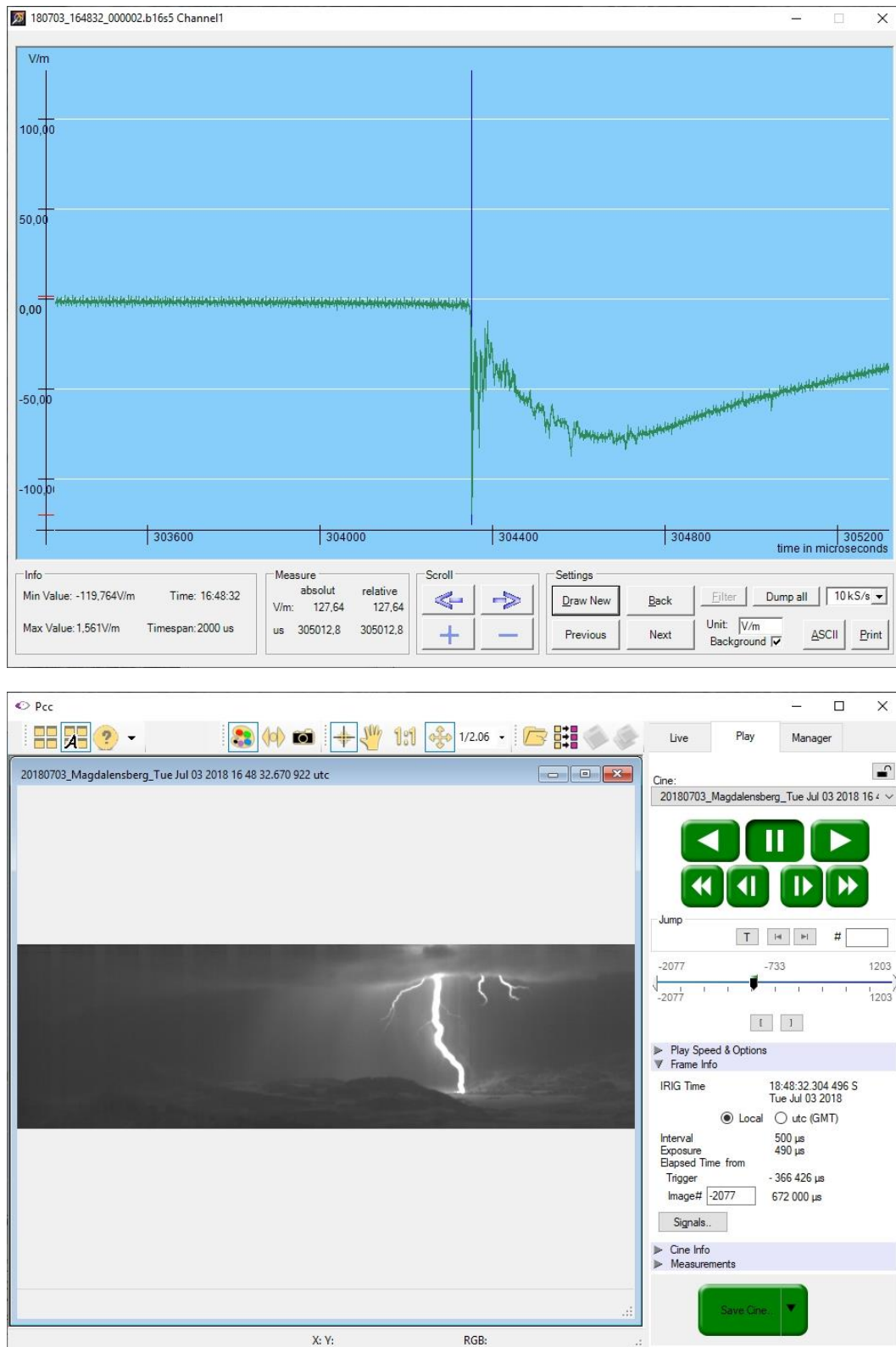


Figure 36: Detailed VFRS electric field record of stroke #1 (vertical blue line shows LLS time stamp) and time correlated video frame for stroke #1 (FI1)

Figure 37 shows the detailed VFRS electric field record and the time correlated video frame for stroke #2 (SU1).

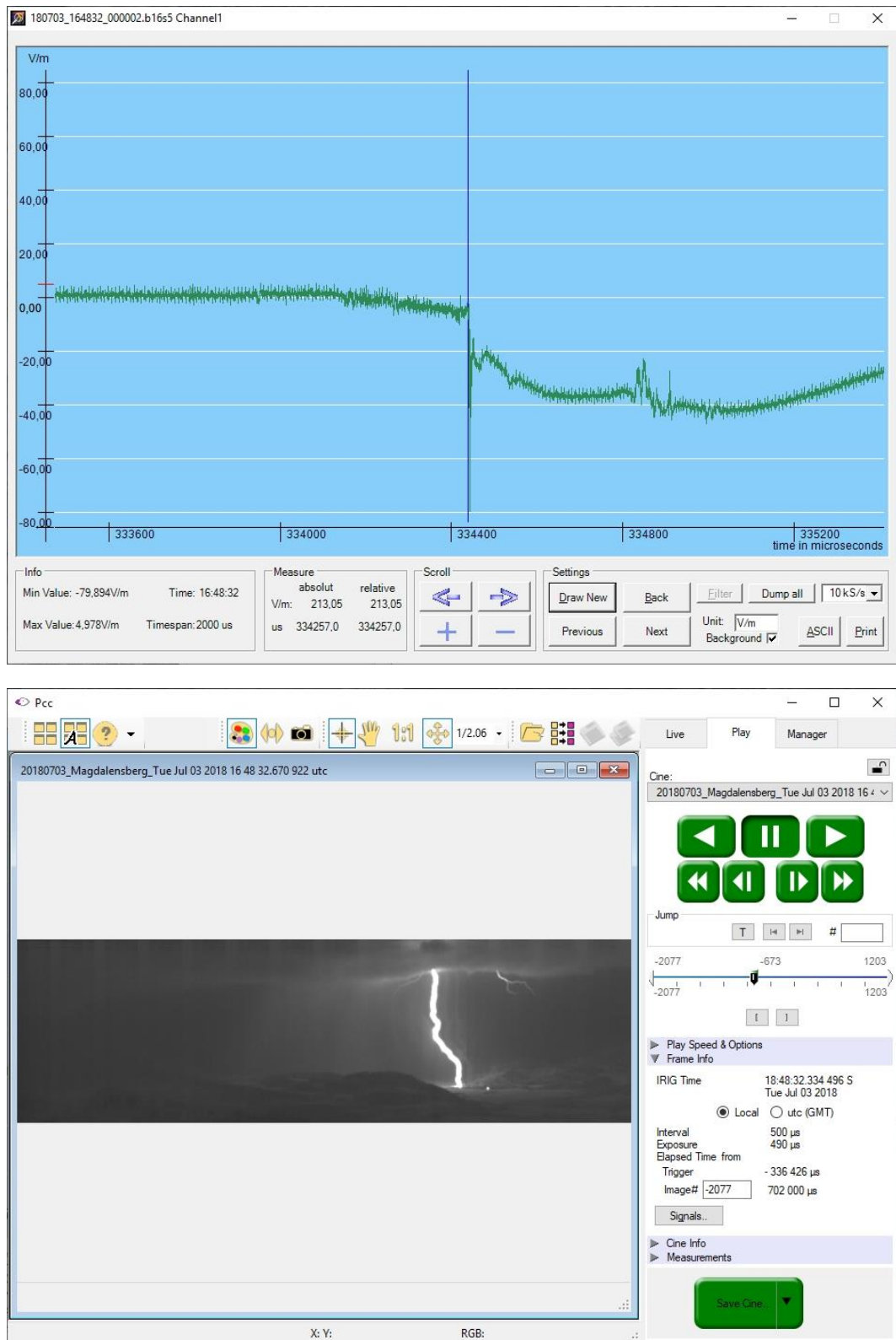


Figure 37: Detailed VFRS electric field record of stroke #2 (vertical blue line shows LLS time stamp) and time correlated video frame for stroke #2 (SU1)

Figure 38 shows the detailed VFRS electric field record and the time correlated video frame for stroke #3 (SU1).

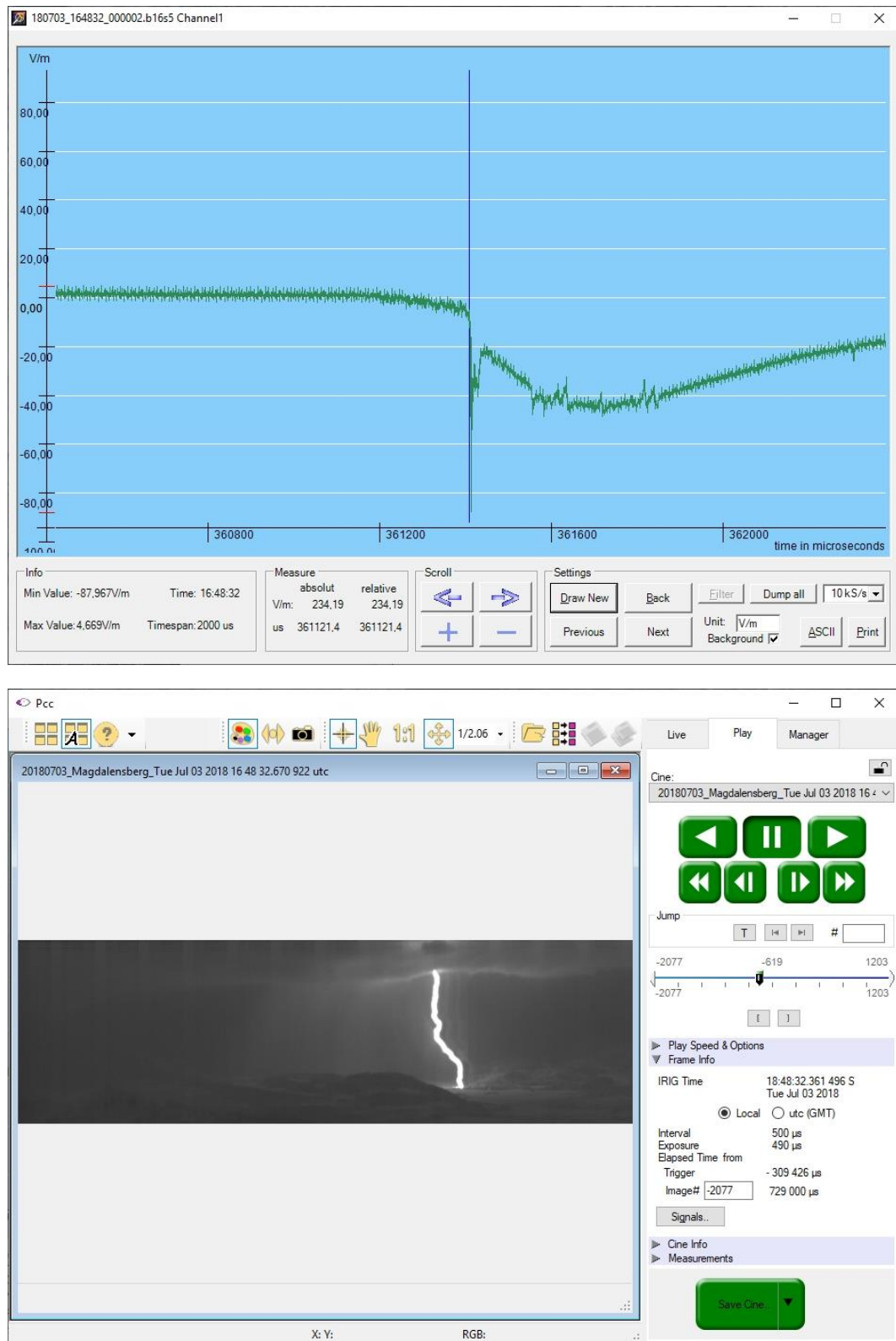


Figure 38: Detailed VFRS electric field record of stroke #3 (vertical blue line shows LLS time stamp) and time correlated video frame for stroke #3 (SU1)